AD748663

TUNNEL SITE SELECTION BY REMOTE [illegible] TECHNIQUES

Final Report

1 April 1971 Through 4 March 1972

THOMAS WAGNER
ROBERT VINCENT
BEN DRAKE
RALPH MITCHELL
PHILIP JACKSON

September 1972

Sponsored by the Advanced Research Projects Agency, Department of Defense, Washington, D. C. 20301 and monitored by the U.S. Bureau of Mines, ARPA Order No. 1879, Amendment 2, Program Code 1F10

Contract H0210041

NOTICES

Sponsorship. The work reported herein was conducted by the Willow Run Laboratories of the Institute of Science and Technology for the Advanced Research Projects Agency, Department of Defense, Washington, D. C. 20301, and monitored by the U. S. Bureau of Mines, under Contract No. HO210041, ARPA Order No. 1579, Amendment 2, Program Code 1F10. Contracts and grants to The University of Michigan for the support of sponsored research are administered through the Office of the Vice-President for Research.

Distribution. Initial distribution is indicated at the end of this document.

Final Disposition. After this document has served its purpose, it may be destroyed. Please do not return it to the Willow Run Laboratories.

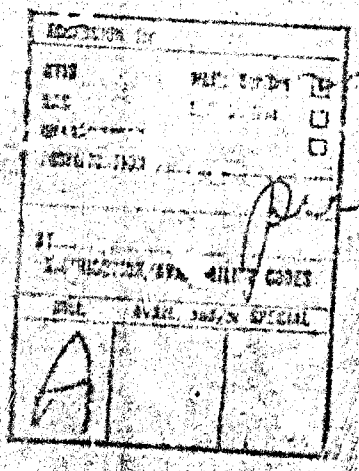

UNCLASSIFIED
Security Classification

DOCUMENT CONTROL DATA - R & D

(Security classification of title, body of abstract and indexing annotation must be entered when the overall report is classified)

1. ORIGINATING ACTIVITY *(Corporate author)*
Willow Run Laboratories of the Institute of Science and Technology, The University of Michigan, Ann Arbor

2a. REPORT SECURITY CLASSIFICATION
UNCLASSIFIED

2b. GROUP
N/A

3. REPORT TITLE
TUNNEL-SITE SELECTION BY REMOTE SENSING TECHNIQUES

4. DESCRIPTIVE NOTES *(Type of report and inclusive dates)*
Final Report, 1 April 1971 Through 4 March 1972

5. AUTHOR(S) *(First name, middle initial, last name)*
Thomas Wagner, Ben Drake, Philip Jackson, Robert Vincent, Ralph Mitchel

6. REPORT DATE	7a. TOTAL NO. OF PAGES	7b. NO. OF REFS
September 1972	x + 91	56

8a. CONTRACT OR GRANT NO.	9a. ORIGINATOR'S REPORT NUMBER(S)
HO210041	10018-13-F
b. PROJECT NO. ARPA Order No. 1579, Amendment 2	
c. Program Code 1F10	9b. OTHER REPORT NO(S) *(Any other numbers that may be assigned this report)*
d.	

10. DISTRIBUTION STATEMENT

11. SUPPLEMENTARY NOTES
This contract was monitored by the U. S. Bureau of Mines

12. SPONSORING MILITARY ACTIVITY
Advanced Research Projects Agency
Department of Defense
Washington, D. C. 20301

13. ABSTRACT

A study of the role of remote sensing for geologic reconnaissance for tunnel-site selection was commenced. For this study, remote sensing was defined as ultraviolet to thermal infrared multispectral scanning, X- and L-band synthetic aperture radar, and aerial photography. Data from these sensors were processed and evaluated in terms of their complementary use. In addition to general geologic interpretation and evaluation of remote sensing, specific work was performed to improve the state of the art and thereby contribute to better geologic interpretation. Our areas of study included: (1) image ratioing to indicate SiO_2 and iron oxide content, representing the final step toward compositional (or lithologic) remote sensing in geology; (2) the analysis and processing of remote sensing data from a glacial drift region for which level slicing, ratioing, and multichannel statistical pattern recognition of multispectral data were employed; also, the correlation of thermal variation studies, aerial photographs, and radar imagery to obtain information on soils, geology, and hydrology; and (3) the analysis of two-frequency multipolarized radar imagery in terms of its capability to delineate geologic features. This report can be used tutorially on the data processing and basic instrumentation of conventional remote sensing. Future research directions are suggested, and the extension of remote sensing to include airborne passive microwave sensor systems, magnetometry, gamma-ray sensors, gravimetry, and airborne electromagnetic sounding systems is discussed.

DD FORM 1 NOV 65 1473

UNCLASSIFIED
Security Classification

14. KEY WORDS	LINK A		LINK B		LINK C	
	ROLE	WT	ROLE	WT	ROLE	WT
Tunnel-site selection						
Geologic reconnaissance						
Remote sensing imagery						
Synthetic aperture radar						
Multispectral scanning						
Image-ratioing techniques						
Multichannel processing						
Statistical pattern recognition						
Level slicing						
Optical processing techniques						

10018-13-F

TUNNEL-SITE SELECTION BY REMOTE SENSING TECHNIQUES

Final Report

1 April 1971 Through 4 March 1972

THOMAS WAGNER
ROBERT VINCENT
BEN DRAKE
RALPH MITCHEL
PHILIP JACKSON

September 1972

RADAR AND OPTICS DIVISION AND INFRARED AND OPTICS DIVISION
Willow Run Laboratories
INSTITUTE OF SCIENCE AND TECHNOLOGY
THE UNIVERSITY OF MICHIGAN
Ann Arbor, Michigan

FOREWORD

The research reported in this final report was performed by Willow Run Laboratories, a unit of The University of Michigan's Institute of Science and Technology. The work was supported by the Advanced Research Projects Agency of the Department of Defense and was monitored by the U. S. Bureau of Mines under Contract No. HO210041, ARPA Order No. 1579, Amendment 2, Program Code 1F10. The inclusive dates for this reporting period are 1 April 1971 through 4 March 1972. The original Project Officer for this project was Benton L. Tibbitts, who was replaced by James Scott; the current Project Officer is Frank Ruskey. The original Principal Investigator was Roger Turpening, who was replaced by Philip Jackson. The Willow Run Laboratories' number for this report is 10018-13-F.

The scientists who have contributed to this project throughout the contract period include Ben Drake, Philip Jackson, Ralph Mitchel, Robert Vincent, and Thomas Wagner. Section 2 of this report was written by Philip Jackson and Thomas Wagner, Section 3 by Thomas Wagner, Section 4 by Robert Vincent, and Section 5 by Ben Drake (with contributions from Philip Jackson and Ralph Mitchel). The remainder of the report was written by Philip Jackson.

The views and conclusions contained in this document are those of the authors and should not be interpreted as necessarily representing the official policies, either expressed or implied, of the Advanced Research Projects Agency or the U. S. Government.

ABSTRACT

A study of the role of remote sensing for geologic reconnaissance for tunnel-site selection was commenced. For this study, remote sensing was defined as ultraviolet to thermal infrared multispectral sensing, S- and L-band synthetic aperture radar, and aerial photography. Data from these sensors were processed and evaluated in terms of their complementary use. In addition to general geologic interpretation and evaluation of remote sensing, specific work was performed to improve the state of the art and thereby contribute to better geologic interpretation. Our areas of study included: (1) image ratioing to indicate SiO_2 and iron oxide content, representing the final step toward compositional (lithologic are remote sensing in geology; (2) the analysis and processing of remote sensing data from a glacial drift region for which level slicing, ratioing, and multichannel statistical pattern recognition of multispectral data were employed; also the correlation of thermal variation studies, aerial photographs, and radar imagery to obtain information on soils, geology, and hydrology; and (3) the discussion of two-frequency multipolarized radar imagery in terms of its capability to delineate geologic features. This report can be used tutorially on the data processing and basic instrumentation of conventional remote sensing. Future research directions are suggested, and the extension of remote sensing to include airborne passive microwave sensor systems, magnetometry, gamma-ray sensors, gravimetry, and airborne electromagnetic sounding systems is discussed.

CONTENTS

FIGURES

TABLES

TUNNEL-SITE SELECTION BY REMOTE SENSING TECHNIQUES
Final Report
1 April 1971 Through 4 March 1972

1
SUMMARY

The purpose of this contract is to evaluate signal-enhancement, data-reduction techniques for an airborne system which would utilize simultaneously aerial photographs, synthetic aperture radar, and multispectral scanning systems (the latter operating in the 0.32- to 13.5-μm spectral region). The data acquired from such a system are to be utilized in the construction of both surface and subsurface geologic maps which could be used to predict subsurface conditions in possible tunneling sites. Ground-truth investigations are to be conducted to verify analyses of the remote sensing data.

For these evaluations, primarily we are using recently acquired remote sensing imagery collected by Willow Run Laboratories. We are presently improving and refining our techniques for collecting and analyzing remote sensing data. Recent advancements in the area include: (1) the development of Vincent's image ratioing method, which utilizes multispectral imagery to detect differences in the SiO_2 and iron content of geologic formations; and (2) development of high-resolution L-band radar, which allows us to acquire like- and cross-polarized images of both X- and L-band. These developments in remote sensing techniques appear to be applicable to the identification of geologic features. Such new techniques may, in fact, be required before the use of remote sensing in tunnel-site selection is feasible.

A literature search was performed on the application of airborne radar and multispectral scanning systems to geologic studies in order to avoid duplication of effort, to build upon work performed elsewhere, and to acquaint ourselves generally with the problems involved in using remote sensing for geologic purposes. We have now acquainted ourselves with much of the significant work in the geologic applications of remote sensing and with most sources of current contributions.

At Willow Run Laboratories, compositional remote sensing (the determination of differences in lithology) has been advanced by two new techniques of image ratioing performed upon multispectral data. These techniques allow the discrimination between silicate and nonsilicate geologic formations and the determination of the amount of ferric oxide in given geologic features. Reflectance and emittance calibrations have been made on rock samples to refine and quantify these methods further, and the laboratory tests for SiO_2 have confirmed the results

obtained in the field. Surficial ferric oxide deposits do not appreciably alter the spectra of underlying rock in the 7- to 14-μm range.

The geology and hydrology of a glaclal drift region were studied through the data-processing techniques of level slicing, two-channel ratioing, and multichannel statistical pattern recognition. In addition, studies of thermal variations, aerial photography, and radar imagery were used for this study.

Several coherent optical processing techniques were applied to available radar imagery in an attempt to reduce the amount of total information and enhance those features applicable to the identification and Interpretation of geologic features. The most successful technique involves an image-enhancement method which removes the low spatial frequency portion of the image's spectrum by means of a spatial filter. This method resulted in the capability to delineate more easily the structural edges and lines separating differently reflecting terrain regions.

During this period, we have also interpreted high-resolution L-band radar imagery along with high-resolution X-band imagery.* With like- and cross-polarized returns in each band, we have the capability for both dual-spectral and dual-polarity returns. Interpretation of these radar images from one geologic region revealed differences in the imagery related to the texture of the surface and to the substratum under a thin surface layer. The differences shown in the L-band and X-band imagery designate those regions for whlch ground-truth investigations should be initiated.

We have accurately quantified our application of compositional remote sensing. With the use of compositional remote sensing and the addition of multispectral and multipolar radar, we presently anticipate that remote sensing will be an economically useful technique to guide field investigations of potential tunnel sites.

No remote sensing data were gathered under this contract. Although both radar and multispectral data were available for several sites, no site was suitable for a case study of remote sensing for geologic areas with crystalline rocks. Fortunately, data from a glacial drift area were recently made available to us. Several kinds of processing were performed on these data to aid in geologic and hydrologic reconnaissance for tunneling.

In the subsequent contract period, it is anticipated that multispectral data will be obtalned from a region containing a wide variety of crystalline and other rock outcrops. A test site in the Black Hills was chosen for a study of tunneling problems. Radar imagery of this area is available from other sources. We hope to provide a test case to evaluate more clearly the contribution of remote sensing to tunnel-site selection.

*Specific examples of the radar imagery cannot be discussed in this report because of security and proprietary reasons.

2
REMOTE SENSING FOR TUNNEL-SITE SELECTION

2.1. INTRODUCTION

Multispectral scanners and radar systems can provide geologic and terrain information useful for exploration and planning purposes. The potential of remote sensing systems results from the new kinds of information collected, the large amounts of data involved, and their compatibility with modern processing facilities. This report describes the results of a one-year effort to process and analyze existing multispectral and radar data to obtain information useful in the selection of tunneling sites and in planning for tunnel construction. Modern remote sensing imagery is used to determine local and regional geologic and hydrological conditions, and examples of high-altitude aerial photography are included and discussed.

2.2. IMAGING REMOTE SENSORS

Imaging sensor systems (cameras, multispectral scanners, and radars) are capable of recording only the surface or near surface of the terrain. Thus, the problem of remote sensing of geologic conditions for tunnel-site selection is one of recording and interpreting the occurrence and nature of surficial materials and conditions as an indicator of the subsurface structures. In many cases, highly accurate predictions of the geology and hydrology of an area can be made through the use of remote sensor imagery. Structural faults and fissures have distinctive appearances on imagery, and rock types are often identifiable by their texture and tone. In other cases, however, because of dense mantles of sediments and/or vegetation, relatively little can be learned about subsurface conditions from surface images. For most geographical areas, remote sensor data can supply much useful information for planning tunnel construction, but seldom all that is required. In no sense can remote sensing techniques replace the ground-survey programs currently carried out in advance of decisions on tunnel location. Remote sensing can, however, reduce ground-surveying efforts by providing early indications of potential problem areas and monitoring surficial changes during and after construction.

To obtain surface information concerning subsurface conditions, remote sensor data can be analyzed in two ways: (1) by an examination of the characteristics and occurrence of rock outcroppings, wherein rock types and their location provide direct lithological information concerning the site; and (2) by a study of the weathered zone of the earth's mantle (e.g., the vegetation patterns, soil and sediment trends, physiographic features, hydrologic conditions, and land-use practices). This report incorporates recent research on remote detection and mapping of rock outcrops (sponsored under this and related contracts) and much of the current state of the art in the remote recording and mapping of nonlithologic terrain features.

2.3. THE ROLE OF REMOTE SENSING IN TUNNEL-SITE SELECTION

In general, the reliability of remotely sensed information concerning probable subsurface conditions decreases with increasing depth below the terrain surface. Necessary information for tunnel-site selection includes knowledge of surface and ground water flow, surficial sediments, and even land use in the form of building locations and existing surface transportation routes. Critical sections in both near-surface and deep tunnel construction are often around portals. Here detailed knowledge of slope materials, their stratification, engineering properties, and drainage are essential. Knowledge concerning the location and transportation of materials for actual tunnel construction can also be useful.

Széchy (Ref. 1) provides the following list of rock properties of interest in geologic reconnaissance for tunnel sites. The items with asterisks are geologic or lithologic properties for which remote sensing can contribute information.

*(1) The orientation of rock stratification (whether horizontal, sheet-like, moderately inclined, steeply sloping, reserved, or overfolded)

*(2) The thickness of individual layers, the regularity of the sequence rock layers, or changes in mountain types

*(3) Mineralogical composition (detrimental components)

(4) The crystalline structure of rocks (uniformly grained, porphyritic, etc.)

(5) The bonds between the individual grains (strong, weak, direct, indirect)

*(6) The hardness of the rocks, whether they would allow for drilling or blasting

*(7) The structural form of rocks (massive, stratified, or shaly)

*(8) Internal structure (whether solid or porous, with closed or open voids)

*(9) Deformations suffered during the origin process (cleavages, crushed zones, faults) or other effects (such as weathering, mylonitization, or kaolinization)

(10) The probable bearing and tensile strength of the mountain at various tunnel sections

(11) The stability of the mountain, the character and magnitude of probable rock pressure

(12) The bulk densities and dead weights of component rocks

(13) The anticipated durability of various rock types to be penetrated, the length of entrance sections to be lined with regard to the danger of frost effects

(14) The depth and composition of cover above each point of the tunnel for each rock constituent

(15) Temperature conditions affecting the mountain

*(16) Hydraulic conditions at the construction site and its environment†

†Springs and watercourses in the vicinity should be observed continuously for years in order to obtain evidence concerning the amount of water flowing into the site and that draining off. The water should also be tested for harmful constituents.

(17) The possibility of the occurrence of harmful gases

(18) The susceptibility of structures to earthquakes and artificial vibrations

*(19) Surface formations

(20) Safety against escaping air in anticipation of operations involving compressed air

*(21) Hazards to structures and especially to entrance portals by forces of nature (e.g., slides, rock falls, avalanches, or slumping)

Of these twenty-one geologic features applicable to the selection of potential tunneling sites, remote sensing techniques can contribute data in at least ten categories.

The importance of the information that remote sensing systems can provide is emphasized by the safety hazards, time delays, and cost increases caused by geologic surprises. Because basic geologic information was incomplete before tunneling was begun, the cost of some tunnels has been multiplied many times and completion delayed for years. Although the increasing sophistication of conventional geologic and geophysical reconnaissance has reduced the problem somewhat, it has not been eliminated. The recent difficulties encountered in constructing the Straight Creek Tunnel on Interstate 70 in Colorado, for example, have resulted in a substantial increase in cost and a significant delay in anticipated completion.

Aerial photography is one type of remote sensing that has been used conventionally in geologic reconnaissance for about 50 years. Geochemistry, measurements of radioactivity, and geobotany have also been introduced into conventional geologic reconnaissance (as distinct from geophysical reconnaissance) during this century. Multispectral scanning and sidelooking airborne radar systems are two of the newer remote sensing systems applicable to the collection of geologic data, and the applications of these systems to geologic investigations are still being analyzed and evaluated.

The economic feasibility of utilizing these newer remote sensing systems in geologic reconnaissance has been questioned, and no precise figures are as yet available. In this regard, however, one must balance the impact of the additional information that such systems can provide against the safety hazards, the scheduling extensions, and the cost increases incurred in construction as a result of inadequate geologic information about the tunnel site. The following points should be considered:

(1) The amount and variety of remote sensing data presently available to U. S. governmental agencies without charge is large and growing larger. The Strategic Air Command has imaged approximately 15% of the United States by sidelooking airborne radar, and the data are available from the Goodyear Aerospace Company for the asking. NASA also maintains three remote sensing aircraft (RB57E, NP3A, and NC130B) with visible, infrared, passive microwave, and active microwave sensing systems. These aircraft are devoted to gathering remote sensing data for governmental or institutional users, and NASA maintains a continuously

growing library of remote sensing data. In addition, the first of the Earth Resources Technology Satellites (ERTS-I) was launched in July 1972. Carrying remote sensors, these satellites are coordinated with underflights for specific research projects and are gathering earth resources data for the public domain. The Earth Resources Observation System (EROS) program will maintain a center in Sioux City, Iowa, to disseminate these data.

(2) Modern structural geology requires a large regional overview, since geologic inferences are made in the context of regional structures. Remote sensing is synoptic and is thus the most economic means of obtaining regional surface features.

(3) Remote sensing is a reconnaissance tool. The basis for reconnaissance is the identification of areas for intensive study. The geologic data presently collected by remote sensing systems are largely indicative rather than definitive, and if remote sensing were the only investigative method available, the lack of complete definitiveness would be a serious drawback. However, when used as a complement to other methods, these data can be highly informative. Remote sensing systems display every portion of the surface that is overflown and serve as a guide for the field geologist. The designation of a distinctive, although undefined, feature is highly useful in reconnaissance. The fact that the data show an outcrop, a dike, an unexplained relief, or a texture is valuable information, since subsequent mapping expeditions can be directed to pertinent features. The time required for geologic mapping is reduced, and, in addition, features may be discovered which would otherwise be overlooked.

(4) Remote sensing collection and data processing techniques are constantly being developed to enable us to define geologic features more clearly, with NASA and other governmental agencies devoting much time and effort toward this goal. Remote sensing instrumentation and data analysis methods are also being developed for application to other disciplines, such as agriculture, ice, soil, and land-use studies, and the new instrumentation and methods that have evolved are being applied to geologic problems. The three basic contributions to the state of the art discussed in this report are examples of the continuing advancement toward more varied as well as more definitive data.

(5) Although geologic reconnaissance is a small portion of the expense of tunneling, the validity of the available geologic information often has a catastrophic impact upon the expense and schedule of the tunnel. Since more complete geologic reconnaissance can potentially eliminate unexpected cost increases, safety hazards, and scheduling extensions, every possible geologic interpretative method must be used, including information provided by remote sensing techniques. Remote sensing has been shown to be useful in detecting fault zones and surface drainage patterns, both of which can impede tunnel construction and produce additional expense.

In summary, the newer remote sensing techniques (i.e., multispectral scanning and synthetic aperture radar systems) are rapidly becoming operational and can provide information useful to the selection of tunneling sites. The potential of these systems results from the new kinds of information collected, the large amounts of data involved, and their compatibility with modern processing facilities. The amount of remote sensing data presently available at no cost is large and growing larger, and extensive libraries of such data already exist and continue to expand. Such data are the most economic means of providing an overview of regional geologic features, and because of widespread development of instrumentation and analysis methods in a number of disciplines, the applications of remote sensing data are rapidly being extended. Although the remote sensing data often do not definitively identify a particular geologic structure, they do serve an important reconnaissance function by designating distinctive features which might otherwise be overlooked. Once the features are located, they can serve as a guide to the field geologist and reduce the time required for geologic mapping. Remote sensing data can contribute information that may eliminate unexpected cost increases, safety hazards, and scheduling extensions. The additional cost of utilizing remote sensing techniques in the selection of tunnel sites is low when compared to the cost of overcoming unexpected geologic difficulties after tunneling has begun. Remote sensing has been shown to be particularly useful in detecting fault zones and surface drainage characteristics, both important geologic features in tunnel construction.

2.4. RELATED LITERATURE SOURCES

In the past two decades there has grown a large body of literature concerned with geologic and geographical interpretations from aerial photographs. Current efforts to obtain geologic information from new types of remote sensors must be regarded as an outgrowth and extension of techniques developed in photogeology, and some familiarity with the literature is required. Extensive bibliographies of photogeology references are contained in Tator et al. [2] and Miller and Schamm [3]. Included here is a listing of some less well-known information sources which relate to remote sensor systems other than or in addition to camera systems.

Undoubtedly the single most comprehensive compendium of reports concerning remote sensor systems (imaging and nonimaging) and their nonmilitary applications are found in the Proceedings of the International Symposia on Remote Sensing of the Environment. These symposia have been held at 18-mon intervals in Ann Arbor, Michigan, since February 1962. While the first four symposia were primarily concerned with the rapidly developing remote sensor technology, since April 1968, the date of the Fifth Symposium, an increasing number of papers have discussed applications of remote sensing to the earth sciences. The Proceedings of the Seventh International Symposium contain 74 papers and are composed of three volumes of 750 pages each. At least half of these papers present the results of research applicable to the earth sciences -- to geology, pedology, hydrology, and geography.

A second, less comprehensive, source of information on current capabilities of remote sensors can be found in the record of the Annual Earth Resources Program Review of the National Aeronautics and Space Administration (NASA). Since NASA, in cooperation with a number of other government agencies, sponsors much of the research in remote sensing, the program reviews provide a useful guide to trends in current applications. The latest review, the fourth is composed of five volumes, including one on geology and geography.

Since 1970, the quarterly Journal for Remote Sensing of Environment (American Elsevier Publishing) has provided a source for publication of current remote sensing research. Also, the monthly journal of the American Society of Photogrammetry, Photogrammetric Engineering, frequently contains articles on current remote sensing applications, although it includes a large range of subjects other than remote sensing.

A number of sources which treat specific aspects of remote sensor applications relevant to tunneling will be referenced where appropriate throughout this report. Many of these are limited-edition reports submitted to sponsoring agencies by Willow Run Laboratories.

2.5. WORK PERFORMED UNDER THIS CONTRACT

This investigation represents a first step in expanding the use of remote sensing in geologic reconnaissance for potential tunnel sites beyond the traditional and operational photogeology, which is now an established discipline [4]. Our investigation has shown that multispectral scanning and sidelooking airborne radar systems not only can provide more geologic and hydrologic information than would be otherwise available, but also can make the available photogeologic data more definitive. Listed below are five areas in which new geologic information can be obtained through remote sensing techniques. The last three of these areas have been under intensive investigation during this contract period.

(1) Extent of Fault Zones. The application of remote sensing techniques to the identification of faults is important, since weathered, brecciated, and water-saturated fault zones are one of the most difficult and expensive problems encountered in tunneling. Rowan et al. [5] have delineated such zones in the Arbuckle Mountains of Oklahoma by means of predawn far-infrared imagery, which reflected a drop in temperature caused by evaporation of water, with a greater amount of moisture in the fault zone than in the surrounding area. Infrared imagery collected in the late morning and afternoon did not display these fault zones, nor did aerial photography.

(2) Crystalline and Sedimentary Rock Outcroppings. When the thermal inertia of different types of rocks (such as granite, dolomite, and limestone) was investigated, it was found that each rock type has a different thermal inertia, and therefore each responds differently to diurnal

temperature variations. Rock outcroppings can, as a result, be mapped and identified by measuring thermal inertia at several different times during the diurnal cycle (Watson, Ref. 6).

(3) Hydrology, Geomorphology, and Surficial Soils. Thermal time variations, single-channel processing, two-channel ratioing, and multichannel statistical pattern recognition have been used to analyze multispectral data. In Section 3 of this report, Thomas Wagner discusses three types of automatic processing of multispectral data useful in the delineation of geologic features; these include single-channel, two-channel, and multichannel processing, the applications of which are each discussed. It was found that multispectral data provided more information about the hydrology, geomorphology, and soils in a glacial region with relatively shallow bedrock than could be determined from aerial photographs. Single-channel processing allowed the identification of standing water areas, which indicate subsurface hydrologic conditions relevant to the choice of tunneling site; such areas were not identifiable on an aerial photograph of the area. The multispectral data also delineated surficial deposits, residual soils, crop vegetation, and various classes of both urban and rural land use—all of which are important considerations in tunneling.

(4) Rock Composition. In Section 4, Robert Vincent describes compositional remote sensing in the field and presents data confirming his laboratory calculations. By using the two-channel ratioing method of processing multispectral data, he has been able to discriminate between silicate and nonsilicate geologic formations and to determine the amount of ferric oxide in a given geologic feature. This ratio method is applicable to the identification of surface outcrops, the tracing of past landslides, and the determination of the number, yield, and pH value of existing springs and water courses.

(5) Lineations, Surface Topography, and Textures. Ben Drake reviews the applications of sidelooking radar to geologic investigations in Section 5, and he considers the parameters that most significantly affect radar returns. As shown in the literature (Dellwig et al., Rowan and Cannon, Refs. 7 and 8), faults, joints, and contacts between different lithologic units commonly have relatively shallow depressions along them which are enhanced by the shadowing effect of SLAR, and regional fold and fracture patterns commonly are more easily identified on SLAR imagery than on aerial photographs. Radar imagery particularly well displays the relationship between the topography and the underlying geologic structure. By means of a new multiplexed radar system, Willow Run Laboratories will soon be able to collect imagery simultaneously in both X-band (3 cm) and L-band (30 cm). The simultaneous collection of data in the two wavelength regions will allow automatic processing of data and the ratioing of the two bands, a capability that should provide more total geologic information about a given region, particularly in regard to surface textures.

In the work performed under this contract, we have assumed that the remote sensors important for geologic reconnaissance were aerial photography, multispectral scanners, and sidelooking airborne radar systems. This assumption ignores, however, other airborne sensing techniques, such as passive microwave sensor systems, gamma-ray sensors, magnetometers, gravimeters, and electromagnetic sounding systems. In Section 6 of this report, Philip Jackson discusses the advantages to be gained by including these additional remote sensors in geologic investigations.

3
MULTISPECTRAL REMOTE SENSING

3.1. MULTISPECTRAL DATA

Up-to-date references are currently available concerning aerial camera systems, and to a lesser extent, radar systems. There is, however, a paucity of available information concerning modern multispectral scanning systems and their applications. This section presents a brief introduction to the concepts and technology of multispectral data collection and processing.* For more details the reader is referred to Shay (1970) [9] and several state of the art reports prepared by Willow Run Laboratories; in particular, see Hasell and Larsen, 1968 [10], Nalepka, 1970 [11], Malila et al., 1971 [12], Nalepka et al., 1971 [13], and Erickson and Thomson, 1971 [14].

3.2. THE MULTISPECTRAL CONCEPT

The concept of multispectral discrimination is relatively simple. The reflectance and emittance of radiant energy by an object are wavelength dependent and usually specific for the materials and conditions of that object [15]. In other words, different objects have different reflectance and emittance characteristics which vary uniquely over the electromagnetic spectrum. By collecting information in a number of spectral bands and by knowing or discovering the unique spectral characteristics of objects or conditions, it is possible to identify these and to distinguish one from another.

An image formed from a broad spectral range may be adequate to distinguish objects which have grossly different radiant characteristics in that range. For example, most

*The term "multispectral" is often confused with the term "multiband" in remote sensing literature. We regard "multispectral" data as data recorded in a number of wavelength ranges through a single aperture. Consequently, all of the data are in exact spatial registration. "Multiband" data are usually the product of multiple aperture camera systems, which do not assure the simultaneity and registration of data.

photographic films are sensitive to all of the visible spectrum, i.e., to the 0.4- to 0.7-μm wavelength range. However, by comparing two or more images of the same object made in different regions of the spectrum, the chances of being able to discriminate and identify that object are increased. As the number of spectral bands is increased, additional information is available about the object of interest. Also, the potential for discriminating between different objects is increased with the addition of spectral information. If the spectral characteristics of objects are not specifically known (generally the case), it is an advantage to have a number of spectral images, because one or more will probably show tone differences between two or more objects better than others. Thus, the inherent ability to distinguish between similar objects is enhanced with an increase in the range and amount of spectral information. The basic strategy in multispectral sensing calls for the accurate detection of spectral characteristics produced by objects of interest in a scene (with use of as many spectral bands as possible) and the correlation of these spectral characteristics with the properties or conditions of the objects.

3.3. A MULTISPECTRAL SCANNING SYSTEM

To take advantage of the spectral information of a scene, the reflected and emitted radiation must be sampled in a number of discrete bands in order to get accurate representation of the energy distribution. For this purpose, an airborne optical-mechanical scanner system, using reflective optics, has certain advantages over multiple aperture systems. First, the spectral information is recorded in electrical form on computer-compatible magnetic tape, and, therefore, certain limitations in data handling and processing inherent in photographic processes are avoided. Second, the detectors in scanner systems are not limited to the rather narrow spectral range over which conventional films are sensitive. Modern scanning systems collect data over a 0.32- to 14.0-μm spectral range (Fig. 1). However, because of atmospheric absorption, surface radiation cannot be recorded in the 2.6- to 3.5-μm and the 5.5- to 8.0-μm wavelength ranges.

Basically, an optical-mechanical scanner consists of a telescope, a rotating mirror, and some sort of radiation-detector configuration. The telescope focuses the radiation from a small portion of the scene onto a detector. Figure 2 shows a schematic diagram of such a scanning system. The rotating mirror causes the scanner's field of view to sweep rapidly across the flight path. The direction of the sweep, or scan, is perpendicular to the direction of flight of the aircraft. The forward velocity of the plane and the rotation of the mirror are such that a complete record of the scene is sequentially recorded in a series of contiguous scans. The resulting scan pattern is similar to a television raster, except that it is continuous for the entire flightline. The rotation rate of our scanning mirror is 60 revolutions/sec. At an altitude of 3000 ft, for example, each scanline represents a ground swath 10 ft wide and almost 1 mile long (90^{o} field of view). In this manner, the spectral data of a scene, composed

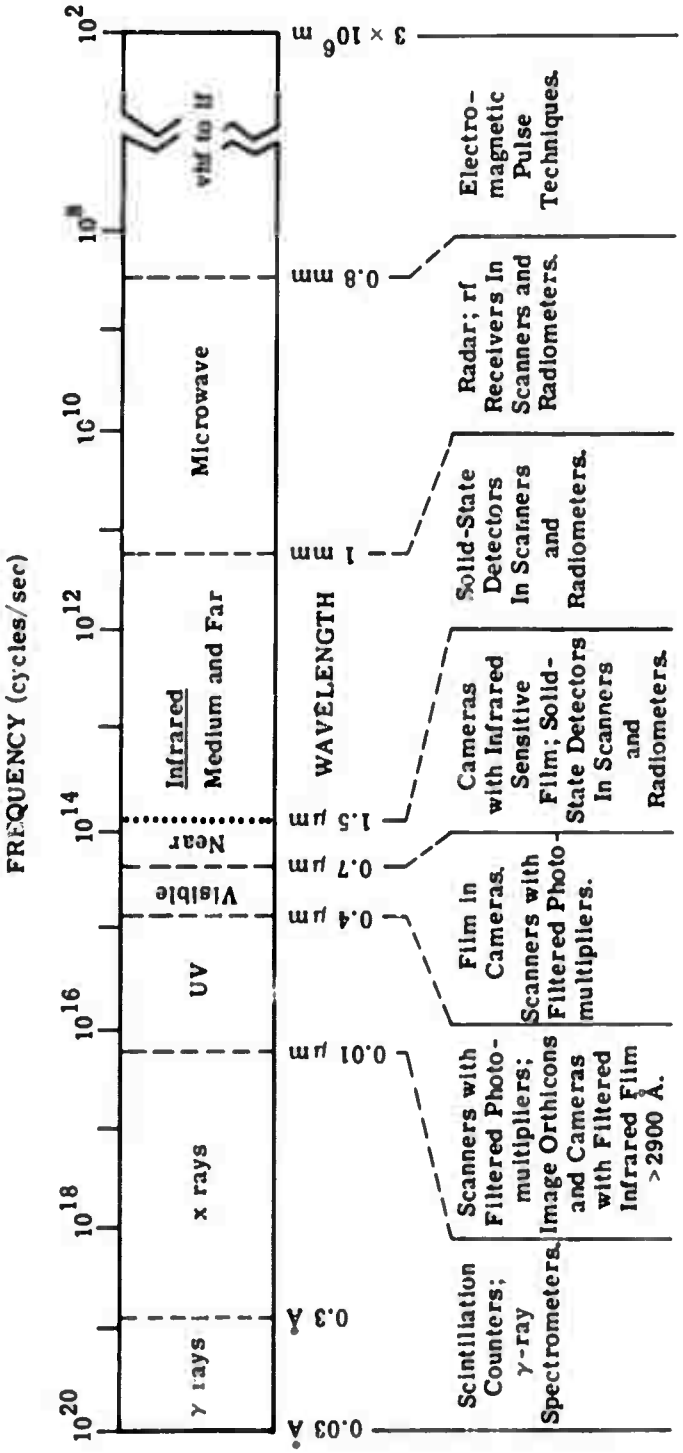

FIGURE 1. THE ELECTROMAGNETIC SPECTRUM AND APPLICABLE SENSING SYSTEMS. Adapted from Research News, Vol. XVIII, No. 8, Office of Research Administration, The University of Michigan, Ann Arbor, February 1968.

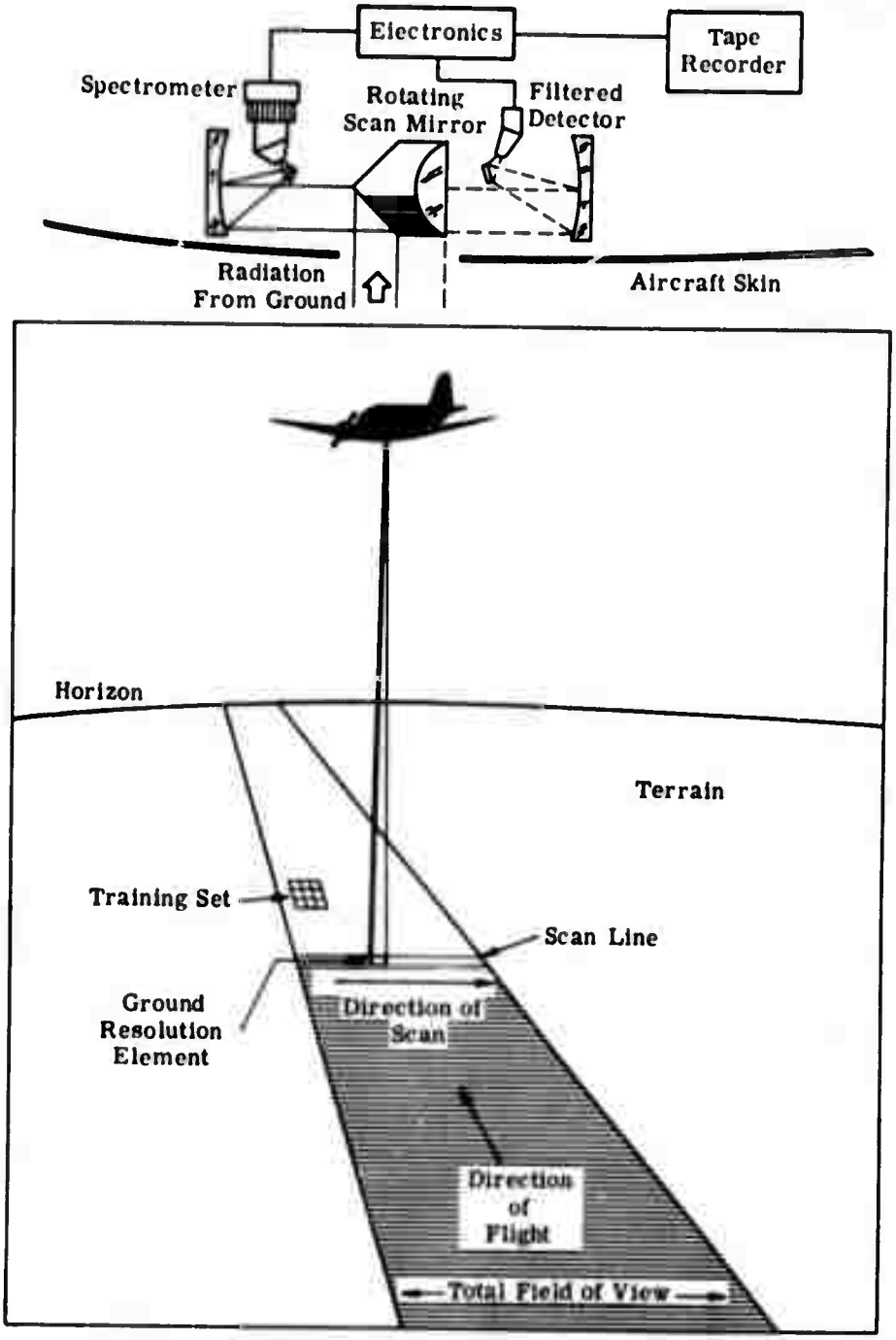

FIGURE 2. MULTISPECTRAL DATA COLLECTION

of many parallel scanlines, are obtained in the length of time it takes for the aircraft to fly over the area.

Modern multispectral systems employ radiation-dispersing prisms behind the single aperture. After the prism disperses the radiation into separate wavelength regions, it is transmitted by an array of relay optics to a number of radiation detectors. Photodetectors are used in the reflective wavelengths and special cooled metal detectors in the infrared wavelengths. These detectors convert the incoming radiant energy to electrical signals, which are then amplified and recorded as voltage levels on multitrack magnetic tape. Radiation calibration is automatically recorded coincident with the scene radiation. Calibration information includes synchronization pulses, upward-looking sun-sensor data, two reference lamps, and two thermal reference plates. The fact that up to twelve spectral bands are recorded simultaneously for a single scene is important. The spectral information of each of the bands is in exact registration with the others, a fact which makes possible the subsequent computer processing of the data.

Willow Run Laboratories' current multispectral scanner system (M-7) went into operation in June 1971 (replacing the M-5 system, which had been operational since April 1966). The spectral bands which can be recorded with this system are listed in Table 1. Because of the magnetic tape's channel limitations, it is not possible to record more than 12 of these spectral bands simultaneously.

3.4. AUTOMATIC PROCESSING

The large amount of information collected by the multispectral scanner system requires that automatic processing techniques be used. There are 540 resolution elements per scanline, and 60 scanlines are recorded each second, which amounts to some 32,400 recorded, quantitative radiation samples per second. A typical 15-mile flightline will be covered in 6.6 min, resulting in over 300 million samples, each sample having 12 voltage levels representing the effective radiance in 12 recorded spectral bands. The conventional tools of image interpretation are not capable of handling this amount of data in a consistent and quantitative manner. Human examination and interpretation of sensor imagery, using accumulated familiarity with specific areas and training with special keys, require much more time than that needed to obtain the original data and can not approach the information potential inherent in modern sensor data. These traditional techniques are neither adequate for analyzing large amounts of data in a short time nor capable of providing results that are not biased by the relative skills and patience of the image interpreter. What is required is a process to reduce the information input rate required of the individual interpreter, i.e., to insert a filter between the sensor system and the person who analyzes the data. The filter should be capable of rejecting much of the undesired information ("noise") so that it is not presented to the interpreter. This data-filtering process must be able to discriminate automatically between objects and materials of potential interest

TABLE 1. SPECTRAL BANDS OF WILLOW RUN LABORATORIES' MULTISPECTRAL SCANNER SYSTEM*

50% Response Points (μm)	Spectral Range
0.32-0.38	Ultraviolet
0.41-0.48	Violet
0.46-0.49	Blue
0.48-0.52	Blue-Green
0.52-0.54	Green
0.53-0.57	Yellow-Green
0.55-0.60	Yellow
0.58-0.64	Orange
0.62-0.69	Red
0.67-0.91	Reflected Infrared
1.0-1.4	Reflected Infrared
1.5-1.8	Reflected Infrared
2.0-2.6	Reflected Infrared
4.5-5.5	Thermal Infrared
8.2-10.9	Thermal Infrared
8.2-13.5	Thermal Infrared
9.4-12.1	Thermal Infrared

*Additional bands may be recorded through the introduction of different filter systems in the 0.32- to 13.5-μm range.

and those potentially not of interest and present the results of this discrimination in an easily interpretable form.

Digital and analog computer systems provide such a capability for processing multispectral data. The analog computer (or processor) can process the data at a near real-time rate, that is, at almost the same rate that the scanner collected the original data. The same filtering operation can be implemented on digital computers, but at a sacrifice of speed and often of the amount of data which can be economically handled. Digital computers have, however, the advantage of providing precise quantitative analysis of the data.

Three types of processing (filtering) of multispectral data can be implemented by computer: (1) single-channel quantization and level slicing; (2) two-channel ratioing; and (3) multiple-channel statistical pattern recognition. These three processing techniques are described below in order of increasing sophistication; examples and applications of these three techniques are discussed in subsequent sections.

3.4.1. SINGLE-CHANNEL PROCESSING

Since a single spectral region contains scene-radiance information distinct from all other regions, it is often useful to select one band for automatic processing. A knowledge of the potential information in individual spectral bands allows their use in extracting certain kinds of information automatically. The objective, then, is to isolate, consistently and objectively, radiance differences which are indicative of conditions or objects of interest. Optimally, the data will be presented in a format readily interpretable to the earth scientist.

This objective is accomplished by playing the recorded signals from a single channel through a data processor. In this case, the processor automatically quantizes the signal levels into a preselected number of discrete ranges. Signal voltages are subsequently recorded as belonging to one of a number of voltage ranges. The total voltage range may include that range recorded on tape for the entire scene or some subset of that range. When the result of this quantization process is printed, a scene image may be portrayed by a number of distinct tones (density levels) on a film transparency, or each discrete range may be separately printed as a black tone on an otherwise clear film transparency. The latter type of image display is known as a level slice or separation. Subsequently a number of quantized separations may be color-coded and overlaid, one with another, to provide a color-coded composite image.

The result of this type of processing is similar to standard techniques of film densitometry, except that the data are taken directly from magnetic tape and the results are portrayed in image form. Some of the difficulties associated with working with nonlinear film and film processing variations are thus avoided. Also, since sensor calibration sources are also quantized, an accurate measure of radiation levels is available. One can use this technique effectively

for quantitative temperature mapping, using a thermal infrared spectral channel, and for surface-water mapping by means of reflective infrared data. (Examples of thermal mapping and surface hydrology are included in Section 3.6.1.1.)

3.4.2. TWO-CHANNEL PROCESSING

With two channels of multispectral data, it is frequently useful to divide the signals in one channel by those of another channel to produce a new ratio image. The shorter wavelength band is divided into the longer wavelength band, and the new image displays differences between the two original images. A ratioed image essentially eliminates the similarities between two bands of spectral data. Also, the resulting ratio (voltage level) is a measure of the average slope of a spectral curve which spans the two wavelength ranges. This technique is found to be useful for obtaining certain types of information from both reflective and thermal multispectral data. The theory and applications of this technique were included in the report by Drake et al., 1971 [16], and further examples are contained in Section 4 of this report.

A ratio of two bands of multispectral data is produced by means of an electronic processor, so that for every scene resolution element the signal level recorded in one channel is divided by the signal level recorded in another. Normalization of the two bands, to adjust for optimal electronic signals on the ratioed image, is accomplished by means of reference standards recorded coincident with the original data. The product is a film transparency in which film density is proportional to the ratio (quotient) of the signals recorded on the original two channels. Usually a neutral grey tone is selected to represent a ratio value of unity. Departures from unity are represented as lighter tones for higher values (greater than one) and darker tones for values less than one. If the ratioed data are electronically recorded directly onto magnetic tape, they can be further processed as a single channel.

Ratioed images from data collected in the reflective wavelengths ($<3.0\ \mu m$) result in information concerning differences in the spectral reflectance of objects. Ratioed images in the thermal wavelengths ($>3.0\ \mu m$) display useful data concerning the emittance characteristics of objects or materials, i.e., the degree to which their thermal radiation characteristics depart from those of a perfect emitter (a so-called blackbody).

3.4.3. MULTICHANNEL PROCESSING

Multichannel processing is the most sophisticated, and potentially the most effective type of multispectral processing. Essentially the technique utilizes computer-implemented pattern-recognition schemes to analyze and discriminate objects or materials within a scene. If one has a sample of object classes of interest within the scene, he needs no other a priori spectral information to use this technique. Both analog and digital computers can be used, and often

extensive statistical analyses of the spectral characteristics of a scene are made before the results are printed out in image form.

There are two phases to the implementation of pattern-recognition schemes. One is the training phase, in which the data are calibrated and corrected for illumination and other types of signal variations. Samples of objects of interest are located on a visual display of the scene, and these areas are then "gated" in such a way that only signals from the sample areas are recorded in the computer's memory. These signals are the statistical means and standard deviations for the sample objects. The combined mean and variance for all channels is known as the spectral signature for a given sample. If that signature represents the recorded spectral characteristics of a sample, it is assumed that the signature indicates the spectral characteristics for all similar members of that class of objects. Thus, once signatures are programmed into the computer, the operational phase consists of having the computer analyze the spectral characteristics of each resolution element from a set of unknown data and determine which of the elements is sufficiently similar to any of the signatures to be recognized as a member of a known class.

For the computer, similarity is defined by a mathematical decision rule. The rule most commonly used is the likelihood ratio. In likelihood-ratio processing, each resolution element of the data is classified as "target" or "not target" by noting if the likelihood ratio, L, is greater than or less than some threshold value, T. In simple form, the likelihood ratio is:

$$L = \frac{P_A(T)P(T/S)}{\Sigma_n P_A(B_n)P(B_n/S)} \begin{matrix} > T = \text{target} \\ \leq T = \text{no target} \end{matrix}$$

where $P_A(T)$ = a priori target probability

$P(T/S)$ = probability of target, given a data sample

$P_A(B_n)$ = a priori probability of background n

$P(B_n/S)$ = probability of background n, given a data sample

The result of this yes/no type of decision rule is a computer recognition map. This map is an image display wherein all areas recognized as being similar to a given signature are displayed as a particular symbol or color. Areas of the test site that are not similar to any of the signatures are left blank, and thus, the recognition map displays only materials of interest. An example of this type of processing is given in Section 3.6.3.

3.5. DATA-COLLECTION PARAMETERS

Important considerations for planning the collection of multispectral data involve the spectral bands to be recorded, the time of day or night, and the altitude and direction of the flight or flights. The attention given to these considerations often determines the relative

success of the remote sensing mission and the subsequent value of the data. A fourth important consideration, often neglected, is the extent and nature of supporting ground-truth investigations.

Multispectral data collected at night are restricted to the thermal wavelengths (> 3 μm). Because of the diurnal cycle of surface temperatures, it is usually advisable not to collect thermal data until several hours after sunset. Prior to this time, the differential rates of cooling of terrain surfaces obscure subtle temperature effects which are diagnostic of certain terrain conditions (such as microrelief, vegetation distribution, or soil moisture). From an operational point of view, dawn provides a convenient time for thermal data collection, in that there is usually sufficient light for aircraft pilots to navigate without ground-marker lights. Ground fog, however, can seriously degrade predawn and dawn imagery, and flights under foggy conditions should be avoided.

Multispectral missions for the collection of data in the visible and near-IR wavelengths are most successful during mid-day hours. For most purposes, low sun angles reduce the quality of the imagery by introducing pronounced terrain and vegetation shadows and by causing radiance variations resulting from bidirectional reflectance differences for objects seen from different scan angles. For the latter reason, flightlines should be oriented as much as possible to insure that the aircraft flies parallel to the sun's rays, i.e., into or 180° from the direction of the solar azimuth. Bidirectional reflectance is not a serious problem when two-channel ratio processing of the data is anticipated, but it can present problems for multichannel discrimination techniques. Daytime thermal data are often best collected during the mid-afternoon hours, at which time the terrain has reached a relative state of thermal equilibrium.

Flight altitude is determined by the trade-off between the degree of image resolution and the total area of coverage desired. Both the resolution-element dimensions and the total area scanned increase linearly with altitude. In Willow Run Laboratories' scanner, the instantaneous field of view (IFOV) is 2 mrad; i.e., a ground patch 2 ft sq will be recorded at 1000-ft elevation. The scanner also has an effective 90° scan, which means that at 1000-ft altitude a swath some 2000 ft wide will be recorded, and at 3000 ft the swath width will be more than 1 mile. However, local variations in terrain influence somewhat the amount of area imaged.

3.6. APPLICATIONS OF AUTOMATIC PROCESSING OF MULTISPECTRAL DATA

This section presents results of the application of the three types of automatic multispectral data processing discussed in Section 3.4. Examples of both processed and unprocessed imagery were selected from existing data files to provide information thought to be applicable to tunnel-site selection. These results represent but a portion of the remote sensing techniques currently being developed for earth resources.

3.6.1. SINGLE-CHANNEL APPLICATIONS

Quantizing of a single channel of multispectral data clearly delineates often subtle contrasts inherent for the scene in the selected wavelength band. Single-channel processing has been useful in the discrimination of surface water and in thermal mapping.

3.6.1.1. Surface Hydrology

For delineation of surface water, a single channel in the near-infrared spectral region was used. Standing water areas were discriminated from all other (background) materials by their low signal levels in the 1.5- to 1.8-μm wavelength range. This data channel was played through a digital processor, and all signals (voltage levels) falling below a selected threshold limit were imaged on a cathode ray tube (CRT) and subsequently recorded by a filmstrip printer. All recorded signals were tallied by a digital counter linked with the system.

Computer-implemented discrimination of standing water consists of setting a threshold level for separating the low signal levels of standing water from those of other scene elements. All signals below the threshold are categorized as standing water. The initial threshold value is empirically determined by adjusting the threshold level to the point that known areas of standing water are adequately imaged on a CRT display, and background elements are not recorded.

Figure 3 compares three images from a flightline which traverses areas of extensive wetlands—lakes, bogs, swamps, and artificial impoundments. As the figure shows, the processed image of standing water provides the location and areal extent of all surface water, while the 0.52- to 0.57-μm image (the spectral range to which the human eye is most sensitive) provides little contrast for discriminating these surface-water areas.

The imagery in Fig. 3 is from a portion of a flightline which crosses such Pleistocene features as outwash gravel, till moraines, kames, and drumlins. A porous dolomite formation underlies this area, often at depths of less than 50 ft. Surface drainage is impeded by the rolling, hummocky glacial topography, and there are no surface streams evident on the imagery. As indicated by the abundance of surface bodies of water and lack of integrated drainage, the probable occurrence of subsurface high-yielding aquifers, either within the surficial sediments or the underlying bedrock, would present serious problems for rapid tunnel construction.

Distribution of surface water as an indication of subsurface hydrologic conditions is further illustrated in Fig. 4. A mosaic of surface-water discrimination images shows a 160-sq-mile area in southern Ontario. (For comparison, a high-altitude photomosaic of approximately the same area is shown in Fig. 5.) The watershed outlined in the center of the image is the 90-sq-mile drainage basin of East and Middle Oakville Creek, which flows into Lake Ontario at the bottom of the image. Surface-water patterns show a marked difference for the

(a) Video Image: 0.52 to 0.57 μm

(b) Video Image: 1.5 to 1.8 μm

(c) Level-Sliced Image: 1.5 to 1.8 μm

FIGURE 3. COMPARISON OF TWO VIDEO IMAGES AND A LEVEL-SLICED IMAGE FOR THE DISCRIMINATION OF STANDING WATER. Imagery collected over No. 6 Highway, between Hamilton and Guelph, Ontario.

FIGURE 4. 1.5- to 1.8-μm IMAGE MOSAIC OF OAKVILLE REPRESENTATIVE BASIN, ONTARIO, FOR DISCRIMINATION OF SURFACE WATER.
Approximate area: 160 sq miles.

FIGURE 5. HIGH-ALTITUDE PHOTOMOSAIC OF OAKVILLE REPRESENTATIVE BASIN, ONTARIO.
Approximate area: 160 sq miles.

upper and lower portions of this mosaic. In the upper portion, numerous lakes, swamps, and bogs indicate the location of glacial sediments underlain at shallow depths by the Anabel dolomite, mentioned above. Most of the central and lower portion of the image show scattered small ponds and the meandering pattern of Oakville Creek. This area is composed of well-drained clay loam tills, underlain by soft shales and sandstones of the Ordovician Queenston formation. The winding course of the creek indicates that drainage is slow over this area, which slopes gently to the Lake Ontario shore. Most of the small ponds are associated with farms. Digital analysis of these two types of terrain indicates that approximately 2.1% of the surface underlain by the massive Anabel dolomite is standing water, whereas the sloping shale plain of the Queenston formation has 0.55% surface water. Except for an occasional sand lens, one would not expect to encounter tunneling problems associated with either rapid surface recharge to the watertable or high-yielding aquifers. Indeed, water supply is known to be somewhat of a problem in this area as a result of the general lack of aquifers and the high rates of surface evaporation associated with land cultivation (Chapman and Putnam, 1966, Ref. 17).

3.6.1.2. Thermal Mapping

For a number of years, useful hydrological and geologic information has been obtained from single-channel thermal images (Fisher et al., 1964; McLerran and Morgan, 1965; Friedman and Williams, 1966; and Quade et al., 1970—Refs. 18-21). To some extent, recent applications of thermal sensing have been hindered by limitations of conventional qualitative approaches to the interpretation of such imagery. Simplistic concepts, such as hot-spot detection, have limited utility in defining natural processes.

Two sets of thermal images (8.0 to 13.5 μm) of a morainal area, the Blue Springs Basin, in southern Ontario illustrate the kind of general land-use information that can be obtained from single-channel processing of thermal imagery.

Data for Fig. 6 were collected at about noon from an experimental watershed near Acton, Ontario. One image shows the thermal data as continuous tone variations, with the warm areas light in tone and the cooler areas relatively darker. The second image, derived from the same data, is a calibrated thermal composite in which four thermal regions are designated by color code. The grey-scale image reveals considerable detail concerning the thermal complexity of the scene but no quantitative information. In many respects, this image appears similar to a conventional panchromatic photograph of the area. Both field patterns and the cool water areas are evident. The color-coded image provides a somewhat simplified view of this area, with the total surface-temperature range for the scene somewhat in excess of 30°F. Some of the fields, coded as green and brown, are characterized by higher temperatures than the rest of the area and are known to be bare soil; the two other thermal ranges correspond to

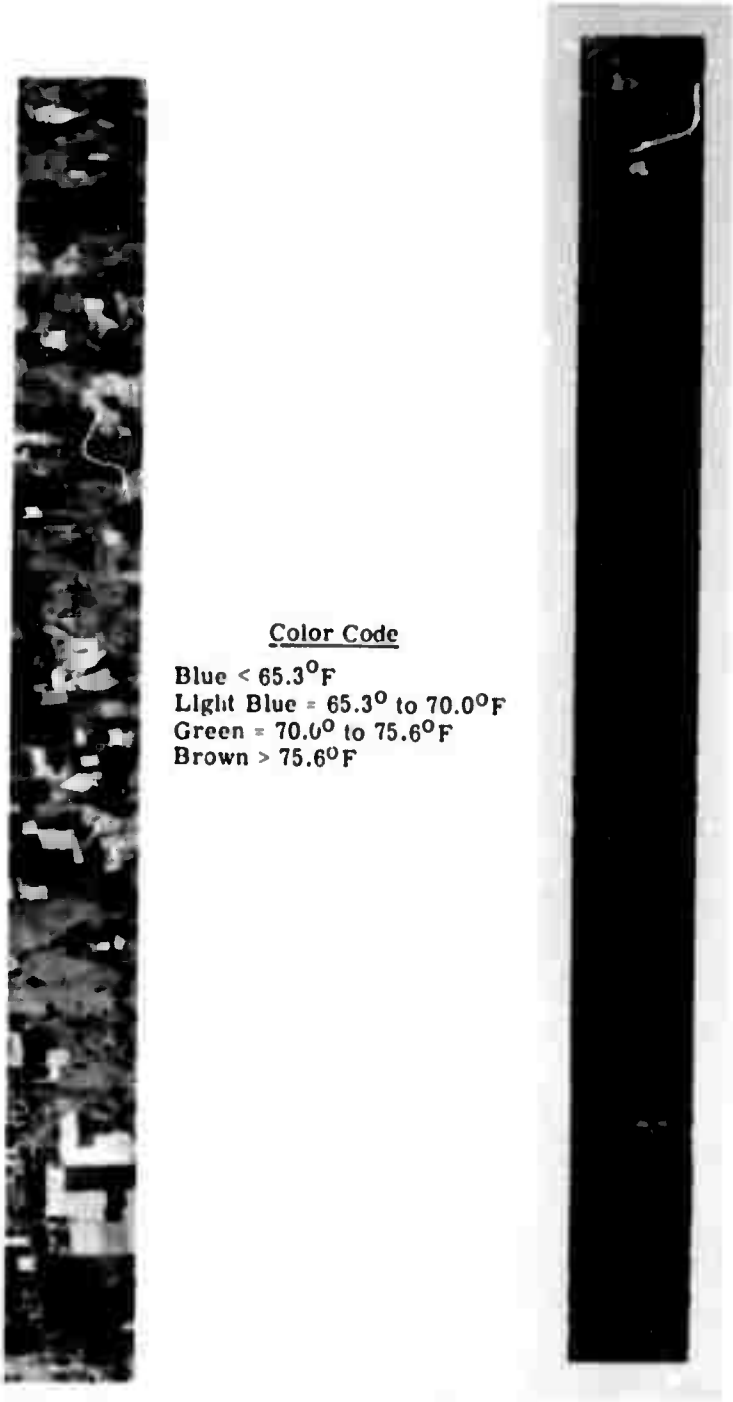

(a) Video Image

(b) Calibrated Thermal Composite Image

FIGURE 6. COMPARISON OF STANDARD THERMAL VIDEO IMAGE WITH CALIBRATED LEVEL-SLICED THERMAL IMAGE; DATA COLLECTED AT 1200 HOURS. Blue Springs Basin, 11 May 1971.

densities of vegetation—the cooler the temperature, the denser the vegetation (perhaps a result of the effects of transpiration).

The data for Fig. 7 were collected at dawn (0400 hours) on the same day as those for Fig. 6. The differential heating and cooling of the surface has produced considerably different thermal contrasts between the mid-day and dawn imagery. The continuous tone image shows many subtle differences between fields; the lighter toned water areas provide the only marked contrasts. On the calibrated composite, the water areas have changed very little in terms of actual temperature, but the terrain surface is considerably cooler. The factors which affect nocturnal surface temperatures are known to be vegetation, moisture, and the movement of cool air from topographically higher areas into lower areas or depressions. The warm areas in the dawn image are either standing water (white) or the upper slopes of drumlins or eskers. The morainal areas are distinguished from the outwash plains and glacial spillways by the complexity of their thermal patterns. The hummocky upland topography of the moraines provides a distinctive thermal contrast to the relatively cool, level plain areas. In other words, nocturnal thermal imagery can be expected to provide information that is influenced by relief, by Pleistocene topography in this case.

Thermal imagery has also recently been used to locate sinkholes in Karst topography. In a study by A. E. Coker et al. [22], temperatures related to water stressed and unstressed vegetation were used to indicate areas of rapid soil-moisture depletion (sink holes).

At one time it was hoped that surficial thermal imagery would provide indications of deep subsurface conditions, but recent results [23] indicate that such information is present only when there are large thermal gradients within the overburden, such as would result from underground mine fires.

3.6.2. TWO-CHANNEL APPLICATIONS

Section 4 of this report is devoted to a study of the lithologic properties of rock outcrops which provide the physical basis for their discrimination by means of a two-channel ratioing technique. This section presents examples of applications of the ratioing technique in regions devoid of rock outcrops. Specifically, the two-channel ratio is applied to three types of surface materials—surficial deposits, residual soils, and natural and crop vegetation.

3.6.2.1. Surficial Deposits

Figures 8 and 9 show the results of ratioing two channels of thermal data—8.2 to 10.9 μm and 9.4 to 12.1 μm—for an area of southern Ontario. Clearly, agricultural development has had a significant effect upon the appearance of this area of glacial tills and outwash sediments.

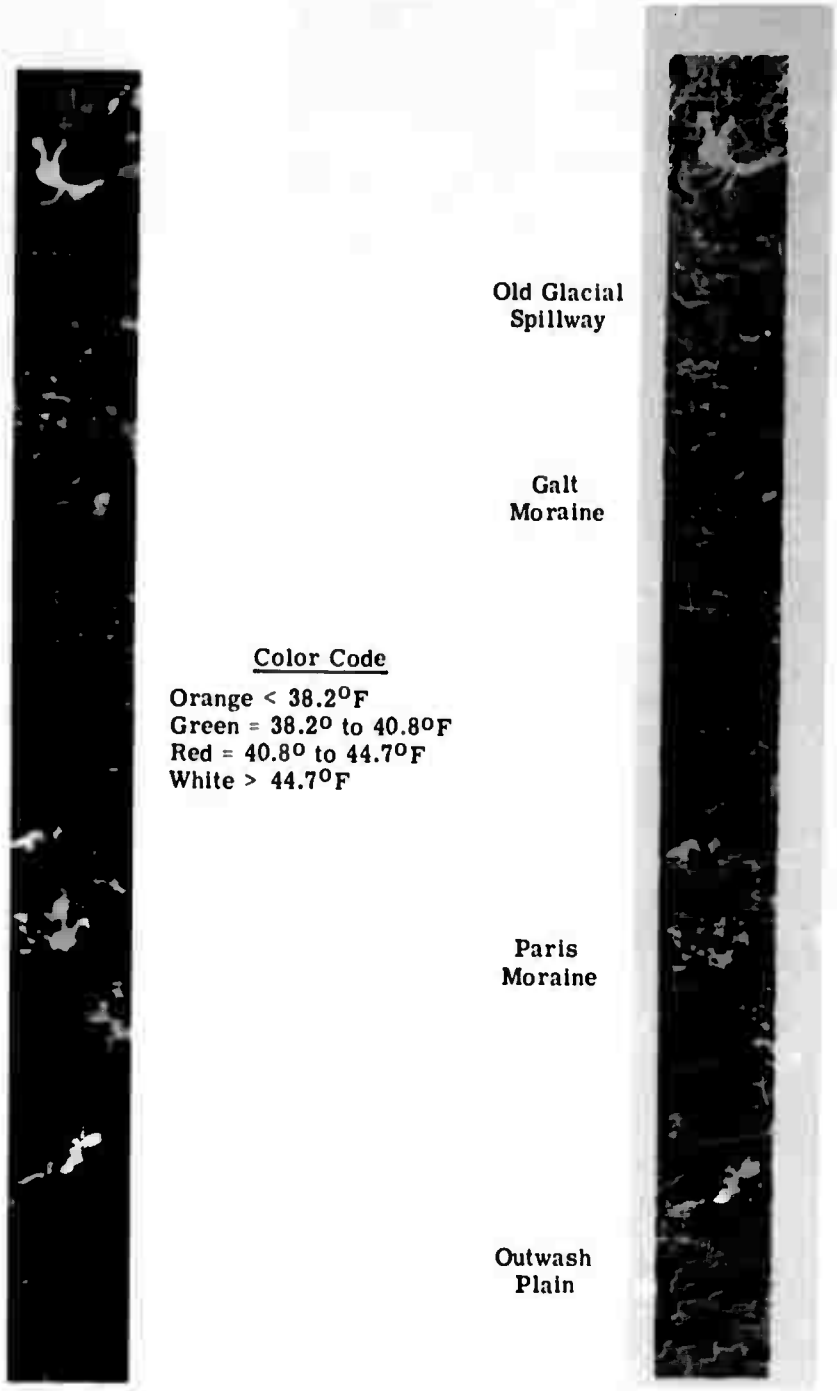

(a) Video Image

(b) Calibrated Thermal Composite Image

FIGURE 7. COMPARISON OF STANDARD THERMAL VIDEO IMAGE WITH CALIBRATED LEVEL-SLICED THERMAL IMAGE; DATA COLLECTED AT 0400 HOURS. Blue Springs Basin, 11 May 1971.

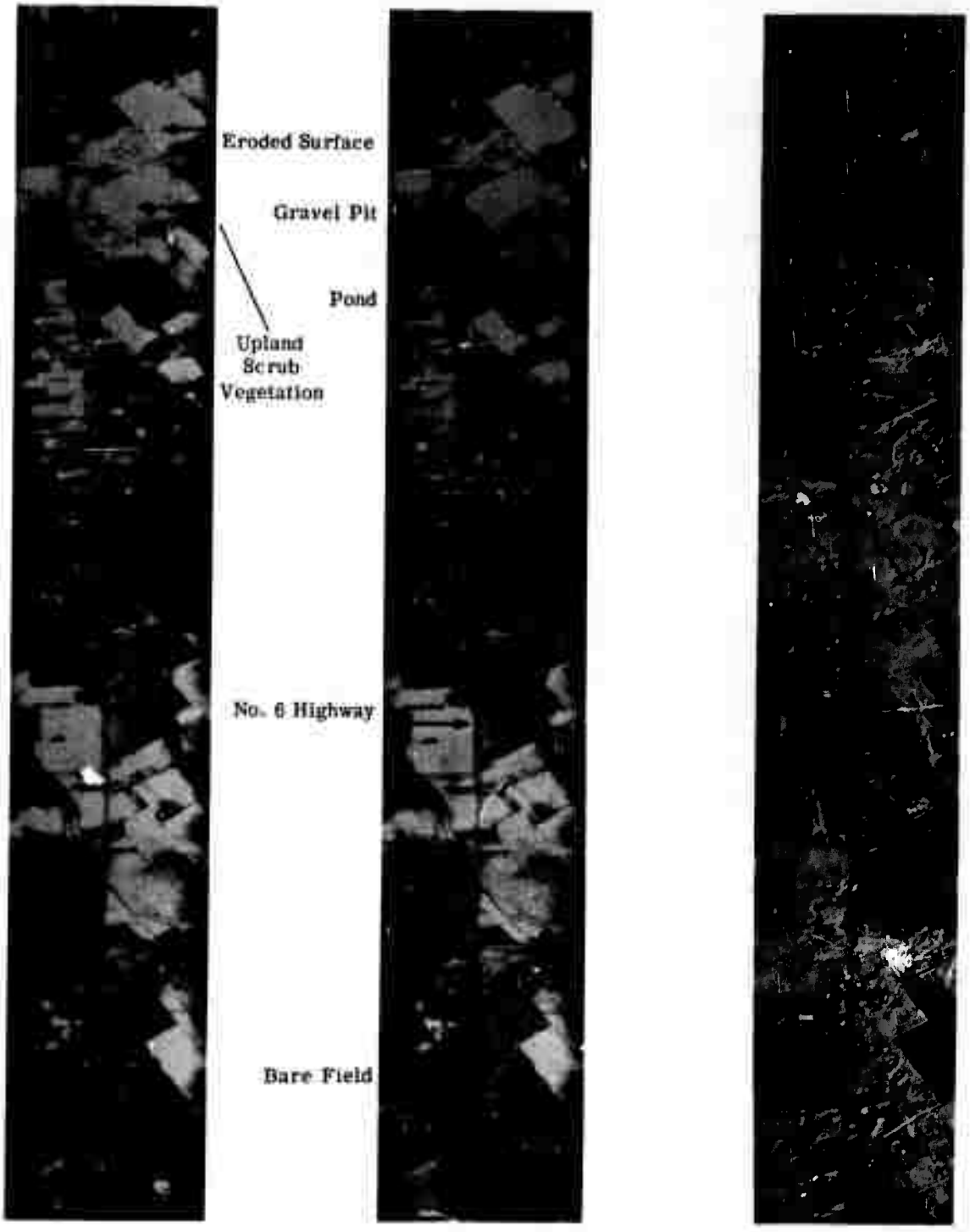

(a) Video Image: 8.2 to 10.9 μm (b) Video Image: 9.4 to 12.1 μm (c) Thermal Ratio Image

FIGURE 8. THERMAL INFRARED IMAGES OF PORTION A OF NO. 6 HIGHWAY BETWEEN HAMILTON AND GUELPH, ONTARIO. Length: 5 miles.

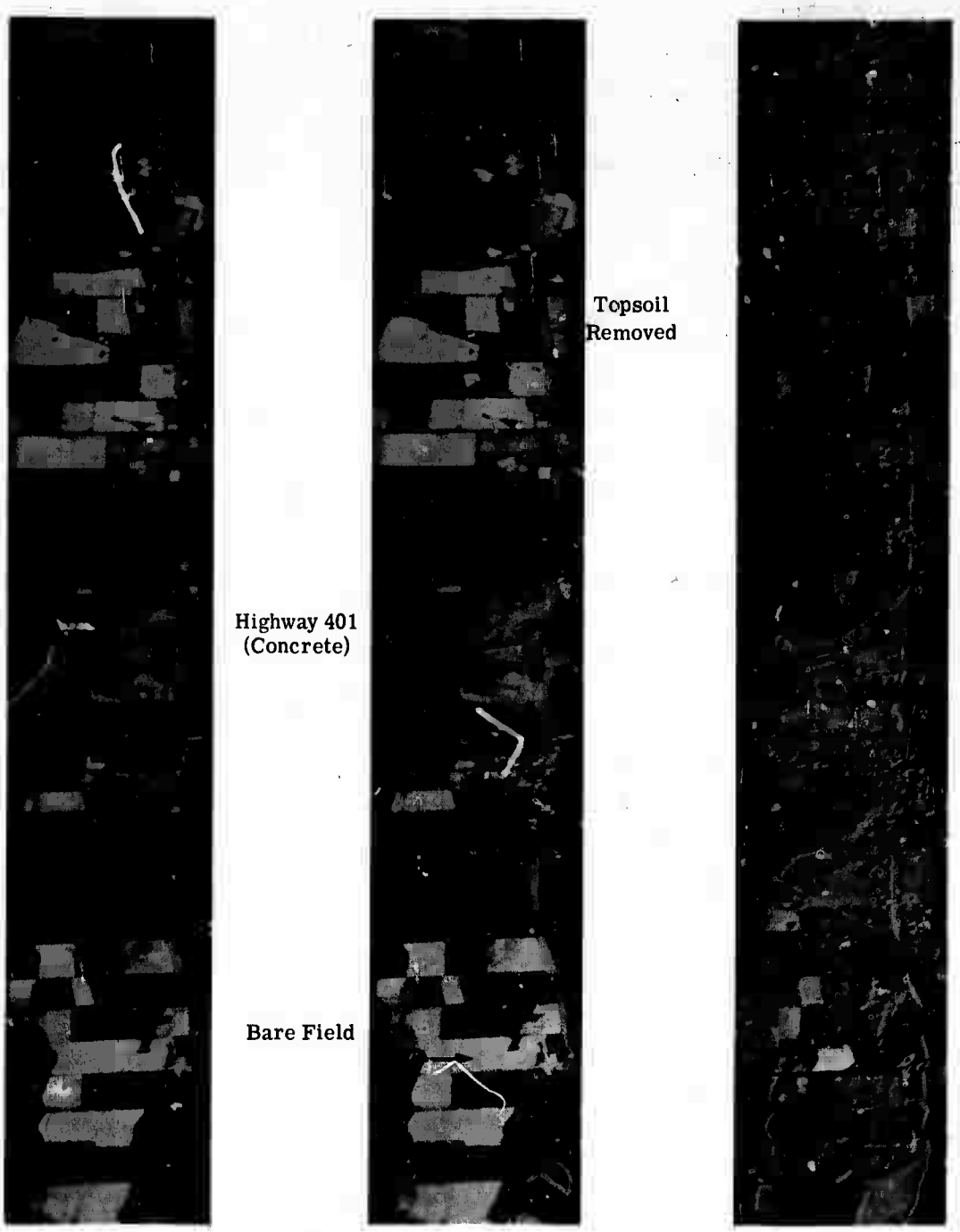

(a) Video Image: 8.2 to 10.9 μm (b) Video Image: 9.4 to 12.1 μm (c) Thermal Ratio Image

FIGURE 9. THERMAL INFRARED IMAGES OF PORTION B OF NO. 6 HIGHWAY BETWEEN HAMILTON AND GUELPH, ONTARIO

On the ratioed thermal images, all of the bare soil areas appear dark, indicating the presence of SiO_2. Areas covered with vegetation and those consisting of water, roads, and man-made structures are medium in tone, indicating no great thermal emittance difference between the two thermal bands, i.e., little or no SiO_2. Therefore, ratioed thermal imagery has the capability of accurately discriminating cultivated fields (those bare of vegetation). In Fig. 8, the ratioed image shows several bare fields which would not have been categorized as such from interpretation of the thermal video images alone. Also, in the upper portion of the image, a sand and gravel pit is also dark. Adjacent to the pit, however, is a bare field which has an anomalous irregular light tone within it. The farmer who cultivates this field indicated that this light area corresponds to an eroded surface on a hill slope. Evidently loss of topsoil exposed the underlying parent materials to view. The ratio of the till parent material is greater (lighter) than the soil cover. These lighter areas may result from a greater percentage of silica in the upper soil level than in the original parent material--a natural result of the soil forming process of podzolization.

The bare field patterns in Fig. 9c also show light areas. In particular, the middle field in a row of three bare fields adjacent to one another appears very light in contrast to the others on the ratioed image. In discussing with the farmer the differences in these fields at the time of the flight, we found no explanation other than that the middle field had been green manured the previous fall. Perhaps, in this field, accumulation of organic matter was sufficient to eliminate the effect of the SiO_2 on the thermal ratio. One additional field shows the effect of the removal of topsoil. Topsoil from the northern half of this field had been removed by a scraper shortly prior to the time of the flight. The remaining portion of the field was bare of vegetation, but still retained its soil cover.

It was originally hoped that a two-channel thermal ratio technique would provide information on the relative distribution of Pleistocene deposits on the basis of differences in their silica content. In retrospect, it appears that cultivation practices induce variations which partially obscure many of the textural differences of the natural terrain.

The ability to discriminate areas containing silicates by means of a thermal ratio does not vary as a result of the time of day that the data were collected. Figure 10 compares two thermal ratio images for the same area. One was produced from data collected at dawn (0400 hours), and the other from data collected at mid-day (1200 hours). The patterns indicating the location of bare soil are the same for the two images. This lack of variance in the thermal ratio image with time of day is in sharp contrast to the results obtained in the single-channel thermal images. (See Section 3.6.1.2.)

(a) Video Image: 8.2-10.9 μm, 0400 hours

(b) Video Image: 9.4-12.1 μm, 0400 hours

(c) Ratioed Image: 0400 hours

(d) Video Image: 8.2-10.9 μm, 1200 hours

(e) Video Image: 9.2-12.1 μm, 1200 hours

(f) Ratioed Image: 1200 hours

FIGURE 10. COMPARISON OF THERMAL IMAGES PRODUCED FROM DATA COLLECTED AT 0400 HOURS AND AT 1200 HOURS

3.6.2.2. Surficial Patterns

Surface soil and vegetation patterns are often indicative of subsurface geologic conditions. In particular, soils derived from residual parent rocks often reflect differences related to their underlying lithology. Rates of erosion, chemical decomposition, and patterns of weakness vary for different types of rocks, giving rise to characteristic variations in topography and the appearances of soils. Variations in color are often indicative of microrelief, drainage, and mineral composition. The purpose of this task was to use ratios of reflective spectral bands to enhance surficial patterns on multispectral imagery.

Figure 11 shows three video images for an area of southeastern Pennsylvania.* The area is intensively cultivated, except for the steep, sloping ridge areas which are left in natural upland hardwood forest. The pattern in Fig. 11 is one of contrasting light field areas and areas of dark natural vegetation or crops (data collected in mid-May). Barely discernible are tonal patterns within the light fields and the dark vegetated areas. A red-green ratio was used for enhancing pattern differences within the bare soil areas, and an infrared-green ratio was used for vegetative patterns.

Figure 12a shows the results of ratioing the 0.66- to 0.72-μm band and the 0.50- to 0.52-μm band. The ratioed image shows almost all of the vegetated areas as dark, but within bare fields are contrasts of light and dark related to slight differences in the redness of the soils. The dark mottled areas correspond to either eroded knobs or to depressions within these fields. Figure 12b shows a ratioed image of the 0.74- to 0.85-μm and the 0.50- to 0.52-μm bands. In this image, all bare fields are uniformly dark, but vegetation patterns are enhanced. In many of the fields, crop patterns show the effects of row direction, but in other cases, soil and relief variations which affect the crops appear as light or dark patterns. Combining the information contained in the first two ratioes, Figure 12c shows soil and vegetative patterns for the entire area. In this ratio, red-plus-infrared divided by green, all contrast between crops and bare soil is lost, but surface patterns which cross soil and vegetated areas can be discerned. Also, man-made features, such as roads, buildings, and farm ponds, are clearly identifiable by their dark tone.

Further applications of this technique will attempt to enhance surface-terrain differences related to variations in the mineral composition of the soil and perhaps to crop types. In a recent work by Karmanov [24] for example, a ratio technique was used to characterize the spectral properties of soils as indicative of the content of organic matter, leaching, podzolization, and ferrallitization. The application of these techniques to areas in which soil patterns reveal underlying lithology are thought to be useful for purposes of tunnel-site selection.

*The data were collected for the Federal Highway Administration, U. S. Department of Transportation.

(a) 0.50-0.52 μm (Green)

(b) 0.66-0.72 μm (Red)

(c) 0.74-0.84 μm (Infrared)

FIGURE 11. COMPARISON OF THREE VIDEO IMAGES FOR AN AREA IN SOUTHEASTERN PENNSYLVANIA

(a) Ratio Image: $\frac{0.66\text{-}0.72\ \mu m}{0.50\text{-}0.52\ \mu m}$

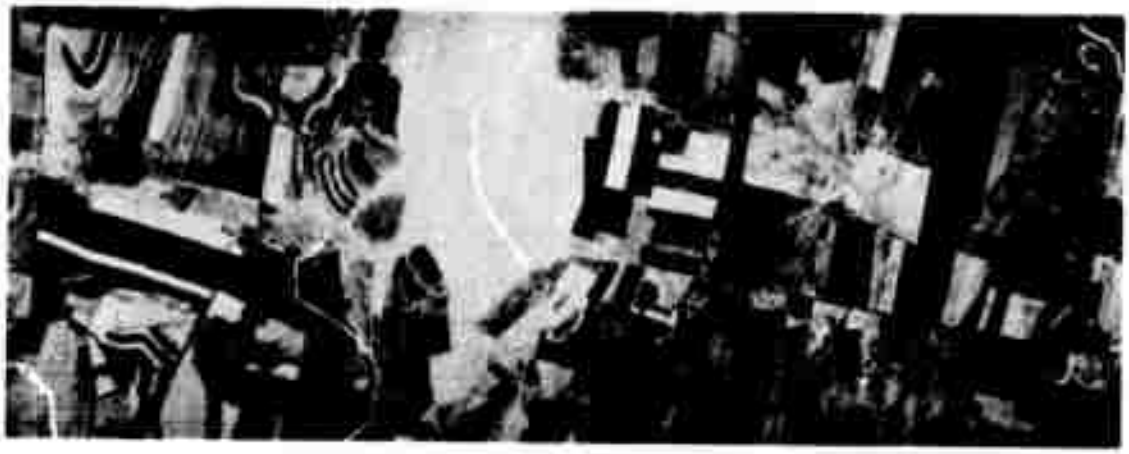

(b) Ratio Image: $\frac{0.74\text{-}0.85\ \mu m}{0.50\text{-}0.52\ \mu m}$

Drainage Channel

(c) Ratio Image: $\frac{0.66\text{-}0.84\ \mu m}{0.50\text{-}0.52}$

FIGURE 12. COMPARISON OF THREE RATIOED IMAGES FOR AN AREA IN SOUTHEASTERN PENNSYLVANIA

3.6.3. MULTICHANNEL PROCESSING TECHNIQUES FOR THE CLASSIFICATION OF LAND USES

Recent research has demonstrated that such terrain features as rock types [25], soils [26], and urban materials [27] (e.g., concrete, asphalt, lawn, gravel, buildings, and trees) can be discriminated on the basis of their spectral reflectance curves. Multichannel processing techniques provide for the development of diagnostic signatures from multispectral data, allowing the distribution of these features to be mapped.

Inherent in the classification of land uses are differing hydrological characteristics associated with each class. In particular, as urban development (characterized by buildings, hard-surface roads, and parking lots) encroaches on rural or agricultural areas, surface permeability and evapotranspiration are reduced, with concomitant changes in runoff and microclimate. These changes in hydrologic characteristics brought about by changes in surface condition can be measured in the field and are well documented. As a result, rapid land-use determinations become important to the hydrologist for assessing watershed conditions and for monitoring changes over time.

Multispectral data of a 1650-hectare (6.4 sq mile) area in the Oakville Creek Basin were processed on a special purpose analog computer. This area encompassed the town of Milton, Ontario, and neighboring agricultural land. (Color aerial photographs of the area are shown in Fig. 13a and b.) Five primarily rural land-use classes, and three urban land uses were identified. These are: (1) crop vegetation, (2) marsh vegetation, (3) forest, (4) bare fields, (5) standing water, (6) asphalt roads and lots, (7) gravel areas, and (8) concrete roads and buildings (roofs). The objective of this task was to discriminate areas of each of the above classes and to compute total areas represented by each.

Automatic spectrum-matching techniques were used. An analog computer identified and printed out the locations of terrain classes for which samples were available. The recognition criteria were based on distinctive characteristics recorded for each sample over the 0.40- to 0.85-μm spectral range. From a total of 12 spectral channels synchronously recorded by the multispectral scanner, a subset of 6 channels provided the means and standard deviations for the spectral signatures. These channels are listed in Table 2.

A likelihood-ratio decision rule was implemented by the computer to determine whether scene elements were spectrally similar enough to be recognized as a given terrain class. If the spectral characteristics of one or more spectral bands for a land-use class of interest are different from the characteristics of all other scene elements, that class is automatically discriminated by the computer and recognized on play-back imagery. In actual practice, multispectral processing techniques are used to establish an average signature for a class of objects, represented by a number of contiguous resolution elements known as a training set. These average signatures have a mean value, variance, and covariance.

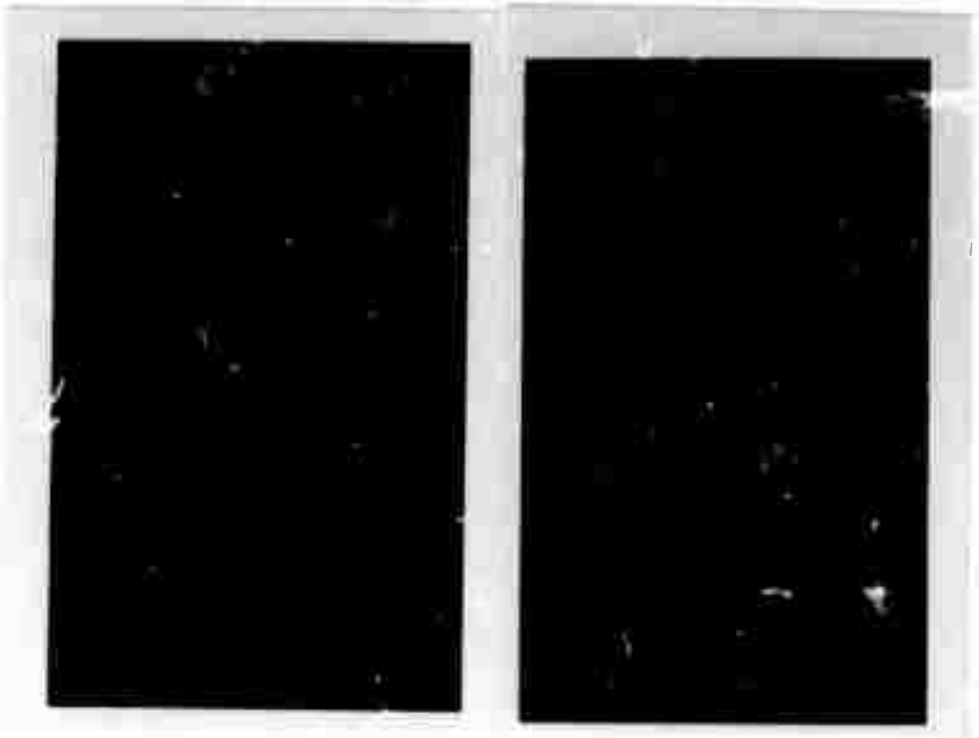

(a) Color Aerial Photograph (b) Color Infrared Aerial Photograph

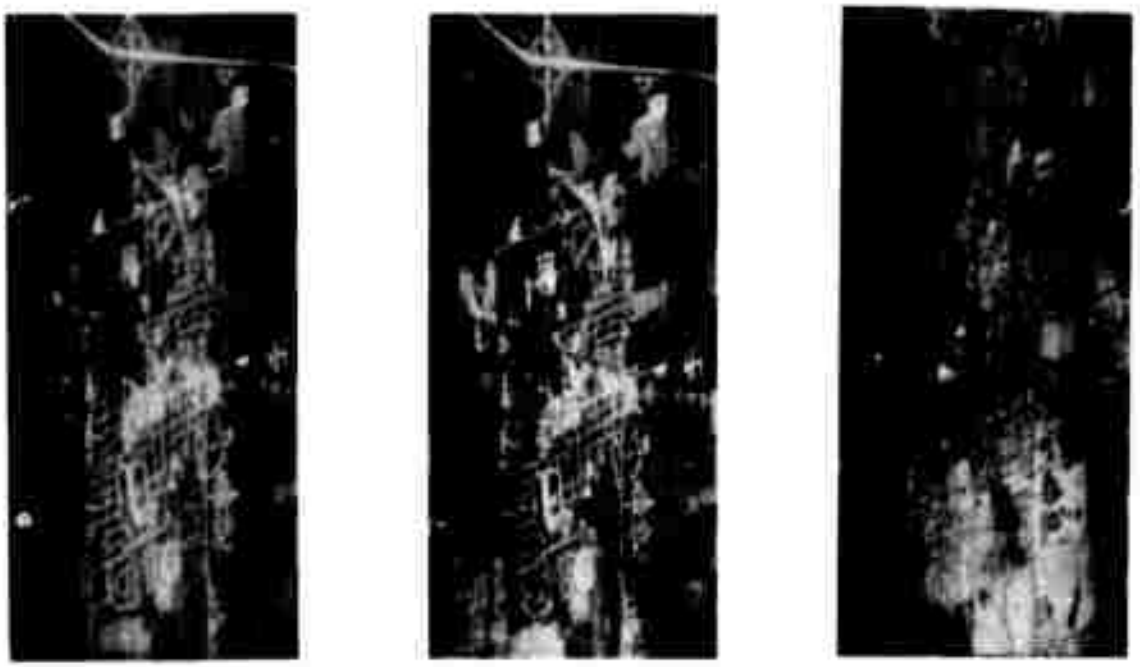

(c) Video Image: 0.43-0.48 μm (d) Video Image: 0.58-0.65 μm (e) Video Image: 0.72-0.92 μm

FIGURE 13. AERIAL PHOTOGRAPHS AND VIDEO IMAGES OF OAKVILLE CREEK BASIN AREA

TABLE 2. SIX SPECTRAL CHANNELS USED FOR RECOGNITION OF LAND-USE FEATURES

Channel	Spectral Range (μm)	Color
1	0.43-0.48	Violet
2	0.46-0.49	Blue
3	0.54-0.60	Yellow-Orange
4	0.58-0.65	Red
5	0.66-0.76	Dark Red
6	0.72-0.92	Reflective Infrared

The ability to establish signatures and to discriminate terrain classes automatically is limited by the resolution of the system. In an optical mechanical scanner system, the ground patch viewed at any given instant by the telescope is a resolution element in size. The resolution of the Michigan scanners is approximately 2 mrad. For this investigation, a resolution element represents an area approximately 24 ft (7.2 m) on a side.

Figures 13c, d, and e show video images in three spectral bands for the Milton area. (The skew in the imagery is caused by cross-wind induced movement of the data-collection aircraft.) The features associated with different land uses have considerably different degrees of contrast in the three images. This consistent change in contrast (or relative radiance) with wavelength allows the identification and mapping of the various land use classes with multispectral data.

Figure 14 contains six examples from twelve different recognition images produced for this Milton area. All white areas in an image are those designated by the computer as being spectrally similar to an example of the given land-use class. In each class, the areas of recognition are mutually exclusive, and no area is identified as more than one class. The images for the eight classes are:

(1) Standing Water. Two irregular reservoir areas were located within the town of Milton and one rectangular reservoir near the highway (401).

(2) Woodlots. Five areas were identified north and west of Milton, with scattered spots of recognition adjacent to portions of Oakville Creek.

(3) Marsh Vegetation. This class was principally located near Oakville Creek before it enters the reservoir in Milton.

(4) Green Vegetation. Recognition is comprised of three images which display differences in the densities of crops and urban lawn vegetation.

(5) Gravel. A single image shows numerous areas of gravel associated with parking lots and the shoulders of roads and highways.

(6) Bare Soil. Two images show areas of plowed fields and numerous roads within the town of Milton. One image shows portions of fields mapped as moderately drained, Chinguacousy clay loam, and the other represents poorly drained areas commonly mapped as Jeddo clay loam.

(7) Concrete. Numerous building roofs and lots and a single lane of the main highway were recognized as a material thought to be concrete.

(8) Asphalt. Parking lot areas and roads not recognized as dirt or concrete were discriminated as a material thought to be asphalt.

The area and percentage of total area of each of these classes are listed in Table 3 below. Of the approximately 1650 hectares which comprise this area, 1340 hectares (81.2%) are

(a) Bare Soil

(b) Crop and Urban Vegetation

(c) Woodlots

(d) Concrete

(e) Asphalt

(f) Gravel

FIGURE 14. RECOGNITION IMAGES OF SIX DIFFERENT LAND-USE CLASSES IN THE OAKVILLE CREEK BASIN AREA

TABLE 3. AREA AND PERCENTAGE OF TOTAL AREA FOR LAND-USE CLASSES IN THE REGION NEAR MILTON, ONTARIO

Land-Use Class	Number of Points	Percentage of Total	Area (hectares)
Standing Water	33,300	1.8	29.4
Woodlots	33,200	1.8	29.4
Marsh	12,300	0.7	10.9
Green Vegetation	715,300	38.3	632.1
Gravel	40,200	2.2	35.5
Bare Soil	387,500	20.8	342.5
Concrete	11,500	0.6	10.2
Asphalt	283,050	15.2	250.1
Not Classified	350,000	18.6	309.4
Total Area	1,866,350	100.0	1650.0

classified. Scene elements not classified are those which, because of their unique spectral properties, do not fall into any of the eight classes. These unclassified scene elements might include such factors as different colored roofs, minor variants in soil and vegetation, and differing surface material within the urban area. Initial inspection of the imagery suggests that areas of vegetation comprise most of the unclassified area.

In addition to some areas not recognized, it is probable that a portion of the areas are classified incorrectly. In other words, it is likely that the spectral characteristics of some scene points will be similar to terrain classes to which they do not belong. Some of the asphalt recognition may fall into this class. Further analysis of the accuracy of the recognition results is proceeding.

4
COMPOSITIONAL REMOTE SENSING OF ROCK OUTCROPS BY IMAGE-RATIOING TECHNIQUES

According to K. Szécchy [1], the first step in geologic exploration prior to tunnel construction is a survey of the morphology, petrography, stratigraphy, and hydrology of the environment, including thorough field reconnaissance and surface explorations. Among the important data needed for decisions on tunnel-site selection are the origin and actual condition of exposed rocks, geochemical correlations between bedrock and topsoil, stream drainage, and pH values of springs and streams. The ratio techniques discussed in this section can be useful in the collection of these and other pertinent data, once the techniques are understood quantitatively. The purpose of this section is to explain the ratioing techniques, to report what has been done to improve them, and to suggest ways in which they can be useful for tunnel-site selection.

The thermal infrared ratio method, originally described in a report to NASA [28] and in the Journal of Geophysical Research [29], was discussed in Section 3 of the semiannual report for this contract [16]. The two references mentioned above show that the ratio magnitude is at least crudely correlated with the gross percentage of SiO_2 in the target; therefore, this technique has been useful for discrimination among widely different silicate rock types [31]. For completeness, the discussion from the semiannual report is repeated here as Section 4.1.

4.1. IMAGERY OPTIMIZATION ANALYSIS

Geologic remote sensing has at its disposal two new techniques of image ratioing which are applicable (1) to the discrimination between silicate and nonsilicate geologic formations and (2) to the determination of the amount of ferric oxide in given geologic features. The first

technique allows the discrimination of silicate rocks on the basis of a ratio of the radiances in two infrared (IR) channels. Utilizing 25 rock samples selected from R. J. P. Lyon [30], Fig. 15, shows the ratio between channel 1 (8.2 to 10.9 μm) and channel 2 (9.4 to 12.1 μm) and the amount of SiO_2 in percentage of weight, with the ratio symbolized by $R_{1,2}$. The crude correlation between $R_{1,2}$ and the percentage of SiO_2 is evidenced by the straight curve on the graph. The wavelengths of the silicon-oxygen reststrahlen bands are monitored by $R_{1,2}$. The more felsic rocks (those with greater SiO_2 content), generally speaking, have reststrahlen bands (relatively large departures from unit emissivity) at shorter wavelengths than do the mafic rocks (those with lesser SiO_2 content), and therefore $R_{1,2}$ increases with decreasing SiO_2.

The second image-ratioing technique involves a ratio of a channel in the visible green region of the spectrum (channel 5, 0.50 to 0.52 μm) and one in the reflective IR (channel 7, 0.74 to 0.85 μm). This ratio can show the rise in reflectance of ferric oxides from the green to the reflective IR wavelengths. This spectral phenomenon is caused by electronic transitions of the Fe^{3+} ion in the ferric oxides hematite and limonite.

The first technique, utilizing the ratio of two IR channels, is demonstrated in Figs. 16-19, which display infrared images of specially processed scanner data gathered by The University of Michigan aircraft at an altitude of 3000 ft over a sand quarry at Mill Creek, Oklahoma, and over an area near Pisgah Crater in Southern California (also at 3000-ft altitude). The Mill Creek data were gathered on June 25, 1970, at 1000 hours local time, while the data from Pisgah Crater were collected at 0800 hours local time on October 30, 1970. Each of the figures includes analog infrared images of two single-wavelength channels of data, plus an image of the ratio of the radiances in the two channels. The ratio image reflects changes in the chemical composition of the rock targets, primarily changes in their SiO_2 content.

Figure 16 shows images of the Mill Creek sand quarry. In the ratio image (Fig. 16c), all features that appear dark (except for wavy noise lines) are either exposed quartz-sand or sandstone. The outcroppings around the lake in the lower part of the images are sandstone. Geologists from both the United States Geological Survey and The University of Michigan have found almost perfect correlation between the dark regions indicated on the ratio image and quartz-sand or sandstone. This type of discrimination should prove useful in explorations for construction materials, such as sand and gravel.

Figure 17 is the first third of a north-to-south flight over Pisgah Crater, located in the right-hand portion of each of the three images. The right half of these images consists primarily of basaltic lava flows which erupted from Pisgah Crater in the late Pleistocene or Recent epochs. These relatively young lava flows (approximately 10,000 to 100,000 years old) erupted in three phases. Although similar in chemical composition, they have quite different surface textures, varying from ropy to blocky. The older fanglomerate in the left half of the images

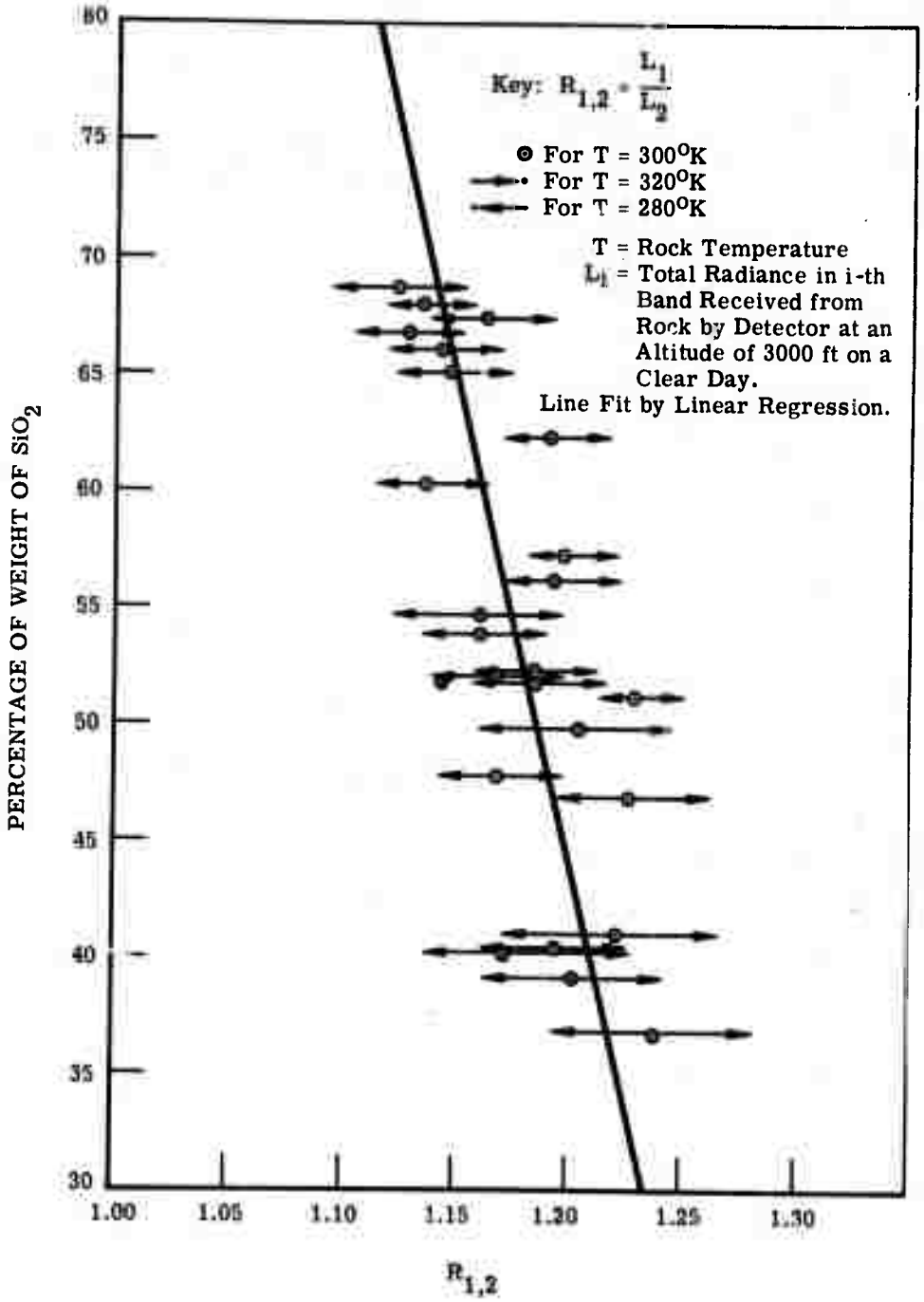

FIGURE 15. RATIO BETWEEN RADIANCES IN CHANNEL 1 AND CHANNEL 2 VERSUS THE PERCENTAGE OF WEIGHT OF SiO_2 IN 25 ROCK SAMPLES.

Samples taken from Ref. [30].

(a) Channel 1: 8.2-10.9 μm

(b) Channel 2: 9.4-12.1 μm

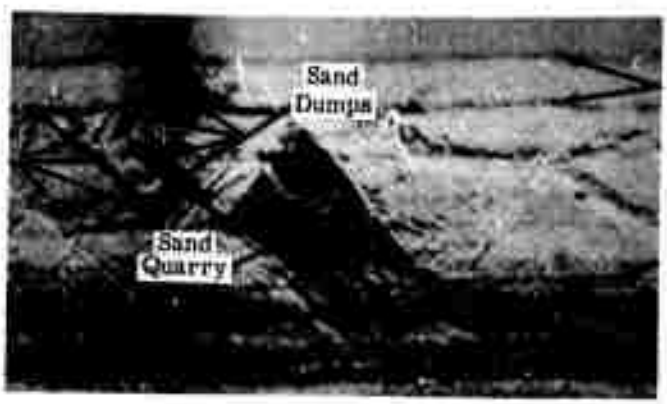

(c) Ratio Image of Channel 1 over 2

FIGURE 16. DISCRIMINATION OF ACIDIC SILICATES NEAR MILL CREEK, OKLAHOMA (SAND QUARRY)

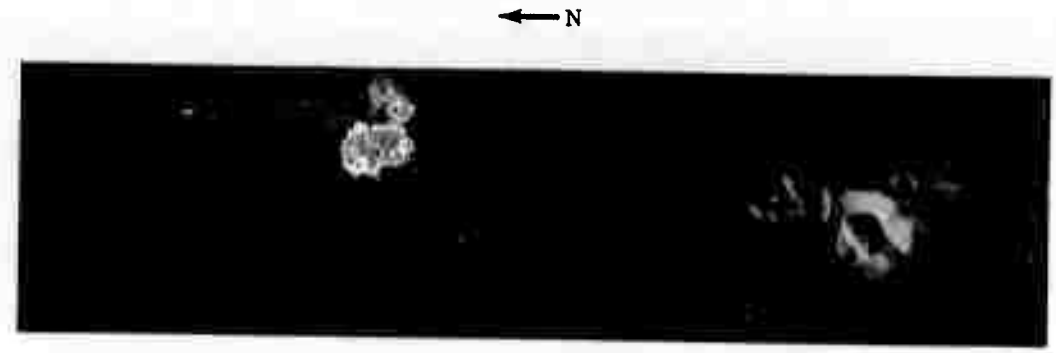

(a) Channel 1: 8.2-10.9 μm

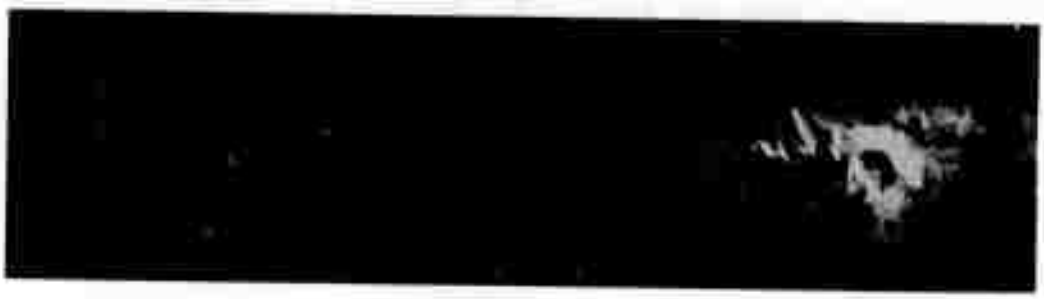

(b) Channel 2: 9.4-12.1 μm

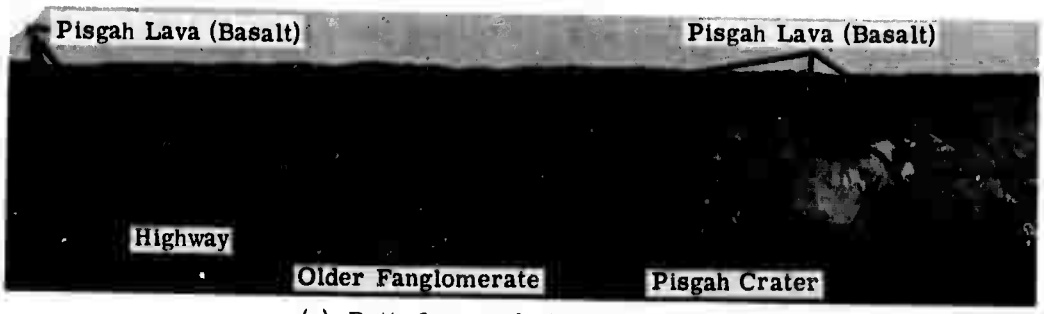

(c) Ratio Image of Channel 1 over 2

FIGURE 17. ANALOG INFRARED IMAGES OF FLIGHT LINE 1, SECTION A, NEAR PISGAH CRATER, CALIFORNIA

(a) Channel 1: 8.2-10.9 μm

(b) Channel 2: 9.4-12.1 μm

(c) Ratio Image of Channel 1 over 2

FIGURE 18. ANALOG INFRARED IMAGES OF FLIGHT LINE 2, SECTION A, NEAR PISGAH CRATER, CALIFORNIA

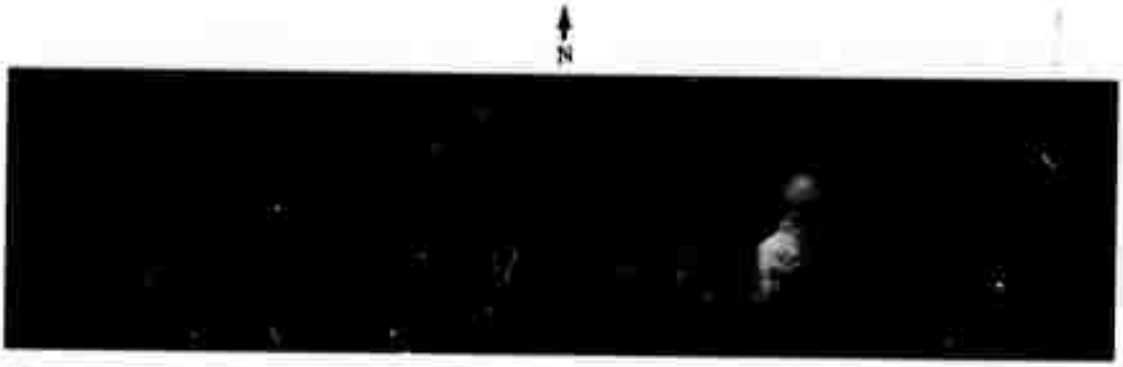

(a) Channel 1: 8.2-10.9 μm

(b) Channel 2: 9.4-12.1 μm

(c) Ratio Image of Channel 1 over 2

FIGURE 19. ANALOG INFRARED IMAGES OF FLIGHT LINE 2, SECTION B, NEAR PISGAH CRATER, CALIFORNIA

consists primarily of rock fragments from both the basaltic lava and the felsic mountains on both sides of this region. North of the highway, parts of the second eruptive phase of the Pisgah lava are partially covered by alluvium.

With the exception of Pisgah Crater, topographically the highest feature in the images, the single-channel images show very little temperature variation across the scene. The ratio image (Fig. 17c), however, shows considerable variation in the wavelengths of the reststrahlen bands over the same region. Lighter and darker areas on the ratio image indicate reststrahlen bands at longer and shorter wavelengths, respectively. The mafic rocks, which contain lower amounts of SiO_2, should appear bright (indicating a high ratio), and the felsic rocks, containing a higher SiO_2 content, should appear dark (evidence of a low ratio). In the ratio image (Fig. 17c), the basaltic lava appears bright in contrast to the darker tones of the fanglomerate and gravel. The basaltic peninsula near the center of Fig. 17c can easily be discriminated from the surrounding fanglomerate and gravel, whereas the single-channel images (Fig. 17a and 17b) show very low thermal contrast for this feature. In addition, the wind-blown sand extending over the lava just south of the peninsula shows up readily in the ratio image, but is not distinguishable in the single-channel images. In the ratio image, the three bright spots on Pisgah Crater are the only experimental artifacts; these resulted from the much higher temperature on the elevated sunward slopes, which caused clipping of the signal in one of the channels. Patches of exposed basaltic lava north of the highway are also evident in Fig. 17c.

Figure 18 shows the westernmost half of a west-to-east flight line over a region south-southeast of Pisgah Crater. From left to right, the warm region (the light area in the single-channel images) in the extreme western part is a dacitic mountain; the adjacent color region is fanglomerate and gravel (grading eastwardly to smaller fragments and sand); and the broad, warm region is the basaltic Sunshine lava flow. Just east of the lava flow is alluvium, followed by playa deposits (primarily clay and carbonates) and the southern tip of the basaltic Pisgah lava flow. Once again, the ratio image (Fig. 18c) shows emissivity variations indicative of rock type. The felsic mountains and fanglomerate appear darker than the mafic lava, and the playa material is contrasted sharply against the alluvium. Because the mountains are warmer than other parts of the scene, computational temperature corrections should heighten the contrast between dacite and basalt by lowering the ratio illustrated in the ratio image. In other words, Fig. 18c shows a higher ratio for this section of the image than would be expected on the basis of the wavelengths of the reststrahlen bands alone. In contrast, the patchy appearance of the playa is caused solely by emissivity variations, since the temperature is uniform across the floor of Lavic Lake of which this section is a part.

Figure 19, a continuation of Fig. 18, shows the western half of the flight line across Lavic Lake. From west to east, the first apparent feature is the Pisgah basaltic lava with playa material below it, then alluvium, a basaltic mountain, and an intermittent stream bed, now dry, which

has eroded down through the surrounding mountains of basalt. Once again, on the ratio image (Fig. 19c), the southern end of the Pisgah lava flow appears similar to the playa material, and the playa-alluvium boundary is sharply demarcated. On the northern side of the basaltic mountain, the small, dark regions near the center of the image have been confirmed by recent field trip to be felsic outcroppings. The two most prominent dark areas in the stream bed are regions of felsic volcanic tuff, which contain minor amounts of malachite, a copper carbonate. The basaltic mountain in the lower right corner of Fig. 19c appears bright, as did the basaltic lava flow in Fig. 18c. As in the previous ratio images, in Fig. 19c the felsic rocks and rock fragments comprising the alluvium appear to have lower ratios (and therefore appear darker in the ratio image) than do the mafic rocks.

These images show that by ratioing images in the two IR channels 8.2 to 10.9 μm and 9.4 to 12.1 μm, one can enhance emissivity variations in the presence of temperature gradients on the order of 10°C or 15°C without computational temperature corrections. Even in shadowed regions, compositional information is still present in the ratio images. Although temperature-corrected ratio maps are available in digital form, they do not show the contrasts in geologic formations as dramatically as the analog infrared ratio images do.

Figures 20 and 21 illustrate the second ratioing method—i.e., the ratioing of channels in the visible green and the reflective IR spectral regions. Figure 20 shows the same area as that of Fig. 18 (south-southeast of Pisgah Crater), except that the data have been recorded in channel 5 (0.50 to 0.52 μm) and channel 7 (0.74 to 0.85 μm). The ratio of these two spectral regions is sensitive to the presence of iron oxides, with the darker areas corresponding to greater contents of iron oxide. In the ratio image of Fig. 20, the andesite dikes in the dacite porphyry mountain are very clearly outlined, while they are hardly discernible in the single-channel maps of the area. The greater amount of iron oxide in the basaltic lava (as contrasted to that in the alluvium) is also clearly illustrated. Figure 21, which covers the same area as that of Fig. 17, shows that the lava flows around Pisgah Crater vary in iron oxide content, a result in agreement with our analysis of samples recently collected in the field from each of the three eruptive phases.

These ratioing techniques have just recently been developed* and are presently being improved. Under the present contract, new laboratory data are being measured, and the results of these measurements should greatly improve our ability to relate the measured $R_{1,2}$ to the chemical parameters of geologic targets. Either the relationship between SiO_2 and $R_{1,2}$ in Fig. 15 will be improved, or a different chemical or mineralogical parameter better related to $R_{1,2}$ will be found. In regard to the $R_{5,7}$ ratio technique, several samples from the Pisgah Crater test site are presently undergoing laboratory analyses (both spectral and chemical) in an effort to prove quantitatively the relationship between spectral reflectivity features and the

*As of September 1971.

(a) Channel 5: 0.50-0.52 μm

(b) Channel 7: 0.74-0.85 μm

(c) Ratio Image of Channel 5 over 7

FIGURE 20. ANALOG VISIBLE AND NEAR-INFRARED IMAGES OF FLIGHT LINE 2, SECTION A, NEAR PISGAH CRATER, CALIFORNIA

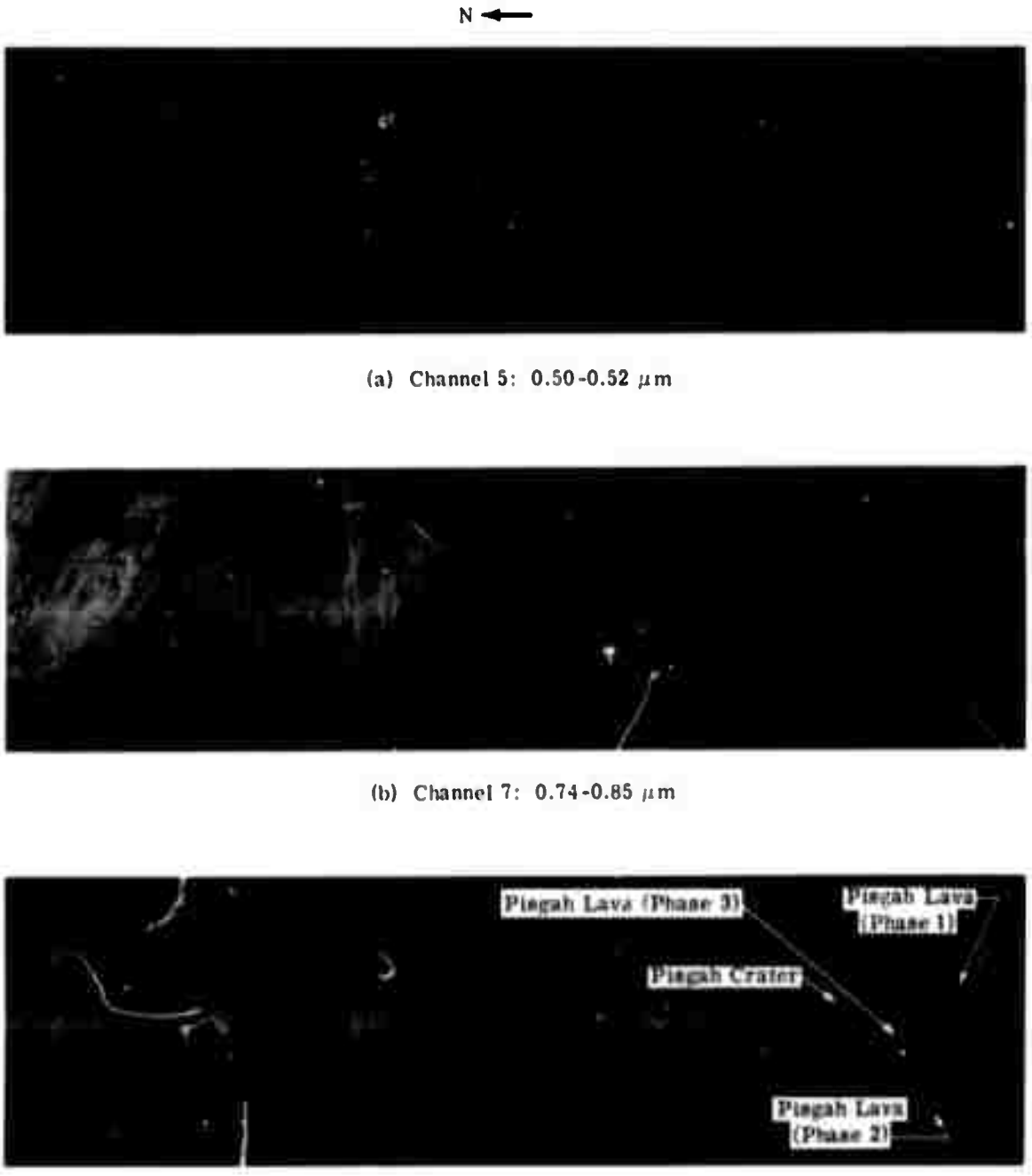

(a) Channel 5: 0.50-0.52 μm

(b) Channel 7: 0.74-0.85 μm

(c) Ratio Image of Channel 5 over 7

FIGURE 21. ANALOG VISIBLE AND NEAR-INFRARED IMAGES OF FLIGHT LINE 1, SECTION A, NEAR PISGAH CRATER, CALIFORNIA

iron oxide content of exposed rock surfaces. It seems likely that the new developments in image-ratioing techniques will lead to improved methods for rapid geologic mapping and lithologic differentiation.

4.2. IMPROVEMENT OF THE THERMAL INFRARED RATIO TECHNIQUE

As indicated in the previous section, the thermal infrared ratio technique has been limited by lack of knowledge about the precise relationships between the infrared spectral features of rocks and their chemical and mineralogical composition. For this reason, a laboratory program was initiated to provide more information about this relationship. Twenty-six igneous rock samples from various parts of the world were selected as a test set. Table 4 lists these rocks and gives the chemical composition of those for which analyses have already been completed. The chemical compositions are currently being determined for the remaining specimens and will be completed by July 1972. The U. S. Geological Survey, through Dr. Larry Rowan of the Branch of Regional Geophysics in Denver, Colorado, supplied all of the rocks except those from Pisgah Crater, California, and also is providing the chemical analyses at no cost to the Bureau of Mines.

As can be inferred from Table 4, the silicate rocks in this group vary from highly felsic to highly mafic. On a parabolic reflectometer (shown in Fig. 22) owned by the Martin-Marietta Corporation, Denver Division, the thermal infrared spectra in the approximate wavelength region from 7.5 to 14.0 μm were measured for an exposed* surface of each of these rocks. Although the reflectometer illuminates the whole hemisphere of the sample, the rock is viewed in a small solid angle of observation. This experimental condition is similar to that of a total integrating sphere, in which the sample is illuminated within a small solid angle of incidence and the observed reflected radiation is collected over the whole hemisphere. However, from a design standpoint, the parabolic reflectometer is superior to the integrating sphere in the thermal infrared wavelength region. First, it is simpler to build and maintain a parabolic aluminum mirror than an integrating sphere which has smooth surfaces compared to wavelengths on the order of 10 μm. Second, the parabolic reflectometer offers an opportunity to observe a given sample in both emission or reflection, with almost the same optical train, whereas this is not feasible with an integrating sphere.

For reflection measurements, a heated blackbody cavity at 600°C acted as the source of infrared illumination. The source radiation was chopped to minimize the contribution of radiation emitted by the sample, which was maintained at a temperature of approximately 300°K by means of ice water circulated through the sample holder and cooled nitrogen vapor blown across

*In this report, an exposed surface is defined as one exposed to air in the sample's natural environment.

TABLE 4. CHEMICAL COMPOSITION OF IGNEOUS SILICATE ROCK SAMPLES

Sample Name and Number	Origin	SiO_2 (%)	Al_2O_3 (%)	Fe_2O_3 (%)	FeO (%)	MgO (%)	CaO (%)	Na_2O (%)	K_2O (%)
Granite (A79)	Antarctica	76.7	12.8	0.49	<.05	0.15	0.11	4.5	4.3
Granite (A119)	Antarctica	66.2	16.5	0.82	2.8	1.1	2.6	3.9	4.9
Granite (A122)	Antarctica	72.4	14.2	0.88	1.2	0.31	1.2	5.6	9.0
Rhyolite (SA-49)									
Rhyolite (Welded Tuff)									
Syenite (E83A)	Montana	61.4	20.3	1.6	0.52	.024	0.99	3.6	9.7
Trachyte (Porphyritic)									
Nepheline Syenite									
Granodiorite (A117)	Antarctica	53.6	18.7	1.3	7.0	3.8	6.2	3.9	2.8
Granodiorite (A127)	Antarctica	62.8	16.0	0.64	1.6	0.90	1.8	3.9	4.4
Dacite (E12A)	Montana	65.7	15.0	1.2	1.3	1.5	3.0	3.9	3.4
Dacite (2A1)									
Dacite (2B5)									
Dacite (2B5, Fresh Surface)									
Diorite (A129)	Antarctica	61.0	16.4	1.8	5.6	1.4	4.6	4.3	2.5
Diorite (E47C)	Montana	56.2	17.4	1.8	5.4	4.4	7.1	3.9	1.8
Andesite (E55A)	Montana	57.8	15.2	2.2	3.3	5.0	5.5	3.2	1.8
Andesite (2A3)									
Gabbro (E80A)	Montana	50.6	15.7	4.0	6.5	6.9	10.7	2.4	0.70
Basalt (1A8)									
Basalt (WI-1-104)									
Basalt (2B5)									
Basalt (5B4)									
Basalt (1A3)									
Anorthosite (AN)									
Diabase									
Peridotite (EP-1)									

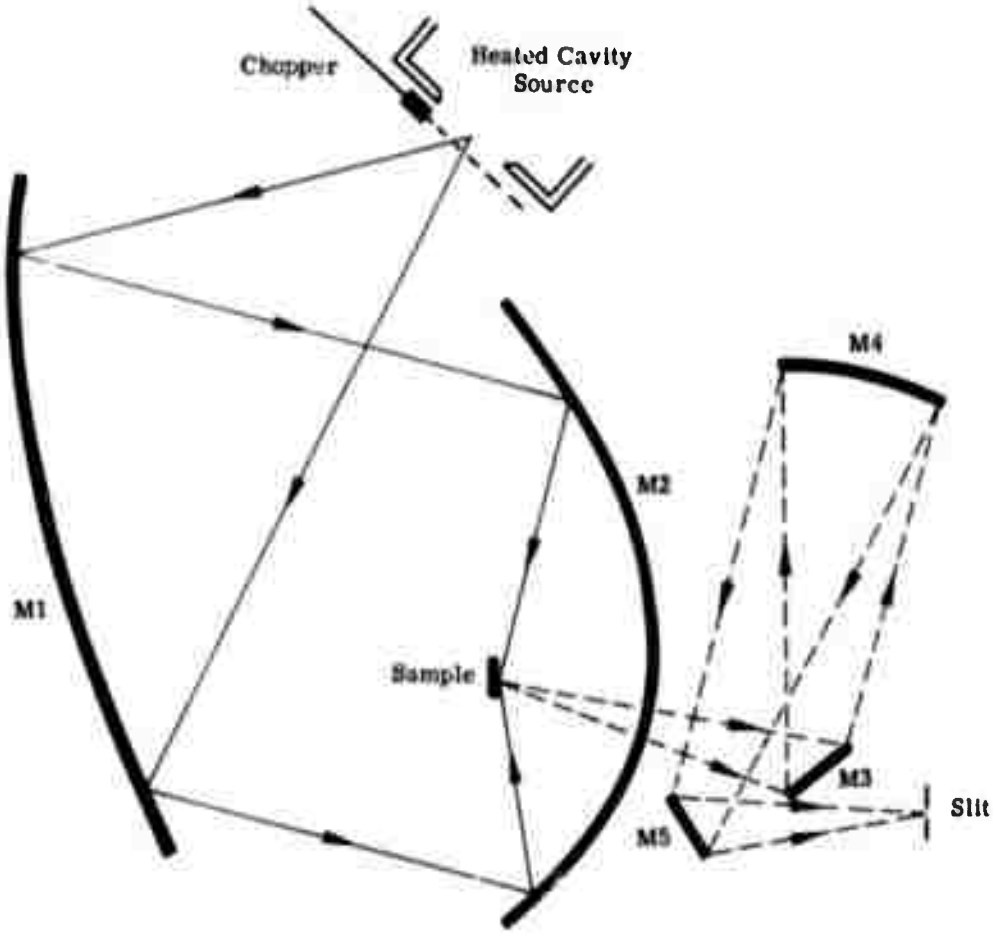

FIGURE 22. PARABOLIC REFLECTOMETER OPTICAL SCHEMATIC

the sample's surface. The observation angle in all cases was 15° to the macroscopic surface normal to the sample. A portion of the radiation from the sample was collected by the transfer optics through a hole in the second parabolic mirror and focused (with an approximate 11° field of view) by mirrors M3, M4, and M5 onto the entrance slit of a Perkin-Elmer Model 98 monochromator. Dispersion in the monochromator was accomplished with a CsBr prism, which had a spectral slit width that varied from $\Delta\lambda = 0.51$ μm at $\lambda = 8$ μm to $\Delta\lambda = 0.29$ μm at $\lambda = 14$ μm. The physical slit width was held at a constant 0.5 mm for all samples, with the physical slit length 12.0 mm. The signal detector was a high sensitivity Reeder radiation thermocouple, with a D^* (detectivity) of approximately 10^9. A gold specular reflectance standard used as a reference varied in reflectance from 0.9921 at $\lambda = 8$ μm to 0.9930 at $\lambda = 14$ μm.

The resulting infrared spectra of the 38 rock samples are shown in Fig. 23. For each sample, the spectral emittance ϵ_λ has been plotted, as calculated from Kirchoff's law

$$\epsilon_\lambda = 1 - \rho_\lambda \tag{1}$$

where ρ_λ is the measured directional spectral reflectance.

The connection between these laboratory spectra and the infrared ratios measured by an airborne scanner will be shown in the following two equations. The total spectral radiance received by an airborne detector from the direction of a given rock target was calculated from the equation

$$\begin{aligned} L_\lambda &= \left[\epsilon_\lambda L_{bb_\lambda}(T) + \rho_\lambda L_{sky_\lambda}\right]\tau_{A_\lambda} + L_{V_\lambda} \\ &= \left\{\epsilon_\lambda\left[L_{bb_\lambda}(T) - L_{sky_\lambda}\right] + L_{sky_\lambda}\right\}\tau_{A_\lambda} + L_{V_\lambda} \end{aligned} \tag{2}$$

where L_λ = total spectral radiance of wavelength λ arriving at the detector

$\epsilon_\lambda = 1 - \rho_\lambda$ = rock spectral emittance taken from the data above and Eq. (1)

$L_{bb_\lambda}(T)$ = spectral radiance of a blackbody at same temperature, T, as rock

L_{sky_λ} = spectral radiance from sky incident on diffuse rock surface

τ_{A_λ} = spectral atmospheric transmissivity

L_{V_λ} = spectral radiance from emission and scattering into the beam by the atmosphere in the path between rock and detector

The atmospheric parameters L_{sky_λ}, τ_{A_λ}, and L_{V_λ} were calculated from a clear, dry summer (visibility of 20 miles) atmospheric model developed at The University of Michigan [32]. Typically, the atmospheric parameters were calculated for geological targets at a base altitude of 0.76 km (3000 ft) and at an aircraft altitude of 1 km above the targets.

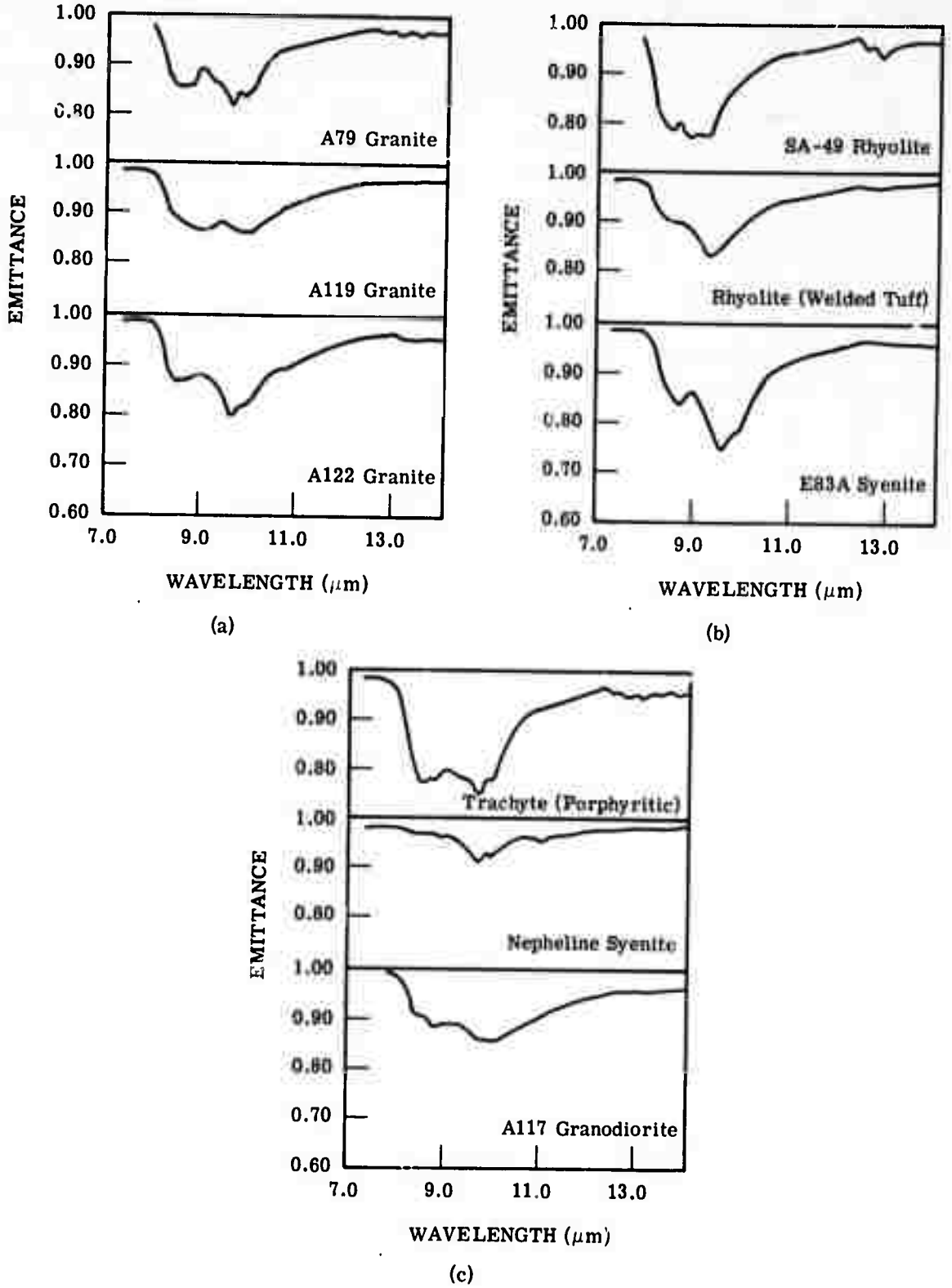

FIGURE 23. INFRARED SPECTRA OF IGNEOUS SILICATE ROCKS

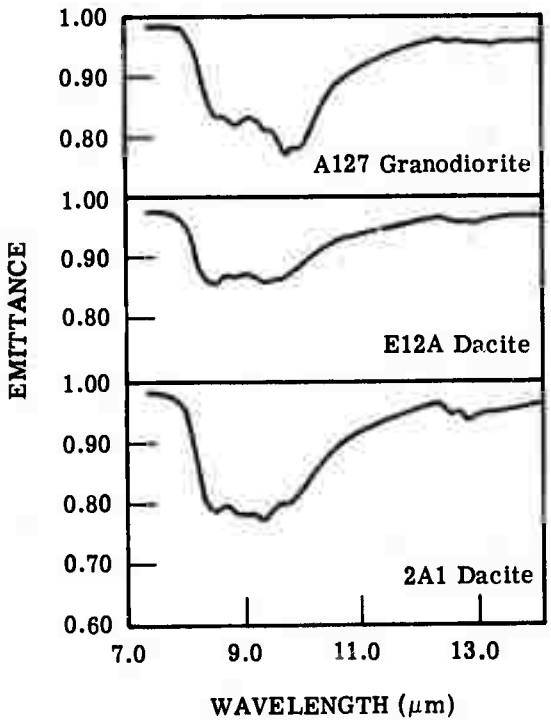

(d)

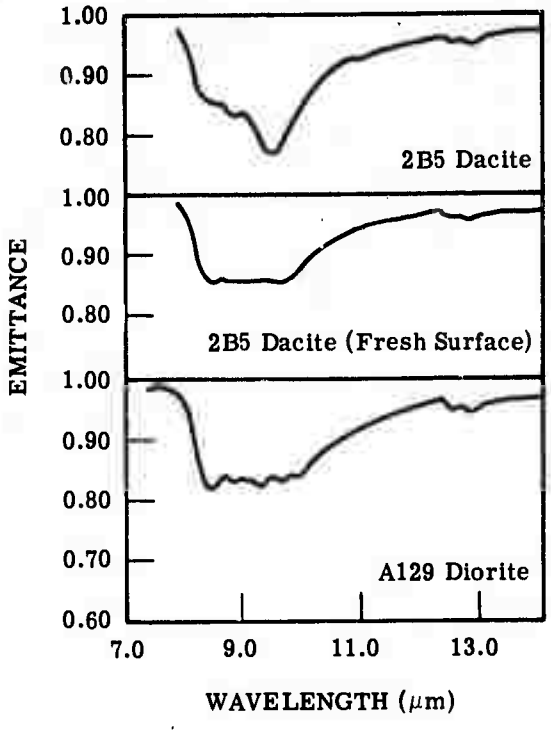

(e)

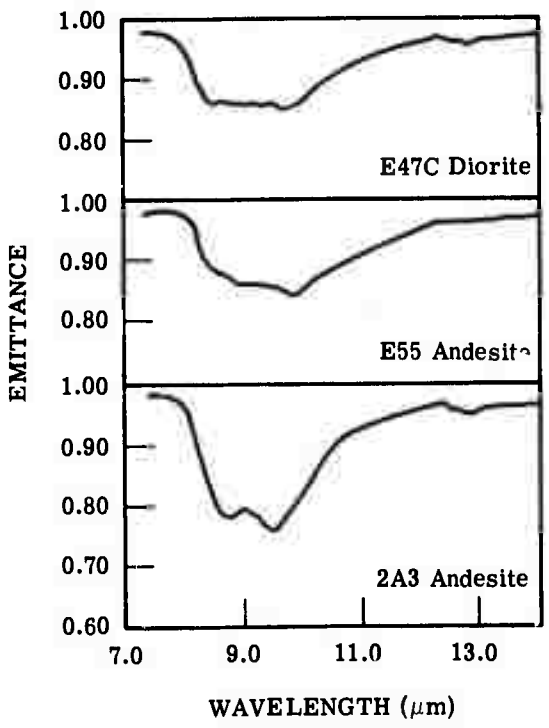

(f)

FIGURE 23. INFRARED SPECTRA OF IGNEOUS SILICATE ROCKS (Continued)

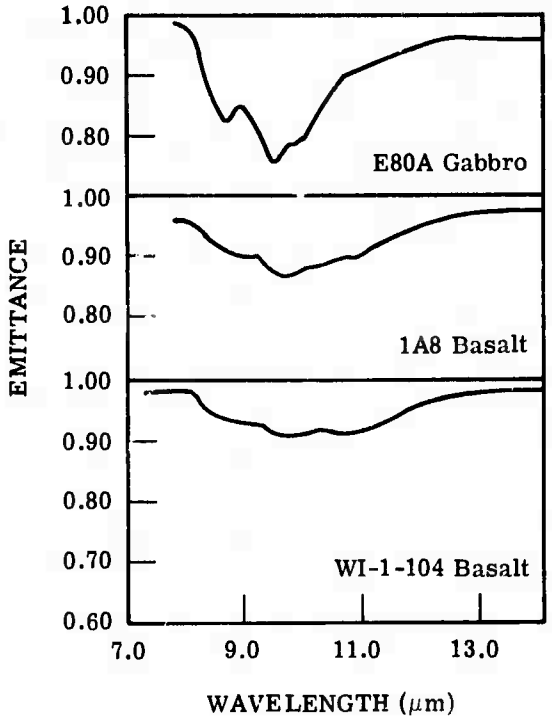

(g)

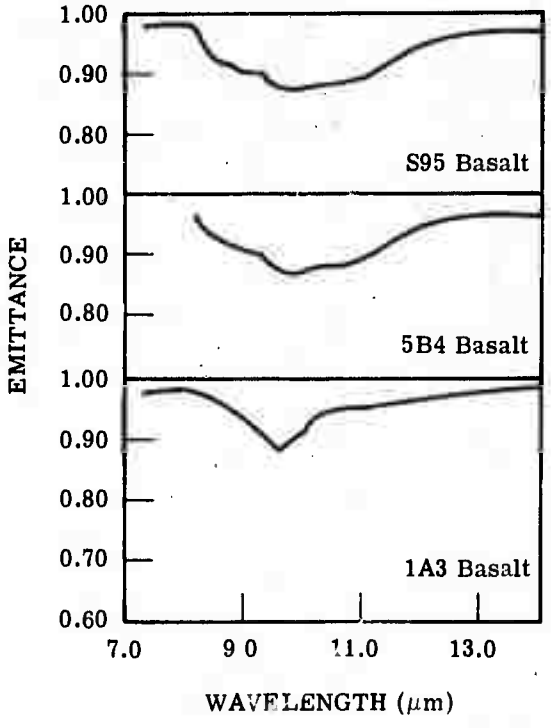

(h)

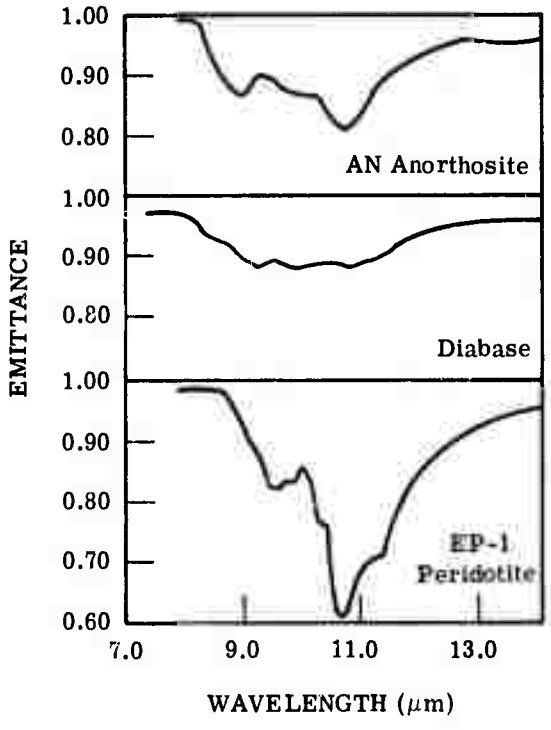

(i)

FIGURE 23. INFRARED SPECTRA OF IGNEOUS SILICATE ROCKS (Concluded)

For two selected bands and an assumed rock temperature, Eq. (2) can be integrated over the respective spectral regions, and a ratio of radiances in the two bands for each of the 26 samples can be calculated. The ratio is then given by

$$R_{1,2}(T) = \frac{L_{\Delta\lambda_1}(T)}{L_{\Delta\lambda_2}(T)} = \frac{\int_{\lambda_a}^{\lambda_b} f_1(\lambda) L_\lambda(T)\, d\lambda}{\int_{\lambda_c}^{\lambda_d} f_2(\lambda) L_\lambda(T)\, d\lambda} \qquad (3)$$

where λ_a and λ_b are the limits of band 1; λ_c and λ_d are the limits of band 2; and $f_1(\lambda)$ and $f_2(\lambda)$ are the exact spectral responses of the detector in the two respective bands. In order that the theoretical results could be compared with an existing set of field data, the two spectral channels first to be considered corresponded to the two wavelength regions covered by Willow Run Laboratories' two-element Honeywell Hg:Cd:Te detector; i.e., $\Delta\lambda_1$ is 8.2 to 10.9 μm and $\Delta\lambda_2$ is 9.4 to 12.1 μm at the 10% spectral responsivity points. Actual filter functions of these two channels were used. The samples were all assumed to be at T = 300°K. With the atmospheric parameters mentioned above, the radiances calculated from Eq. (2) were substituted into Eq. (3) to yield a ratio for each sample, as measured by this specific detector at an above-ground altitude of 1 km. The resulting $R_{1,2}(300^\circ K)$ ratios are given in column 1 of Table 5.

In column 2 of Table 5 are shown ratios $R^0_{1,2}(300^\circ K)$ for no atmosphere $\left(\tau_{A_\lambda} = 1,\ L_{sky_\lambda} = L_{V_\lambda} = 0\right)$, with the same filter functions. In column 3 are ratios, which will be called $R_{I,II}(300^\circ K)$, for two hypothetical channels with square-filter functions between 8.2 and 9.2 μm (channel I) and 10.3 and 11.3 μm (channel II); the same experimental conditions as were used to calculate $R_{1,2}(300^\circ K)$ were assumed. Finally, in column 4 are the ratios $R^0_{I,II}(300^\circ K)$ for these same two hypothetical channels without atmosphere. Based on previous studies [28], channels I and II are nearly optimum for discrimination on the basis of percentage of SiO_2.

The end product of the analysis of these data will include plots of the ratios listed in Table 5 versus percentage of SiO_2, or possibly versus some better chemical or mineralogical parameter(s). Although the analysis cannot be completed until the next contract year, three experimental problems merit discussion, and three useful results can be derived from the data in their present state. The three experimental problems involve the small spot size of the reflectometer, the spectral effects of surface contaminants (weathering products) on a few samples, and, for some samples, the lack of agreement between spectral reflectance and direct spectral emittance measurements.

TABLE 5. CALCULATED THERMAL INFRARED RATIOS BY A DETECTOR AT AN ABOVE-GROUND ALTITUDE OF 1 km ON A CLEAR, DRY SUMMER DAY

Sample Name and Number	$R_{1,2}(300^{\circ}K)$	$R^{0}_{1,2}(300^{\circ}K)$	$R_{I,II}(300^{\circ}K)$	$R^{0}_{I,II}(300^{\circ}K)$
Granite (A79)	1.1761	1.1541	0.6756	0.6383
Granite (A119)	1.1946	1.1812	0.6977	0.6868
Granite (A122)	1.1987	1.1828	0.7030	0.6918
Rhyolite (SA-49)	1.1266	1.0886	0.6366	0.5960
Rhyolite (Welded Tuff)	1.1741	1.1555	0.6852	0.6731
Syenite (E83A)	1.1784	1.1540	0.6960	0.6846
Trachyte (Porphyritic)	1.1442	1.1053	0.6561	0.6211
Nepheline Syenite	1.2094	1.2058	0.7030	0.7016
Granodiorite (A117)	1.2134	1.2054	0.7149	0.7097
Granodiorite (A127)	1.1723	1.1461	0.6834	0.6636
Dacite (E12A)	1.1724	1.1512	0.6715	0.6485
Dacite (2A1)	1.1436	1.1062	0.6566	0.6203
Dacite (2B5)	1.1574	1.1264	0.6737	0.6497
Dacite (2B5, Fresh Surface)	1.1686	1.1457	0.6704	0.6476
Diorite (A129)	1.1685	1.1420	0.6730	0.6456
Diorite (E47C)	1.1795	1.1693	0.6818	0.6617
Andesite (E55A)	1.1962	1.1820	0.7033	0.6934
Andesite (2A3)	1.1394	1.1007	0.6587	0.6277
Gabbro (E80A)	1.1810	1.1567	0.6993	0.6870
Basalt (1A8)	1.2154	1.2087	0.7184	0.7151
Basalt (WI-1-104)	1.2204	1.2180	0.7188	0.7190
Basalt (S95)	1.2246	1.2216	0.7280	0.7303
Basalt (5B4)	1.2255	1.2225	0.7280	0.7287
Basalt (1A3)	1.2018	1.1943	0.7047	0.7026
Anorthosite (AN)	1.2458	1.2494	0.7547	0.7648
Diabase	1.2204	1.2168	0.7245	0.7236
Peridotite (EP-1)	1.3723	1.4178	0.9092	0.9776

The physical area observed on each rock during the spectral measurements was approximately 0.5 mm × 12.0 mm (the slit dimensions), which presented a problem with coarse-grained polymineralic rocks. The greatest variability in ρ_λ or ϵ_λ with a change in sample position was found in the granite samples, as expected. Figure 24 shows the spectral variations caused by taking measurements at various locations on three of the coarsest grained samples: granite, granodiorite, and peridotite. Whereas such variations add to uncertainty of detection via the ratio method, this problem is minor, except possibly for the granites. Monetary constraints made it impossible to take more measurements for various sample positions or to alter the optical train to enlarge the spot size without losing spectral resolution.

Surface contaminants, in the form of weathering products (both authogenic and allogenic), constituted a second problem, although one that was deliberately allowed to occur. In most cases, the surfaces examined on these samples were those naturally exposed in the field, because these are the surfaces that a remote sensing experiment would encounter. Thus, some idea of how such contamination can affect this type of experiment can be gained from the more contaminated samples, such as the 1A3 basalt, 2B5 dacite, and the nepheline syenite. Both 1A3 and 2B5 are Pisgah Crater area samples contaminated with a silt that seems common to the playa sediments of Lavic Lake, which is within a 2 or 3 mile radius of the location from which each of these rocks was collected. The 1A3 basalt sample surface was quite silty. In contrast to the cleaner 1A8 basalt sample, collected within 100 yards of 1A3, the 1A3 sample has an emittance minimum at about 9.5 μm; this emittance minimum is most likely caused in part by the silt, in agreement with R. J. P. Lyon's recent airborne spectrometer data of Lavic Lake playa sediments [33]. In Fig. 23e, curves of both exposed and fresh surfaces of the 2B5 dacite sample are shown. They demonstrate that the 9.5-μm emittance minimum in the weathered 2B5 curve is caused by the surface contaminant, which appears to be the same type of silt as that found on 1A3, i.e., a light-colored silt that seems to be composed of clay particles.

The final problem encountered involved an experiment that compared emittance calculated from reflectance measurements by means of Eq. (1) with directly measured emittances. A 45° folding mirror was placed in front of the source, facing down into a container of liquid nitrogen. A hemisphere of approximately 100°K radiation (limited by the emittance of the mirrors) was thus effectively produced around the sample, which was maintained at approximately 300°K by means of warm water circulating through the sample holder. The chopper was moved to a new position, in front of the monochromator slit. This experiment was designed to determine what spectral emittance differences one might expect when the sample temperature is changed from one that decreases toward the interior of the sample (negative temperature gradient) to one that increases toward the interior (positive temperature gradient). For a negative temperature gradient, the emittance is calculated from reflectance measurements, while for a positive gradient, direct emittance measurements are used.

Figure 25 compares the spectral emittances from Eq. (1) and from direct spectral emittance measurements for SA-49 rhyolite, A79 granite, A117 granodiorite, and EP-1 peridotite. Other samples measured in this way, with results now shown, are 2A1, 2B5, 2A3, E80A, 5B4, 1A3, 1A8, and AN. In almost all of the direct spectral emittance measurements, a local emittance minimum, which seems independent of sample composition, occurs in the 8.3- to 8.5-μm region. This result is thought to represent an experimental artifact, although its origin has not yet been deduced. Besides this anomalous minimum, the emittances measured directly are higher than those derived from reflectance measurements and Eq. (1). The lack of quantitative agreement is believed to result from the different temperature gradient in the two experimental cases and to an overestimate of the sample's surface temperature in the direct emittance case. The measured emittance is simply the detected emitted radiance divided by a blackbody radiance at the sample's surface temperature, which is estimated via thermocouples. Because of these difficulties, the reflectance measurements were chosen as the principal data set. The emittances from Eq. (1) (plotted in Fig. 23) are for samples with a negative temperature gradient near the outermost surface, as one would expect for rocks in the day-time. Figure 25, with the exception of that artifact in the 8.3- to 8.5-μm region, indicates that a positive temperature gradient, which would be expected under night-time conditions, should not produce emittances greatly different from day-time emittances.

The three useful results which can be derived from these data in their present state involve (1) the apparent transparent behavior of ferric oxide coatings in the 7- to 14-μm wavelength region, (2) the very uniform emittance of 25 of the 26 silicate samples in the 11.75- to 13.75-μm region, and (3) the excellent agreement between ratios calculated from the Pisgah Crater samples in this data set and those actually measured in scanner-produced ratio imagery from Pisgah Crater, California.

Sample 2A1 dacite is stained dark reddish-brown by ferric oxide, and yet, in the wavelength region from 7-14 μm, it has a distinctly different spectral structure from the ferric oxide coated basalt samples (including 1A3 and 1A8 from Pisgah Crater). This result indicates that in this wavelength region ferric oxide coatings do not appreciably alter the spectra of the underlying rock (for coating thicknesses on the order of 100 μm). As support for this argument, Fig. 26 shows an emittance spectrum calculated from Eq. (1) for a thick layer of rust (a millimeter or more in depth) on a piece of iron. The few spectral features of rust are not observed on the 2A1 dacite, 2A3 andesite, 1A3 basalt, or 1A8 basalt samples.

The second immediate result is the uniform emittance of all the samples, excluding peridotite, in the 11.75- to 13.75-μm wavelength region. The mean emittance for those samples in that spectral region is 0.956 ± 0.008, while peridotite, the most highly mafic sample, has a lower mean emittance, about 0.895. This uniform emittance for so many silicates indicates

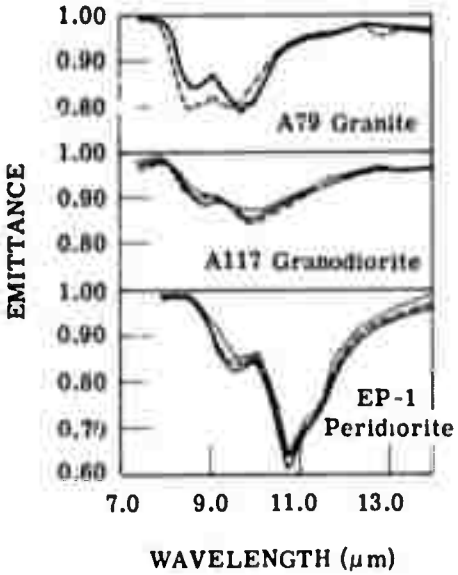

FIGURE 24. SPECTRAL VARIATIONS RESULTING FROM MEASUREMENTS TAKEN AT DIFFERENT LOCATIONS ON THE SAMPLES

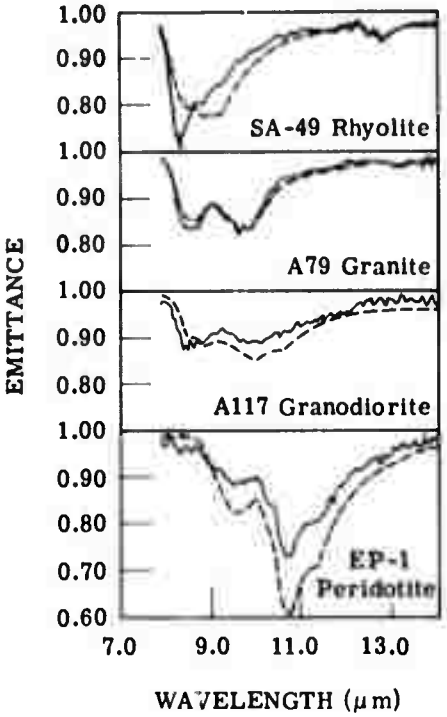

FIGURE 25. COMPARISON OF DIRECT SPECTRAL EMITTANCE MEASUREMENTS (SOLID LINE) WITH SPECTRAL EMITTANCE CURVES DERIVED FROM KIRCHOFF'S LAW AND SPECTRAL REFLECTANCE MEASUREMENTS (DASHED LINE)

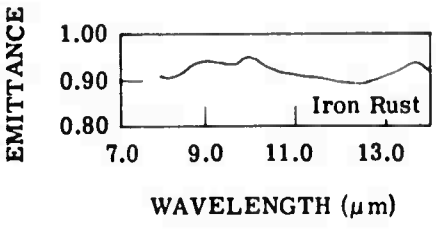

FIGURE 26. SPECTRAL EMITTANCE OF IRON RUST

that the 11.75- to 13.75-μm region is an excellent one in which to determine the temperature of a silicate target. Previously that assumption was made to facilitate temperature corrections of the Pisgah Crater scanner data [34]. Now it is quantitatively verified to be a valid assumption. Such knowledge should also improve the accuracy of absolute temperature measurements, which are important in the interpretation of thermal variations across the scene.

Finally, the $R_{1,2}(300^{\circ}K)$ values of Pisgah Crater samples from Table 4, when multiplied by a temperature correction factor $R_{gb}(300^{\circ}K) = 0.8429$ [34], agree quite well with the measured values from scanner data collected in an October 1970 flight under NASA Contract No. 9-9784. Figure 27 is a reprint of a figure from Ref. [35], which shows a digital ratio map of part of flight line 2, section A, 5 miles southwest of Pisgah Crater. The dacite in Fig. 27 marked D is represented by sample 2A1, which has a temperature-corrected ratio of 0.964, correctly represented by the lightest color range $R < 0.969$, where $R = R_{gb}(300^{\circ}K)R_{1,2}(300^{\circ}K)$. Also correctly in that range is the 2A3 andesite sample, located adjacent to 2A1. The alluvium A consists primarily of rock fragments of these two rock types. The Pisgah basalts 1A3 and 1A8 have temperature-corrected ratios of 1.013 and 1.025, respectively, which would make them fall into the darkest color range ($R > 0.992$). Accordingly, the basaltic Sunshine lava flows marked LA (not very different from the Pisgah basalt in percentage of SiO_2) are dark in Fig. 27. The playa material marked P consists mostly of clays that have a spectral behavior similar to sample 1A3, and hence patches of the playa appear to be in the darkest color range. In summary, there is excellent quantitative agreement between laboratory results as shown in Table 4 and field results (Fig. 27).

4.3. DESCRIPTION AND IMPROVEMENT OF THE VISIBLE-REFLECTIVE INFRARED RATIO TECHNIQUE

The visible-reflective infrared ratio technique, originally described in the NASA report of Ref. [34], is discussed in Section 4.1 of this report, excerpted from Ref. [16]. In short, a ratio of radiances collected in channel 5 (0.50-0.52 μm) to those collected in channel 7 (0.74-0.85 μm) was hypothesized as useful for mapping variations of iron oxides on exposed rock surfaces. That technique had not, however, been verified by laboratory data. The first step in proving its validity required a demonstration that the scanner data represent true spectral variations in the observed rocks. It is a crucial step, since good quantitative atmospheric data have not previously been available for this spectral region.

To correct this deficiency, spectral reflectance measurements of 14 Pisgah basalt samples were made on a Beckmann spectrophotometer with an integrating sphere reflectance attachment. The sample was illuminated near normal incidence, and reflected radiation was gathered over the whole hemisphere. The samples were of three eruptive phases of Pisgah basalt, including sample 1A3 (phase-3 basalt) and 1A8 (phase-1 basalt). Figure 28 shows the

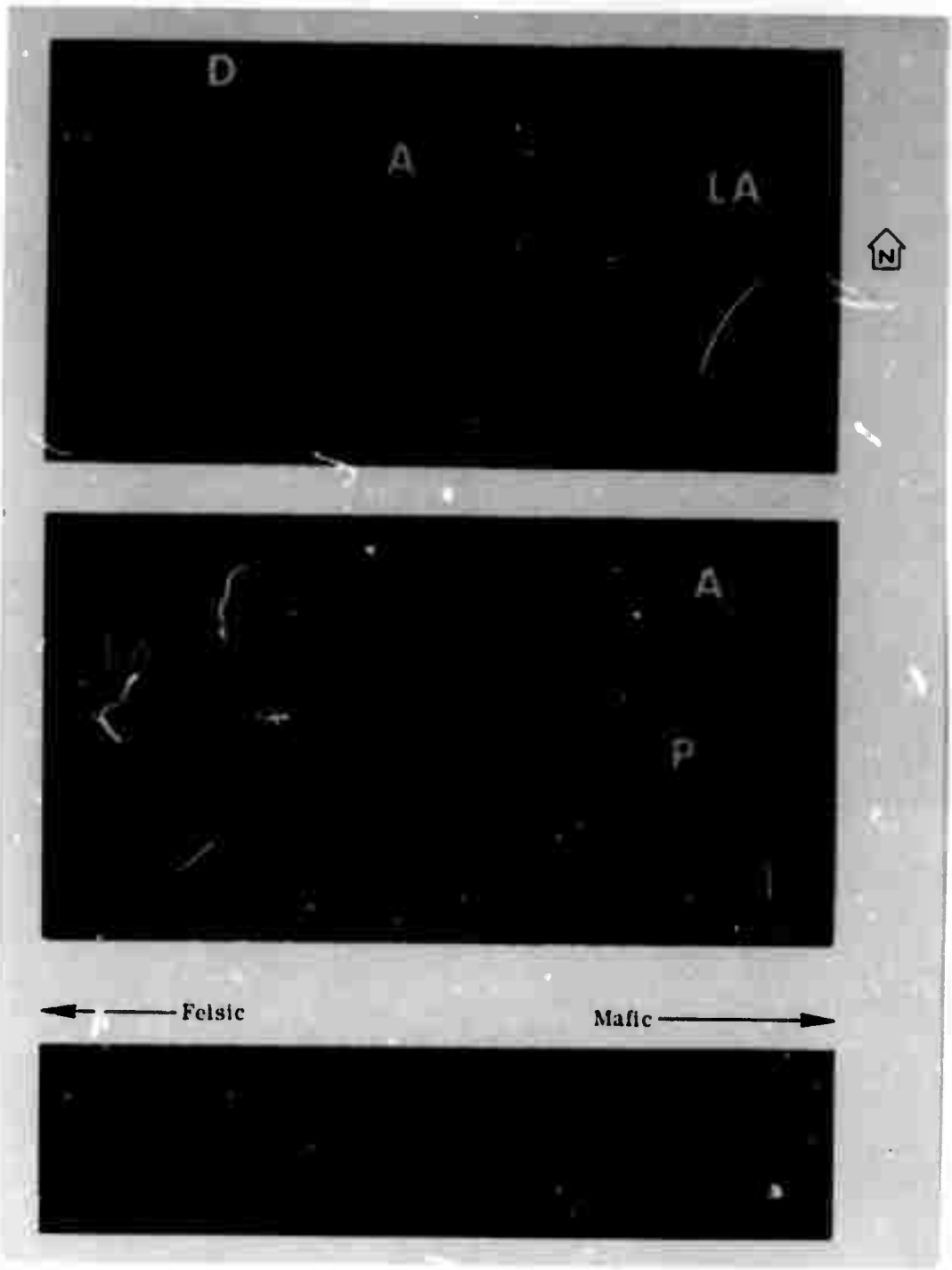

FIGURE 27. TEMPERATURE-CORRECTED RATIO RECOGNITION MAP OF SILICATE ROCKS NEAR PISGAH CRATER, CALIFORNIA. From Ref. [34].

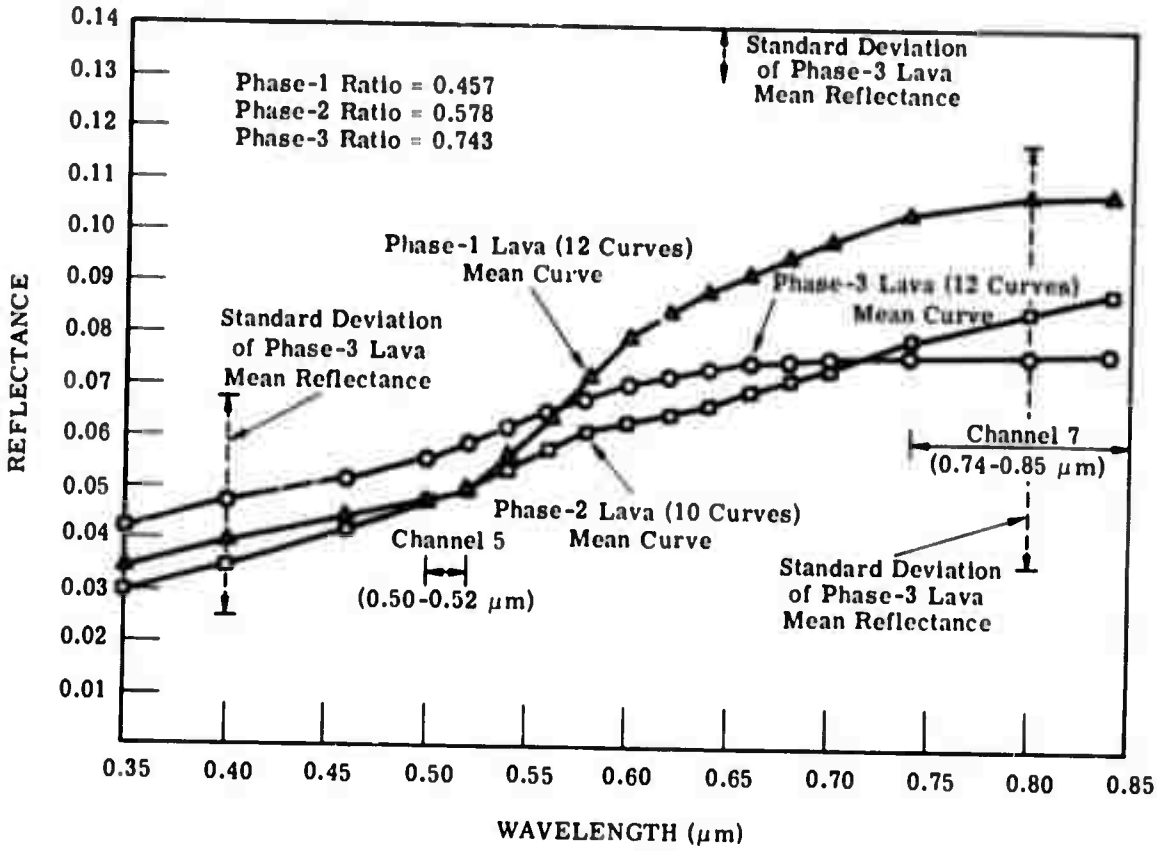

FIGURE 28. MEAN REFLECTANCE OF THREE LAVIC PHASES OF PISGAH CRATER BASALTS

mean curves for the oldest phase-1 lava (averaged over 12 curves), phase-2 lava (averaged over 10 curves), and the youngest phase-3 lava (averaged over 12 curves). The individual curves were taken from randomly collected samples and at randomly located spots on the samples. Some samples were measured at more than one spot. Although the standard deviation is large within a given lava phase, the mean curves indicate that the visible-to-reflective infrared ratios should increase from phase 1 to phase 3. The average reflectance ratios of channel 5 (0.50-0.52 μm) to channel 7 (0.74-0.85 μm) for lavic phases 1, 2, and 3 are 0.457, 0.578, and 0.743, respectively. On the average, then, phase-1 lava should appear the darkest of the three on the $R_{5,7}$ ratio image; phase 3 should appear lightest; and phase 2 should be an intermediate tone. An examination of Fig. 21, which shows single channel and $R_{5,7}$ ratio images of flightline 1, section A, confirms that the relative magnitude of the $R_{5,7}$ ratios as measured by the airborne multispectral scanner agree well with the laboratory-measured values. A more complete quantitative analysis is not possible because of lack of accurate atmospheric parameters.

Therefore, the $R_{5,7}$ ratio measured by a scanner can be used to monitor spectral variations of exposed rock surfaces, in spite of the fact that shadowing, scan-angle effects, and target-geometry variations are present across the scene. When the chemical analyses are completed, an attempt will be made to correlate the $R_{5,7}$ variations with Fe_2O_3 content of the basalt samples.

4.4. RELEVANCE OF THESE METHODS TO TUNNEL-SITE SELECTION AND OTHER BUREAU OF MINES PROBLEMS

The observation of surface outcrops, tracing of past landslides, and the determination of the number, yield, and pH value of existing springs and water courses are all important in tunnel-site selection. The ratio methods presented can aid in each of these areas. For instance, initial outcrop rock-type discrimination can be done quickly over large areas via airborne scanners. Although only igneous rocks have been considered in this report, these techniques should also be useful with sedimentary and metamorphic rocks. Discrimination between silicate and nonsilicate rocks is relatively easy, as has been shown between quartz sandstone and limestone [35]. Image ratioing is also a good method for detecting outcrops, even if they are only a few feet in diameter (for lower altitude flights) and in small clearings between the trees. These techniques should prove superior both to aerial photography and field observation for the location of outcrops, except in very dense vegetation.

These techniques should prove as good as aerial photographic methods for tracing past landslides and could prove to be even better if the rock types involved are appreciably different in SiO_2 content, but similar in visible color. The infrared technique has been useful, for instance, in distinguishing volcanic rhyolitic ash flown from less acidic detritus, where the two materials were indistinguishable in aerial photographs [34].

The determination of the number, yield, and pH values of existing springs and water courses can probably also be assisted via these techniques, although there have been no test cases of that nature as yet. Stream-bed sediments can probably be correlated with their parent materials, if the whole upstream channel is flown. Although water is opaque to thermal infrared radiation, the water edges can be identified. From these data, one could calculate volume flow, if the standard channel width (including the whole stream bed) to channel depth model is used, along with the measured water level. Finally, some information regarding the pH values of streams might be obtained by mapping ferric oxide stains on the banks of acidic streams or on the bottoms of intermittent acidic stream beds. Such mapping could be accomplished with the visible-reflective infrared ratio technique. Although false-color photography would also detect the ferric oxide stains, the scanner ratio method is insensitive to shadowing effects, which makes it superior for shadowed stream beds. The ferric oxide stain mapping procedure might also be useful for monitoring acidic water runoffs from either surface strip mines or abandoned underground coal mines, both considerable water-pollution hazards.

Finally, these techniques should eventually be useful for rapid assaying of identifiable regions of surface ore deposits, although more laboratory measurements similar to the ones presented in this section would be needed, so that correlations could be made between observed ratio values and bulk content of the mineral resource to be mined. The use of these techniques should be especially useful when rapid decisions must be made by the Department of Interior concerning the designation of wilderness areas.

5
APPLICATIONS OF SIDELOOKING RADAR TO GEOLOGIC INVESTIGATIONS

5.1. INTRODUCTION

Sidelooking airborne radar (SLAR) has imaging capabilities that both supplement and complement the passive remote sensors. Although SLAR effectively collects geologic information when used alone, maximum data will be obtained if it is used prior to ground studies in conjunction with other sensors, each contributing its special information. Sidelooking radar has the same limitation as multispectral scanning and aerial photography in that it provides information, often relatively detailed, about surface and very near-surface geology, but no definite information about geologic features more than a few inches beneath the surface, since the wavelengths presently being used (mainly K-, X-, and L-bands) have very limited penetration into geologic materials. Radar penetration of geologic materials increases as the wavelengths get longer. The use of much longer radar wavelengths (several to tens of meters) should provide useful information, depending upon the terrain conditions, about deeper geologic

features (such as buried structures and rock types), but the interpretation of such imagery will be more difficult and more subject to error than that of present radar imagery. In general, the major geologic advantage of SLAR is that it detects and identifies surface features more thoroughly and therefore aids the geologist in making inferences about subsurface features.

Sidelooking radar has several advantages over multispectral scanning and aerial photography aside from the fact that it collects information from a different part of the electromagnetic energy spectrum. As an active sensor, SLAR provides its own source of illuminating energy and records the energy reflected back. Therefore, radar imagery can be obtained without regard to sun conditions. Radar penetrates fog, haze, and all types of clouds except cumulonimbus (thick, dense moisture-laden clouds). Although rain attenuates the radar signal, the extent of attenuation depends upon the radar wavelength and the rate of rainfall; some radar wavelengths will not penetrate a heavy rain. Thus, SLAR is essentially an all-weather, day or night sensor which is not affected by daily variations in temperature and sun illumination. Radar is the only sensor capable of producing the same high quality imagery of a region regardless of the time of day or season of year. The advantages of using SLAR to gather geologic data in regions of adverse weather and/or sunlight conditions are obvious. Such adverse conditions commonly exist in the polar regions, especially during winter. Sidelooking radar recently provided the first imagery of the entire Darien Province, Panama, which is essentially cloud covered year around. In the past 20 years, only a small portion of the province was ever photographed because of the cloud conditions. Berlin and Schaber [36] state that it is readily becoming apparent that SLAR (operating at K-band and longer wavelengths) is the only sensor that can be used with a high degree of success in the humid tropics.

Although it appears possible that some radar wavelengths penetrate certain types of vegetation, other radar wavelengths will not penetrate any vegetative cover. Longer wavelengths than those presently being used very likely will be able to penetrate vegetation and provide information on the nature of the ground surface. Much more research is needed to determine the penetrating capabilities of various radar wavelengths, to ascertain the types and characteristics of vegetation that can be penetrated, and to provide information on the extent to which the vegetation and ground surface each contribute to the total radar return.

Radar shadows are created when the unidirectionally transmitted energy is blocked by a terrain feature which prevents the energy from reaching the shadowed area behind the feature. Relative relief and roughness of the terrain are portrayed on SLAR imagery mainly by the distribution of radar shadows. Radar imagery is similar to a shaded-relief topographic map in that the shadowing creates a three-dimensional effect. Extensive and/or excessively dark shadows, particularly in high relief areas, commonly mask features and details and hinder geologic interpretation. By careful choice of the look direction and depression angle, radar

shadowing can emphasize any preselected direction of topography. Radar shadows are extensively used in interpreting structural, geomorphic, and local lithologic units seen on the imagery. Because of the high depression angles (45-60°), shadowing will be much less extensive on radar imagery obtained by satellites scheduled to be launched in the next several years. Although the reduced amount of shadowing will somewhat hinder interpretation, more total terrain area and more geologic features will be visible.

5.2. SIMULATION OF RADAR IMAGERY BY MEANS OF LOW SUN-ANGLE PHOTOGRAPHY

Lyon, Mercado, and Campbell [37] have shown that low sun-angle photography (LSAP), taken under specified conditions, approximates SLAR imagery made at comparatively high depression angles. They state that by using a low sun-angle (around 20-30° above the horizon) combined with an increase in the γ-contrast of the prints to intensify the blackness of the shadows, one can produce aerial photography with some of the shadowing features of radar imagery used in geologic interpretation. Low sun-angle photography has some advantages over SLAR: it is less expensive over limited areas than radar imaging and requires no electronic gear. Also, the quality of the imagery, when conditions are optimum, appears to be equal to that of SLAR imagery. However, in addition to the necessity for clear weather, LSAP has other important disadvantages: (1) sun angles can only be chosen from a finite set of elevation and azimuth angles; (2) a particular solar elevation and azimuth must be used at different times of the year for a specific latitude to get photographs which closely simulate radar imagery. Lyon et al. [37] report that "one should plan the use of the sun in azimuth, as well as in elevation, to enhance the lineations. If north-south linears are present, one should use the dawn or dusk sunlight; if east-west, the winter sun, and so on. Above all, one should plan to use several illumination angles." Normally it would not be possible to wait long enough to satisfy the conditions necessary for LSAP simulation of radar imagery.

It should be remembered, however, that low-sun angle photography and SLAR do not present similar information for at least two reasons. First, unlike optical wavelengths, radar wavelengths interact with surface textures with roughness on the order of radar wavelengths. Second, the albedo of the surface does not correspond to the dielectric constant at microwave frequencies.

5.3. STEREOSCOPIC SLAR IMAGERY AND AREAL COVERAGE

It is presently possible to generate limited amounts of stereoscopic SLAR imagery by overlapping adjacent flight lines. Stereoscopic SLAR imagery enables one to interpret the imagery qualitatively to determine if the shadowing is caused by topography or by the differing reflective properties of materials.

Without stereoscopic coverage, techniques which aid in the differentiation of areas of diverse relief are very helpful. As indicated earlier, limited shadowing can give SLAR imagery a pseudo three-dimensional appearance. Dellwig, MacDonald, and Kirk [38] describe a simple, relatively inexpensive technique which imposes a pseudo three-dimensional effect upon monoscopic SLAR imagery. This technique is easily applicable to the present methods employed for monoscopic imagery viewing and interpretation and facilitates the interpretation of radar imagery in areas of low relief, such as the Gulf Coast. Magnification by a binocular microscope causes the three-dimensional effect to become even more pronounced, allowing an interpreter to identify readily features that formerly were on the threshold of recognition [38]. The technique is known only to exaggerate the relative relief, its radargrammetric value not having been investigated.

Sidelooking radar is capable of providing broad areal coverage, on either a single film or on a mosaic, in a minimum amount of flight time. This coverage is difficult to obtain by any other sensor. The continuity of regional structures and landforms can easily be traced for long distances on SLAR single images and mosaics, and the regional, commonly deeper extending, structural pattern can be determined. This identification would not be possible with aerial photography without extensive use of mosaics, which could very possibly hinder the tracing of the desired structure or landform.

5.4. RADAR RETURN PARAMETERS

Sidelooking radar imagery portrays the reflectance characteristics of the terrain for certain wavelengths of the electromagnetic spectrum that are much longer than those of visible light. Those parameters generally agreed upon as most significantly affecting the general radar return are surface roughness, topography (including orientation and slope of surfaces), complex dielectric constants of soils and rocks, object geometry, moisture content of the feature (especially near the surface), type and extent of vegetation, moisture content of low vegetation (such as brush, crops, and grasses), and the incidence angle, wavelength, and polarization of the transmitted radar energy. Rydstrom [39] also considers the manner of illumination by radar, i.e., unidirectional illumination, to be a fundamental parameter. The relative value of the different parameters commonly is difficult to assess, even after a comprehensive study. Generally, several parameters contribute to the magnitude of the radar return, but one parameter may be dominant. The relative importance of each parameter depends upon the feature and region being imaged.

A surface with roughness less than the wavelength of the incident electromagnetic energy appears smooth and flat to the energy and acts as a specular or mirror-like reflector. The specular reflection may be either a strong return or a no-return, depending upon the angle at which the energy strikes the surface. Rougher surfaces appear multifaceted to the incident

energy and act as diffuse reflectors, scattering energy unequally in all directions. Diffuse reflectors return only a fraction of the energy to the antenna. Because radar wavelengths are much longer than those of visible light, many more surfaces appear smooth to radar energy than to visible light. Thus, radar imagery displays a greater number of specular reflections than does aerial photography. Depending upon the particle diameters and radar wavelength, silt, sand, and gravel deposits can act as specular reflectors. Water bodies with smooth horizontal surfaces act as specular reflectors and are recorded as no-returns on the imagery.

The complex dielectric constant of the soil or rock is directly determined by its chemical and mineralogical composition, moisture content, conductivity, and porosity. What part each of these factors, plus possibly others, plays in determining the complex dielectric constant of a material is generally hard to determine. Gillerman [40] noted a difference in the return on simultaneously obtained like- and cross-polarized K-band radar imagery of rhyolitic to basaltic Tertiary volcanic rocks in the western United States. He suggests that mineral composition an and glass content may play a part, although very likely a subtle one, in causing the difference in return. He also speculates that the age of the rocks, as it might be related to compositional differences and degree of weathering, may be a factor contributing to the difference in the radar return of the lava domes and craters of Mono Craters, California. The complex dielectric constant varies directly with the moisture content of the soil or rock, and high moisture content, especially near the surface of the feature, causes a bright or very light toned return on the radar imagery. Examination of imagery during the course of this contract suggests that a high moisture content of soil and rock may so dominate the other radar-return parameters as to be essentially the only parameter influencing the return. Accordingly, radar imagery of a region generally should be obtained during a dry period. The texture of the rock, including crystal orientation and possibly crystal size, influences the rock's conductivity. Cosgriff, Peak, and Taylor [41] discuss the variations in radar return from materials of many different compositions.

The angular relationship between the surfaces of a geologic feature, i.e., the object geometry, greatly influences the strength of the radar return. Radar energy may or may not be specularly reflected back to the antenna from a right-angled dihedral corner reflector. A trihedral corner reflector in which the three surfaces are mutually perpendicular will return a strong specular reflection to the antenna regardless of the look direction. Rydstrom [39] ably illustrates the relationship between dihedral corner reflectors and specular reflection.

Vegetation causes diffuse radar reflections. Because the radar energy is primarily returned from the first reflecting surface that is encountered, the return may be mainly from, and thus more indicative of, the vegetative cover than the underlying soil or rock. Thus, the type and extent of vegetation are very important radar return parameters. Radar imagery of

areas with a heavy vegetative cover will appear much different than that of areas without vegetation or with only sparse vegetation. The differences in the radar images of various types of vegetation may indirectly indicate differences in the underlying soil or rock, such as the thickness of the soil or the mineral content of the soil. The occurrence and distribution of substantial forested areas may indirectly indicate the topography. The radar return varies directly with the moisture content of low vegetation; high moisture content causes high-energy, light-toned returns.

The incidence angle, wavelength, and polarization of the transmitted radar beam are the only radar-return parameters which can be chosen and directly controlled. The incidence angle on a particular surface(s) and object geometry control how much energy, if any, is specularly reflected from the surface(s) back to the antenna. Radar shadowing, radar layover, and radar foreshortening of a particular terrain are functions of the general incidence angle of the terrain, which is the complement of the depression angle of the radar beam (Refs. 42 and 43).

The same feature commonly looks different on imagery of different wavelengths, and the interpretation of the imagery of the two wavelengths commonly yields different information about the feature. Thus, it is desirable to image the same area with different radar wavelengths, simultaneously if possible. Not only are the penetration characteristics of the various wavelengths different (although none of the present radar wavelengths can penetrate to more than a very shallow depth), but the specular-diffuse reflection boundary in terms of particle size is different. Even though more areas are being imaged by two different radar wavelengths, it has not been possible previously to do so simultaneously. The inability to image simultaneously has obvious disadvantages, since return parameters such as moisture content of the soil or rock and vegetation characteristics (type, extent, moisture content) can easily change between flights. Willow Run Laboratories, by means of a new multiplexed radar system, will soon have the capability of simultaneously imaging an area with two different radar wavelengths.

A feature commonly appears different on the simultaneously produced like- and cross-polarized radar imagery of a particular wavelength, and the difference in appearance provides information about the feature. Four differently polarized images generally are obtained for one radar wavelength. Radar energy is transmitted linearly polarized (either vertical or horizontal) and is returned to the antenna either linearly polarized to produce like-polarized (HH and VV) radar imagery or orthogonally polarized to produce cross-polarized (HV and VH) radar imagery.

Certain return parameters are more important than others in determining the appearance of geologic features on radar imagery. The most important parameters generally are topography, surface roughness, object geometry, complex dielectric constants, and the incidence angle, wavelength, and polarization of the transmitted radar energy. Rydstrom [39] would add the unidirectional illumination of the terrain by radar as a fundamental return parameter; it

may or may not be, but certainly it is a large factor in how the geologic feature looks on the radar imagery.

At the present time, the other parameters are generally considered to be much more important than the complex dielectric constant (composition) of the soil or rock in determining the radar return of a geologic feature; indeed the contribution to the return by the other parameters masks the lesser contribution made by the composition of the material. However, certain compositional characteristics of rocks may be inferred from their physical configurations, which affect the radar image more directly [39]. Generally, it is only possible to differentiate between crystalline and sedimentary rocks and then only on the basis of the inherent characteristics of the rock classes (bedding, jointing, object geometry) and not on the basis of mineralogy or chemistry.

The unidirectional illumination of the terrain by radar energy creates radar shadows which give the imagery a pseudo three-dimensional appearance and indicate the topography and relative relief. Radar imagery generally shows smaller variations in surface relief than does aerial photography. The topography and relief, discussed later, are important parameters used in identifying structural and geomorphic features, especially linear ones.

Look direction is an important factor in whether structural lineaments or linear geomorphic features are readily recognized. A study by MacDonald, Kirk, Dellwig, and Lewis [44] showed that lineaments normal to or at a high angle to the look direction are much more easily seen than those that are not. Lineaments parallel to the look direction commonly are not seen at all. Obviously, the geologic feature may be enhanced or not seen depending upon its orientation to the look direction. Lineaments not seen or only faintly seen on the imagery obtained with one look direction may be clearly visible on the imagery obtained from another look direction. MacDonald et al. [44] state that the maximum geologic information from radar imagery of an unmapped or poorly mapped region can be obtained by imaging the region from four orthogonal look directions, but that imagery taken using only one look direction can still contain significant information.

A surface composed of particles with diameters less than the wavelength of the incident radar energy appears smooth and flat and generates specular reflections. Thus, silt, sand, gravel, and glacial deposits commonly can be differentiated as to the type of deposit, but not as to composition, by determining whether they act as a specular or diffuse reflector for a particular wavelength. This differentiation of grain size is best done by imaging the deposit with two or more radar wavelengths, such as will be done with the new multiplexed radar system. Surfaces that appear rough to one wavelength may appear smooth to another. Smooth, essentially horizontal, specular surfaces (such as playas) are recorded as no-returns and generally are easily recognized in arid environments. However, areas within a playa of high

near-surface moisture content and/or vegetation content may be imaged as local bright spots. Using shorter wavelength radars, alluvial fans can be readily distinguished from playas by their diffuse reflections as well as by their characteristic fan shape. Coarser debris such as boulders in a dry stream bed, distributary channels of coarse material, and talus slopes generally will show as high returns on shorter wavelength radar imagery, a result which can be misleading. Lava flows have rough surfaces and thus generally show a moderate to high return on radar imagery.

Topography and surface roughness are particularly important parameters in determining the radar-return signal that is especially applicable to the recognition of linear features and geologic boundaries (Gillerman, Ref. 45). There commonly is a correspondence between the topography and the underlying structure or geomorphic feature, and this relationship is particularly well displayed on SLAR imagery. The topography can reflect either different resistances of rocks to erosion or structural or geomorphic patterns. MacDonald's study [42] of the radar imagery of Darien Province, Panama, showed that in areas of substantial forest cover, where the radar return is primarily from the foliage, the imagery indirectly depicts topography.

Faults, joints, and contacts between different lithologic units commonly have relatively shallow depressions along them which are enhanced by the shadowing effect of SLAR. Generally, many more of these structural features can be seen on SLAR than on aerial photography or as proven by many studies, such as multispectral scanning, Gillerman [45]. Topographically expressed folds are clearly displayed and traced on SLAR imagery. Indeed, the regional fold and fracture patterns commonly are more easily delineated on SLAR imagery, with its synoptic view, than on aerial photographs.

It must be kept in mind that shapes are distorted by the near-range compression of slant range radar imagery. The elongated distortion of shapes parallel to the ground track is a problem when delineating landforms which might have structural significance (Lewis and MacDonald, Ref. 43). Wing [46] and Wing, Overbey, and Dellwig [47] point out that is is important to distinguish on slant range imagery, with its nonuniform distortion, between lineaments that are truly straight and those that only appear to be. Straight parallel lines on the ground do not appear such on the imagery, unless they are either 90^{o} or 180^{o} to the flight line. Slightly curved lineaments, approximately parallel to the flight line, may appear straighter in the near range, and straight lineaments can appear curved if they are long enough and not oriented 90^{o} to the flight line. Much of the problem of lineament distortion is compensated for by plotting the lineaments on topographic maps, provided large scale coverage is available [46, 47].

The object geometry of rocks plays a large part in their appearance on radar imagery. Rocks with surfaces that form dihedral or trihedral corner reflectors commonly return much

more energy to the antenna, and thus they appear much lighter toned on the imagery than they would if the natural reflectors were not present. Trihedral corner reflectors will return a high amount of energy regardless of the look direction, but the highest return from dihedral corner reflectors is from those oriented normal to the look direction. Sedimentary rocks, such as limestone or dolomite, in which there are a large number of joint planes perpendicular to each other and to the bedding planes commonly contain many dihedral and trihedral corner reflectors. High returns can be expected from the cliff faces of such rocks and from valleys cut into them. The irregular surfaces of lava flows commonly form corner reflectors so that the return from lava flows is both specular and diffuse. Plutonic igneous rocks should contain few, if any, corner reflector surfaces, while the number of corner reflectors to be found on metamorphic rocks is determined by the amount of foliation on the rock, its resistance to erosion, and the degree of jointing.

5.5. USE OF WIDE DYNAMIC RANGE OF RADAR

Both synthetic and real aperture radar systems are capable of a wide dynamic range of up to approximately 60 db. However, images used for interpretation are most often recorded on photographic paper with a dynamic range of perhaps 15-20 db. Geologic diagnostics available from subtle tonal gradations are lost when such processing methods are used. Usable data are degraded and useful diagnostic information destroyed. The degradation of the imagery is approximately $1/2^{10}$ (1/1024) in energy or $1/2^{5}$ (1/32) in amplitude of the available tonal gradation (conservatively based on 50-db recording and 20-db photographic printing).

Although the signal film of the synthetic aperture radar will only record a dynamic range of approximately 20 db, the signal is spread over a relatively large area and is then compressed to a small area. The ratio of areas is the factor of improvement in dynamic range. Recently N. Massey of Willow Run Laboratories developed a means of making from signal film a hologram which can be viewed, or scanned, in a simple optical viewer. The subtle gradations of tone resulting from the larger dynamic range are thus accessible. Also, Willow Run Laboratories is presently installing an image dissector with analog to digital conversion to obtain a wide dynamic range and to enable sophisticated digital processing. During this contract, however, we did not have holograms of suitable geologic features, nor was the image dissector available to determine the usefulness of a wide dynamic range to the selection of tunnel sites.

A wide dynamic range, properly used, might allow for the successful identification of fault zones, an important feature in the selection of tunnel sites. Without such a wide dynamic range, our ability to identify such zones has been limited. For example, in the Arbuckle Mountains of Oklahoma, a fault zone had been identified by means of predawn far-infrared imagery [5] which revealed a drop in temperature caused by evaporation of water, with a slightly greater amount of moisture in the fault zone than in the environs.

We examined classified radar imagery of the area in an attempt to identify this fault zone, assuming that radar's sensitivity to moisture would help in the delineation of the feature. Difficulties in optical processing produced unsubdued speckle patterns, and the feature could not be identified. Later a technique termed noncoherent integration was used to process the imagery to bring out ground painting. In the processed imagery, the fault zone appeared slightly darker in tone, and the tonal difference was similar to that found in some published works illustrating the use of radar imagery in identification of fault zones. This tonal difference might have been caused by a slight difference in vegetation, however, and microdensitometer traces across the film were inconclusive. Had a larger dynamic range been available, the subtle gradations in tone might have allowed precise identification of this fault zone.

During the period of the ensuing contract, we will have available holograms of geologic features and an image dissector with analog to digital conversion, both of which will produce a wide dynamic range. With the image dissector, level slicing can be performed on the digital output of the optical processor. Either the output of the optical processor or the holographic viewer image can be used for level slicing. With the larger dynamic range from which to choose, level slicing becomes a powerful diagnostic tool, which may well be used effectively in the identification of geologic features.

5.6. OPTICAL PROCESSING FOR ENHANCEMENT OF GEOLOGIC FEATURES*

Coherent radar imagery has shown considerable usefulness for all-weather mapping of terrain. The complex scattering mechanism in radar imaging is strongly affected by geomorphic factors and tends to enhance subtle topography and vegetation [39]. The ability of a radar image to reveal small tectonic features and lineaments has been recognized by others; Rowan and Cannon [8] have utilized radar imagery to locate both previously mapped and newly discovered faults in the Mill Creek, Oklahoma area.

Although radar imagery effectively displays a large number of geomorphic features, it still absorbs a considerable amount of a geologist's activity to locate and map tectonic features. Particularly in view of the image coverage afforded by a radar sensor, whereby geologic mapping can be extended over much of the earth's surface, the present capacity to collect radar imagery is far beyond that of geologists to examine, analyze, and interpret it adequately.

This problem could be alleviated by processing the imagery to reduce the amount to be examined, allowing the geologist to use his talents for interpretation of the structural signatures. Since the images are two-dimensional, it is natural to consider a form of optical processing which can operate upon the imagery without transformation.

*Section 5.6, authored by Ralph Mitchel, was originally published in the semiannual report on this contract, Ref. [16].

Coherent optical systems, in particular, are suitable for interpreting radar imagery. Along with the capability of analyzing each point of the image simultaneously, coherent optical image-processing systems possess a physically accessible Fourier transform plane, allowing the spectrum of an image to be modified. Thus, linear filtering operations can be performed upon the imagery very rapidly. Examples of the filtering operations commonly performed by a coherent optical-processing system are directional filtering, matched filtering, and image enhancement.

A series of experiments was performed on some high-resolution, synthetic-aperture radar imagery collected by The University of Michigan to evaluate the usefulness of coherent optical processing as an aid to the geologist. The area mapped was near Mill Creek, Oklahoma, an area underlain by gently folded, severely faulted pre-Pennsylvanian rocks, parts of which are covered by Pennsylvanian sandstone and conglomerates of the lower part of the Pontotoc Group. The major faults and folds in these pre-Pennsylvanian rocks run northwest-southeast. In many regions, the conglomerates lack the extensive structures which might reveal offsetting. Rubble along a fault trace appears similar to the parent rock, making the recognition of a fault difficult, even with meticulous field work.

Optical directional filtering experiments were attempted on this imagery with little success. Narrow angular wedges placed in the optical system to modify the spectrum of the radar imagery produced poor discrimination. Although the filtered image had poor contrast, it did contain many streaks identifying lineaments. However, this type of filtering did not effectively reduce the information to be interpreted. Similar results were obtained when a two-dimensional Gaussian slit was used to modify the spectrum of the imagery.

In an effort to obtain better discrimination, optical matched filtering was attempted. The mathematical model that we utilized for the radar energy reflected from a fault trace and recorded on a radar image was as follows:

$$i(x, y) = I_o \, \mathrm{Rect}\frac{x - x_o(y)}{2\Delta(y)} \, \mathrm{Rect}\frac{y - y_o}{2a}$$

where i = the radar imagery reflected from a fault trace and recorded on a radar image

x = coordinate across width of fault trace

y = coordinate along length of fault trace

I_o = a constant

2Δ = width of the fault trace

$2a$ = length of the fault trace

x_o = path taken by a fault trace

$x_o(y)$ = center of fault trace as a function of the location along its length

y_o = center of fault length

2Δ and x_o are written as functions of the length y, since the trace may not be of constant width or exactly straight.

We defined probability measures over x_o, Δ, and a, along with the associated probability density functions $f_{x_o}(x)$ and $f_\Delta(x)$ over x, as well as $f_a(y)$ over y. $x_o(y)$ and $\Delta(y)$ are random processes; i.e., for each y they are random variables. We assumed that $f_{x_o}(x)$ is symmetric around some value $x_o(y) = M$ (the centroid of a fault trace in the x-direction); that $f_\Delta(x)$ is symmetric at about $\Delta(y) = \lambda$ (average width of a fault trace); and that $f_a(y)$ is symmetric at about some mean value $a = \alpha$ (average length of a fault trace).

The probability $i(x, y) = I_o$ is the probability (P) that $x_o - \Delta \le x \le x_o + \Delta$ and $-a \le y \le a$, which can be computed to be:

$$P[i(x, y) = I_o] = \left\{[f_\Delta(-x) - f_\Delta(x)] * F_{x_o}(x)\right\}[F_{-a}(y) - F_a(y)]$$

$$= \left\{[F_{-\Delta}(x) - F_\Delta(x)] * f_{x_o}(x)\right\}[F_{-a}(y) - F_a(y)]$$

where F = the probability distribution function.

A particular case should, however, be noted; when the fault trace is narrow, having a constant width ($2\Delta = 2\epsilon$), where 2ϵ is on the order of the radar image's resolution, we have:

$$P[i(x, y) = I_o] = f_{x_o}(x)(2\epsilon)[F_{-a}(y) - F_a(y)]$$

That is, the probability of the fault trace's existence at a particular point is defined in terms of the probability density function of the random variable defining its path.

For the case of uniform noise, a coherent optical correlator using a matched filter in the form of a complex spatial filter can display an output light amplitude distribution proportional to the cross correlation between a reference signal (stored on the filter) and the input image. The results of the experiment utilizing optical matched filtering were mixed. Some of the known faults were not detected. However, with the filter described above, we were able to locate the contact separating the Deese and Dornick Hills formations.

The last experiment performed was image enhancement, designed to eliminate from the radar image that information which is unnecessary to geologic interpretation. The low spatial frequency portion of the image's spectrum was removed by means of a spatial filter. In the processed image, structural edges and lines dividing differently reflecting terrain regions were emphasized. As a result, this experiment allowed geologic interpretation with much less time and effort than that required by the unprocessed pictures.

6
FUTURE RESEARCH

6.1. RECOMMENDATIONS

Future research in the applications of remote sensing techniques to tunnel-site selection should be concentrated in three categories: (1) field test cases; (2) continued development of remote sensing systems as defined under this contract, i.e., multispectral scanning, sidelooking radar, and aerial photography; and (3) the addition of other kinds of sensors, including physical field sensors, for a complete remote sensing system.

6.1.1. FIELD TEST CASES

Although we know that we can obtain synoptic remote sensing data which can complement information acquired from other types of geologic investigations, these data must be evaluated experimentally. For such an evaluation, we need a test area comprised of crystalline and other rock outcrops in which folding, faulting, tilting, jointing, and weathering have occurred.

In the continuation of the work described in this report, we have chosen as a test site a region in the Black Hills, South Dakota, where the surface exhibits great geologic and lithologic diversity. Sidelooking radar imagery of this region has been received from the Strategic Air Command, and multispectral scanning and concurrent stereographic aerial photographic flights were obtained in May 1972. Ground-truth studies of the test site were made at the time of the flights. We will undertake to use all of the remote sensing data to infer the geology and lithology by attempting to reconstruct, extend, and possibly correct the present knowledge of the geology of the region, and we will then evaluate our efforts.

Remote sensing tests of present tunnel sites in which geologic difficulties have been encountered should also be undertaken. If the precise geologic features which caused the difficulties could be identified or detected for subsequent identification, the value of remote sensing techniques in tunnel-site selection would be confirmed. Unfortunately, no tests of this kind are presently funded.

6.1.2. CONTINUED DEVELOPMENT OF MULTISPECTRAL SCANNING AND RADAR SYSTEMS

Within this contract period, for the first time multispectral scanning systems have been shown to be capable of identifying the chemical content of rocks. As described in Section 4, SiO_2 and ferric oxides have been identified by means of a ratioing technique which takes advantage of the fact that spectral characteristics of radiation depend upon the material which emits or reflects that radiation. Although Vincent has demonstrated this capability with only two chemical compositions, the basic technique could be used for many different geologic materials. Investigations into the applicability of this technique to the identification of other

geologic materials should be continued. With the further development of such techniques, more complex lithology could be classified and more effective geologic reconnaissance performed.

Although multichannel processing of data by means of statistical pattern recognition is quite well developed, its application to geologic investigations has been limited. Wagner shows, however, the applicability of the method to the identification and classification of surface features. Although much remains to be done to correlate this technique with other data processing methods, without doubt multichannel processing not only utilizes the spectrum in a more sophisticated way than does ratioing but also can be used to identify materials relevant to the selection of tunneling sites.

The structural geologist may be able to utilize the technique at optimal effectiveness by interacting directly with the computer, since geologic inferences require considerable knowledge and experience. The scene could be presented on the screen, and the interpreter could choose the spectral bands he wished to use and the defined area he wished to investigate. With a double cursor, he would define the area, and the computer would immediately present on the screen those areas which were within a preset deviation of the channels found within the defined area. The geologist could then draw upon his experience to ascertain if the rock in the different areas was of similar composition or possibly from the same formation. Such interaction with the computer might offer more effective data processing for geologic investigations, and such processing techniques should be developed to be used with known spectral signatures.

The emphasis of future developments in sidelooking radar is upon multipolarity and multifrequency radiation. Willow Run Laboratories is presently capable of collecting both X-band (3 cm) and L-band (30 cm) radar imagery; however, data are not presently collected simultaneously in the two bands. On one pass imagery is collected in one band, and then the antenna is changed and an attempt made to collect imagery of the same area and the same flight direction in the other band. Since the imagery from the two flights can not be superimposed, we have not been able to process both bands automatically by means of ratioing or image subtraction.

Willow Run Laboratories will soon, however, install a new multiplexed radar system which will allow the simultaneous collection of both X- and L-band imagery on one pass over an area. Superimposible imagery will allow automatic processing, and the bands can be ratioed to delineate surface textures. Simultaneously collected radar data will extend the possible geologic applications discussed in Section 5.

6.1.3. THE ADDITION OF OTHER KINDS OF SENSORS FOR A COMPLETE REMOTE SENSING SYSTEM

If remote sensing is used for geologic reconnaissance (and this report has shown the benefits to be gained from its use), all types of airborne sensors should be included, preferably aboard a single aircraft. The latter requirement might not be feasible, however, in certain cases, such as the inclusion of both a gamma-ray sensor and sidelooking radar; gamma-ray sensing is most effective at very low altitudes, while radar is used at a relatively high altitude.

Even if different aircraft must be used, however, the increase in the amount of confirming data that could be gathered by the additional systems offset the cost. Thus far, we have been concerned with detecting, identifying, and mapping geologic units, and we have emphasized surface structural details, such as faults, joints, soil moisture, drainage patterns, and general geomorphology, since these data are necessary to infer geologic features at depth. To increase our ability to define and map surface features, a passive microwave sensor system and a gamma-ray (nuclear radiation) sensing system should be added.

Sensors of volume characteristics rather than of surface characteristics should also be utilized, particularly since the geologic formations at depths of a mile or more are important in tunneling. The direct sensing of the extent of buried rock masses could provide valuable geologic information. Also, just as inferences about structures at depth can be made from surface data, knowledge of surface formations can be rendered more complete by data on subsurface features. The most complete knowledge of the geology of a region is achieved when both kinds of data are used. Three volume sensors that should be considered are the magnetometer, the gravimeter, and an electromagnetic sounding system.

The two additional surface sensors and the three volumetric sensors are discussed below.

6.1.3.1. Additional Surface Sensors

Passive Microwave Sensor Systems. A passive microwave system is similar to a multispectral scanning system in that it depends upon the sensing of natural radiation that is reflected and emitted from objects. The power received by the radiometer is considered in terms of an equivalent temperature known as the "apparent temperature" or "antenna temperature." Two types of passive microwave sensor systems have been developed—the single-value sensing system and the scanning system. The former establishes a single value for any location under the flight path, while in the latter, successive scans are recorded normal to the flight path and a two-dimensional image is obtained. The scanning system is, of course, considerably more expensive than the single-value sensing system, but the two-dimensional image that it produces increases the potential information to be gained and allows correlation with other types of remote sensing imagery.

Edgerton et al. [48] state that "microwave brightness temperatures of soils and sediments are dependent upon . . . moisture content, density, surface roughness (including microrelief, particle or fragment size and shape, vegetal cover, etc.), thermometric temperature, and stratigraphy (layering, etc.)." These dependencies have been demonstrated experimentally [48], and since data indicating each of these physical properties can be used to locate geologic mapping units, the value of passive microwave systems in geologic reconnaissance is obvious. Since it is known that fault zones can be identified by far-infrared detection of predawn evaporative cooling [5], the capability for detection of moisture becomes particularly applicable to tunnel-site selection. Passive microwave sensor systems might, in fact, be more effective than infrared systems in the detection of fault zones, since the underlying volume, particularly that close to the surface, plays a part in microwave emission.

Gamma-Ray Sensors. Airborne gamma-ray surveys conducted in Canada (Darnley and Fleet, Ref. 49) and in Puerto Rico (Schwarzer et al., Ref. 50) have shown the applicability of nuclear remote sensing to geologic investigations. In these surveys, low-altitude flights were used to establish gamma-ray signatures for several substances, such as thorium, uranium, potassium, bismuth, and thallium. Once the signatures were known, rock types could be identified on the basis of the amount and ratios of these elements. Schwarzer et al. state, ". . . this study suggests that it is possible not only to discriminate between various bedrock lithologies but to identify them, provided there is adequate rock exposure or the overlying soil cover accurately reflects the composition of the underlying parent material . . . . Gamma-ray remote sensing . . . can be an effective method of revealing geologic patterns and serving as a guide for minimum investigation on the ground."

6.1.3.2. Volumetric Sensors

Airborne Magnetometer. Airborne magnetometers have been employed operationally since World War II in mineral and oil exploration (Dobrin, Ref. 51), and any thorough geologic reconnaissance program should incorporate aeromagnetic interpretation. The magnetometer can easily be incorporated with the other sensors in a single aircraft. Magnetometer data should also be correlated with other remote sensing data, although research into the possibilities of combining and processing the data is necessary. For example, meaningful image ratioing might be performed with a magnetic intensity map and other remote sensing data.

Airborne Gravimetry. Nettleton et al. [52] first investigated airborne gravimetry, the purpose of which is to measure the variation in the gravitational field by detecting small differences in the weight of a constant mass at different points on the earth's surface. The location and composition of deeply buried features can be inferred from knowledge of the gravitational field. Unlike the airborne magnetometer, the airborne gravimeter has not yet been incorporated into operational use in mineral and oil exploration. According to Garland [53],

"It is now generally agreed that the greatest limitation to gravity measurements from moving vehicles is the lack of navigation systems which could be used anywhere on earth to give a continuous record of the vehicle's velocity."

Research on airborne gravity surveys is still continuing, however. Hall and Townsend [54] produced Bouguer anomaly maps with data gathered from a helicopter survey, and contour lines differing in 10 milligals were plotted as close together as 2 km. In Szabo and Anthony's discussion [55] of aerial gravity measurements (in which Doppler radar, astrotracker, hypsometer, terrain clearance radar, and aerial camera data were used), a typical result was a total $5^{o} \times 5^{o}$ error of 11.8 milligals. In the continuing research on airborne gravimetry, one of the problems that must be solved is the determination of the relative accuracy required in tunnel-site selection in comparison to that required for mineral exploration.

Airborne Electromagnetic Sounding. Airborne electromagnetic sounding (AEM) systems are essentially very low-frequency, intensity-measuring nonranging radars (a few hertz to a few thousand hertz), in which the transmitter and receiver are separated, usually by more than 60 m. The separation is achieved either by towing a glider or by using two aircraft. According to Dobrin [51], the AEM technique can be used to a maximum depth of approximately 1500 ft. The depth of penetration is an inverse function of frequency, where the optimum frequency, f, for greatest penetration [51] is

$$f = \left(\frac{100}{h^2}\right)\rho$$

where h is depth of penetration in meters and ρ is resistivity in ohm · cm.

In a tutorial article, Ward [56] states, "The purpose of all of the totally airborne [AEM] systems is to locate, rapidly, good conductors of electricity within the top several hundred feet of the earth's surface. Such good conductors might include graphitic schists, carbonaceous sediments, fault and shear zones, swamps, etc., as well as the primary target, massive sulfide mineralization." Although not basically used for mapping, airborne electromagnetic sounding is particularly suited for locating fault and shear zones (probably because of the increased moisture content in these zones), and the ability to identify such zones is an obvious benefit in tunnel-site selection.

6.2. RATIONALE OF APPROACH TO FUTURE RESEARCH

Geologic reconnaissance for tunnel-site selection has much in common with mineral and oil exploration and general geologic mapping in that it seeks to infer features that cannot be directly seen. For such a purpose, every possible confirming method should be used, particularly in investigations involving tunneling, where the cost of construction is so much greater

than the cost of a complete geologic and geophysical survey and where one geologic oversight can cost many times more than the total survey.

In future research into geologic applications of remote sensing data, test sites must be utilized to evaluate present techniques, to provide a framework for improvement of these techniques, and to develop new methods of acquiring useful data. The progress that we have made in geologic applications of image ratioing, statistical pattern recognition, and sidelooking radar should be continued. All available remote sensing systems should be incorporated; the correlation of data from many different types of sensors enables us to make more reliable geologic inferences than we could make on the basis of any one type of remote sensing data or on a limited number of types.

Because of the increasing availability of remote sensing data (such as the Strategic Air Command's sidelooking radar imagery and the data resulting from the ERTS project), reconnaissance geologists will in the near future be required to use such data effectively. Research should currently be directed toward the determination and development of the most effective techniques of utilizing these data in geologic investigations.

REFERENCES

1. K. Széchy, "The Art of Tunneling," Akadémiai Kiadó, Budapest, Hungary, 1967.
2. B. A. Tator et al., "Photo Interpretation in Geology," in Manual of Photographic Interpretation. American Society of Photogrammetry, Washington, D. C., 1960, pp. 169-342.
3. V. C. Miller and S. A. Schumm, "Aerial Photographs and Surface Features," in Aerial Surveys and Integrated Studies: Proceedings of the Toulouse Conference, UNESCO, Paris, 1968, pp. 41-79.
4. C. F. Miller, Photogeology, McGraw Hill Book Company, New York, 1961.
5. L. C. Rowan, T. W. Offield, K. Watson, P. J. Cannon, and R. D. Watson, "Thermal Infrared Investigations, Arbuckle Mountains, Oklahoma," Geol. Soc. Amer. Bull., Vol. 81, December 1970.
6. R. D. Watson, "Spectral Reflectance and Photometric Properties of Selected Rocks," J. Remote Sensing of Environment, Vol. 2, No. 2, 1972, pp. 95-100.
7. L. F. Dellwig, H. C. MacDonald, J. N. Kirk, "The Potential of Radar in Geological Exploration," Proceedings of the Fifth International Symposium on Remote Sensing of Environment, Willow Run Laboratories of the Institute of Science and Technology, The University of Michigan, Ann Arbor, April 1968, pp. 747-763.
8. L. C. Rowan and P. J. Cannon, "Remote Sensing Investigations Near Mill Creek, Oklahoma," Oklahoma Geology Notes, Vol. 30, No. 6, December 1970.
9. R. J. Shay (ed.), Remote Sensing with Special Reference to Agriculture and Forestry, National Academy of Sciences, Washington, D. C., 1970, p. 421.
10. P. G. Hasell and L. M. Larsen, Calibration of an Airborne Multispectral Optical Sensor, Report No. 6400-137-T, ECOM-00013-137, Willow Run Laboratories of the Institute of Science and Technology, The University of Michigan, Ann Arbor, 1968.
11. R. F. Nalepka, Investigations of Multispectral Discrimination Techniques, Report No. 2264-12-F, Willow Run Laboratories of the Institute of Science and Technology, The University of Michigan, Ann Arbor, 1970.
12. W. A. Malila et al., Studies of Spectral Discrimination, Report No. 31650-22-T, Willow Run Laboratories of the Institute of Science and Technology, The University of Michigan, Ann Arbor, 1971.
13. R. F. Nalepka et al., Investigations of Multispectral Sensing of Crops, Report No. 31650-30-T, Willow Run Laboratories of the Institute of Science and Technology, The University of Michigan, Ann Arbor, 1971.
14. J. D. Erickson and F. J. Thomson, Investigations Related to Multispectral Imaging Systems for Earth-Resources Surveys, Report No. 31650-17-P, Willow Run Laboratories of the Institute of Science and Technology, The University of Michigan, Ann Arbor, 1971.
15. R. N. Colwell et al., "Basic Matter and Energy Relationships Involved in Remote Reconnaissance," Photogram. Eng., Vol. 29, 1963, pp. 761-799.
16. B. Drake et al., Tunnel-Site Selection by Remote Sensing Techniques (Semiannual Report, 1 April Through 30 September 1971), Report No. 10018-7-P. Willow Run Laboratories of the Institute of Science and Technology, The University of Michigan, Ann Arbor, November 1971.

17. L. J. Chapman and D. F. Putnam, The Physiography of Southern Ontario, University of Toronto Press, Toronto, 1966, pp. 292-296.

18. W. A. Fisher et al., "Infrared Surveys of Hawaiian Volcanoes," Science, Vol. 146, No. 3645, 1964, p. 733.

19. J. H. McLerran and J. O. Morgan, "Thermal Mapping of Yellowstone National Park," Proceedings of the Third International Symposium on Remote Sensing of the Environment, Willow Run Laboratories of the Institute of Science and Technology, The University of Michigan, Ann Arbor, 1964.

20. J. D. Friedman and R. S. Williams, "Infrared Sensing of Active Geologic Processes," Proceedings of the Fifth International Symposium on Remote Sensing of the Environment, Willow Run Laboratories of the Institute of Science and Technology, The University of Michigan, Ann Arbor, 1968, pp. 787-815.

21. J. G. Quade et al., Multispectral Remote Sensing of an Exposed Volcanic Province, Technical Memorandum 33-453, Jet Propulsion Laboratory, 1970. pp. 9-13.

22. A. E. Coker, R. Marshall, and N. S. Thomson, "Application of Computer Processed Multispectral Data to the Discrimination of Land Collapse (Sinkhole) Prone Areas in Florida," Proceedings of the Sixth International Symposium on Remote Sensing of the Environment, Vol. 1, Willow Run Laboratories of the Institute of Science and Technology, The University of Michigan, Ann Arbor, 1969, pp. 65-77.

23. W. M. Knuth, W. Fisher, and R. W. Stingelin, "Detection, Delineation, and Monitoring of Subsurface Coal Fires by Aerial Infrared Scanning," Proceedings of the Fifth International Symposium on Remote Sensing of the Environment, Willow Run Laboratories of the Institute of Science and Technology, The University of Michigan, Ann Arbor, 1968, pp. 877-882.

24. V. V. Karmanov, "Studies of Soils from the Spectral Composition of Reflected Radiation," Trans. in Soviet Soil Science, 1970, pp. 226-238.

25. R. D. Watson, "Spectral Reflectance and Photometric Properties of Selected Rocks," J. Remote Sensing of Environment, Vol. 2, No. 2, 1972, pp. 95-100.

26. H. R. Condit, "Application of Characteristic Vector Analysis to the Spectral Energy Distribution of Daylight and the Spectral Reflectance of American Soils," Appl. Opt., Vol. 11, No. 1, 1972.

27. J. E. Colwell, Multispectral Remote Sensing of Urban Features, Report No. 2772-6-F, Willow Run Laboratories of the Institute of Science and Technology, The University of Michigan, Ann Arbor, 1970.

28. R. K. Vincent, R. Horvath, F. Thomson, and E. Work, "Remote Sensing Data Analysis Projects Associated with the NASA Earth Resources Spectral Information System," Report No. 31650-26-T, Willow Run Laboratories of the Institute of Science and Technology, The University of Michigan, Ann Arbor, 1971.

29. R. K. Vincent and F. Thomson, "Spectral Compositional Imaging of Silicate Rocks," J. Geophys. Res., Vol. 77, No. 14, May 1972, pp. 2465-2471.

30. R. J. P. Lyon, Evaluation of Infrared Spectrophotometry for Compositional Analysis of Lunar and Planetary Soils: Rough and Powdered Surfaces (Final Report, Part ii, under NASA Contract NASr-49(04), Stanford Research Institute, Menlo Park, California, 1964.

31. R. K. Vincent and F. Thomson, "Rock-Type Discrimination from Ratioed Infrared Scanner Images of Pisgah Crater, California," Science, Vol. 175, 1972.

32. D. Anding, R. Kauth, and R. Turner, Atmospheric Effects on Infrared Multispectral Sensing of Sea Temperature from Space, Report No. 26760-5-F, Willow Run Laboratories of the Institute of Science and Technology, The University of Michigan, Ann Arbor, 1970.

33. R. J. P. Lyon, "Infrared Spectral Emittance in Geological Mapping: Airborne Spectrometer Data from Pisgah Crater, California," Science, Vol. 175, 1972.

34. R. K. Vincent, Rock-Type Discrimination from Ratio Images of the Pisgah Crater, California Test Site, Report No. 31650-77-T, Willow Run Laboratories of the Institute of Science and Technology, The University of Michigan, Ann Arbor, 1972.

35. R. K. Vincent, F. Thomson, and K. Watson, "Recognition of Exposed Quartz Sand and Sandstone by Two-Channel Infrared Imagery," J. Geophys. Res., Vol. 77, No. 14, May 1972, pp. 2473-2477.

36. G. L. Berlin and G. G. Schaber, "Geology and Radar Mosaics," J. Geol. Ed., Vol. 19, No. 5, 1971, pp. 212-217.

37. R. J. P. Lyon, J. Mercado, and R. Cambell, Jr., "Pseudo Radar," Photogram. Eng., Vol. 36, No. 12, 1970, pp. 1257-1261.

38. L. F. Dellwig, H. C. MacDonald, and J. N. Kirk, "Technique for Producing a Pseudo Three-Dimensional Effect with Monoscopic Radar Imagery," Photogram. Eng., Vol. 36, No. 9, 1970, pp. 987-988.

39. H. O. Rydstrom, "Interpreting Local Geology from Radar Imagery," Geol. Soc. Amer. Bull., Vol. 78, 1967, pp. 429-438.

40. E. Gillerman, Investigation of Cross-Polarized Radar on Volcanic Rocks, CRES Report No. 61-25, The University of Kansas, 1967.

41. R. L. Cosgriff, W. H. Peak, and R. C. Taylor, "Terrain Scattering Properties for Sensor System Design," Terrain Handbook II, Ohio State University, Eng. Exp. Sta. Bull., Vol. 181, 1960.

42. H. C. MacDonald, "Geological Evaluation of Radar Imagery from Darien Province, Panama," Mod. Geol., Vol. 1, No. 1, 1969, pp. 1-63.

43. A. J. Lewis and H. C. MacDonald, "Interpretive and Mosaicing Problems of SLAR Imagery," J. Remote Sensing of Environment," Vol. 1, No. 4, 1970, pp. 231-236.

44. H. C. MacDonald, J. N. Kirk, L. F. Dellwig, and A. J. Lewis, "Significance of Look Direction in Detection of Geologic Features," Proceedings of the Sixth International Symposium on Remote Sensing of Environment, Willow Run Laboratories of the Institute of Science and Technology. The University of Michigan, Ann Arbor, 1969, pp. 637-650.

45. E. Gillerman, "Roselle Lineament of Southeast Missouri," Geol. Soc. Amer. Bull., Vol. 81, 1970, pp. 975-982.

46. R. S. Wing, "Cholame Area—San Andreas Fault Zone, California: A Study in SLAR," Mod. Geol., Vol. 1, No. 3, 1970, pp. 173-186.

47. R. S. Wing, W. K. Overbey, and L. F. Dellwig, "Radar Lineament Analysis, Burning Springs Area, West Virginia—An Aid in the Definition of Appalachian Plateau Thrusts," Geol. Soc. Amer. Bull., Vol. 81, 1970, pp. 3437-3444.

48. A. T. Edgerton, F. Ruskey, D. Williams, A. Stognyn, G. Poe, D. Meeks, and O. Russell, Microwave Emission Characteristics of Natural Materials and The Environment, Technical Report No. 9016R-8, Aerojet General Corporation, February 1971.

49. A. G. Darnley and M. Fleet, "Evaluation of Airborne Gamma Ray Spectrometry in the Bancroft and Elliot Lake Areas of Ontario, Canada," Proceedings of the Fifth International Symposium on Remote Sensing of Environment, Willow Run Laboratories of the Institute of Science and Technology, The University of Michigan, Ann Arbor, 1968.

50. T. F. Schwarzer, B. G. Cook, and J. A. S. Adams, "Low Altitude Gamma Spectrometric Surveys from Helicopters in Puerto Rico as an Example of the Remote Sensing of Thorium, Uranium, and Potassium in Soils and Rocks," J. Remote Sensing of the Environment, Vol. 2, No. 2, 1972.

51. M. B. Dobrin, Introduction to Geophysics, McGraw-Hill Book Company, New York, 1960.

52. L. L. Mettleton, L. LaCoste, and J. C. Harrison, "Tests of an Airborne Gravity Meter," Geophysics, Vol. 25, No. 1, February 1960.

53. G. O. Garland, Introduction to Geophysics: Mantle, Core, and Crust, W. B. Sanders Company, Philadelphia, 1971.

54. M. Hall and I. J. Townsend, "Helicopter Gravity Survey of Areas Marginal to the W. Gt. Artesian Basin," Mineral Resources Rev., No. 130, Department of Mines, South Australia, June 1969.

55. B. Szabo and D. Anthony, "Results of AFCRL's Experimental Aerial Gravity Measurements," J. International Assoc. Geodesy, No. 100, June 1971.

56. S. H. Ward, "The Electromagnetic Method," in Mining Geophysics, Vol. II, Theory, Society of Exploration Geophysicists, 1967.